Charles University
Faculty of Science

Study programme: Biology

Branch of study: Genetics, molecular biology and virology

Bc. Michaela Myšáková

Investigation of the role of the KEAP1-NRF2 antioxidant pathway in the therapy of secondary acute myeloid leukaemia

Výzkum role antioxidační dráhy KEAP1-NRF2 v terapii sekundární akutní myeloidní leukémie

Diploma thesis

Supervisor: RNDr. Kristýna Pimková, PhD.

Prague, 2024

Prohlášení:

Prohlašuji, že jsem závěrečnou práci zpracovala samostatně a že jsem uvedla všechny použité informační zdroje a literaturu. Tato práce ani její podstatná část nebyla předložena k získání jiného nebo stejného akademického titulu.

V Praze, 29.4.2024

Bc. Michaela Myšáková

Abstract

The development of therapy resistance is a long-standing problem in treating cancer, particularly in the treatment of myelodysplastic syndrome (MDS) and acute myeloid leukaemia (AML), where the hypomethylating agent 5-azacytidine (AZA) is the first choice of treatment. To enhance therapeutic efficacy, AZA is often combined with other agents such as pevonedistat (Pevo), a NEDDylation inhibitor targeting the ubiquitin-proteasome system. While initial results showed a synergistic effect of the AZA and Pevo combination in treating MDS and AML, dual resistance has been described, underlining the importance of understanding the mechanisms behind the resistance development.

Our previous data demonstrated an essential role of redox homeostasis and antioxidant system represented by Nuclear factor erythroid 2-related factor 2 (NRF2) in AZA resistance. The Kelch-like ECH-associated protein 1 (KEAP1)-NRF2 pathway is the master regulator of antioxidative defence in cells crucial for maintaining redox balance. However, hyperactivation of NRF2 has been implicated in therapy resistance and cancer progression. We hypothesised that NRF2 is crucial in MDS/AML therapy resistance, particularly in resistance to combined AZA and Pevo therapy.

We worked with cells sensitive and resistant to AZA and Pevo and monitored their redox state and NRF2 activity through flow cytometry and immunodetection techniques. Our findings revealed that the development of resistance to AZA and Pevo is associated with redox changes and persistent NRF2 activation. Paradoxically, our results underscore an important role for NRF2 both in the mechanism of action of AZA and Pevo and in the resistance to this combined therapy. Additionally, using a mass spectrometry-based redox proteomics method, we analysed specific oxidative modifications of protein thiols and we found that Pevo resistance is accompanied by significant changes in the redox state of proteins regulating key survival pathways.

Key words:

Acute myeloid leukaemia (AML), myelodysplastic syndrome (MDS), Kelch-like ECH-associated protein 1 (KEAP1), Nuclear factor erythroid 2-related factor 2 (NRF2), Isocitrate dehydrogenase 1 (IDH1) gene, Isocitrate dehydrogenase 2 (IDH2) gene, mutations, redox homeostasis, antioxidant pathway, mass spectrometry, proteomics, flow cytometry

Abstrakt

Vznik rezistence na terapii je dlouhodobým problémem při léčbě nádorových onemocnění, zejména při léčbě myelodysplastického syndromu (MDS) a akutní myeloidní leukémie (AML), u nichž je hypomethylační lék 5-azacytidin (AZA) první volbou. Pro zvýšení terapeutické účinnosti se AZA často kombinuje s dalšími látkami, jako je pevonedistat (Pevo), inhibitor NEDDylace zaměřený na ubikvitin-proteazomový systém. Ačkoliv první výsledky ukázaly synergický účinek kombinace AZA a Pevo při léčbě MDS a AML, byla popsána duální rezistence, což podtrhuje důležitost pochopení mechanismů stojících za vznikem této rezistence.

Naše předchozí výsledky prokázaly zásadní roli redoxní homeostázy a antioxidačního systému reprezentovaného Nuclear factor erythroid 2-related factor 2 (NRF2) v rezistenci na AZA. Dráha Kelch-like ECH-associated protein 1 (KEAP1)-NRF2 je hlavním regulátorem antioxidační obrany v buňkách, která je klíčová pro udržení redoxní rovnováhy. Hyperaktivace NRF2 se však podílí na rezistenci k léčbě a progresi rakoviny. Předpokládali jsme, že NRF2 má zásadní význam v rezistenci na terapii MDS/AML, zejména v rezistenci na kombinovanou léčbu AZA a Pevo.

Pracovali jsme s buňkami citlivými a rezistentními na AZA a Pevo a sledovali jejich redoxní stav a aktivitu NRF2 pomocí průtokové cytometrie a imunodetekčních technik. Naše zjištění odhalila, že rozvoj rezistence k AZA a Pevo je spojen s redoxními změnami a přetrvávající aktivací NRF2. Naše výsledky paradoxně zdůrazňují důležitou roli NRF2 jak v mechanismu účinku AZA a Pevo, tak v rezistenci na tuto kombinovanou léčbu. Kromě toho jsme pomocí metody redoxní proteomiky založené na hmotnostní spektrometrii analyzovali specifické oxidační modifikace thiolů proteinů a zjistili jsme, že rezistence na Pevo je doprovázena významnými změnami redoxního stavu proteinů regulujících klíčové dráhy přežití.

Klíčová slova:

Akutní myeloidní leukémie (AML), myelodysplastický syndrom (MDS), Kelch-like ECH-associated protein 1 (KEAP1), Nuclear factor erythroid 2-related factor 2 (NRF2), Isocitrát dehydrogenáza 1 (IDH1) gen, Isocitrát dehydrogenáza 2 (IDH2) gen, mutace, redoxní homeostáza, antioxidační dráha, hmotnostní spektometrie, proteomika, průtoková cytometrie

Acknowledgements:

Firstly, I want to express my deepest thanks to my supervisor, RNDr. Kristýna Pimková, PhD., for her excellent academic guidance and mentorship. I am grateful for her readiness to help, her insightful advice, and her patience in explaining things. Her enthusiasm for her work and the effort she puts into it continue to inspire me.

I would also like to thank my colleagues from our laboratory for their constant willingness to help. I am grateful to be a part of such an amazing collective of driven individuals.

Finally, my heartfelt thanks go to my partner for his endless support and to my parents, who have made it possible for me to pursue my passions.

Table of Contents

List of abbreviations

α-KG	Alpha-ketoglutarate
7-AAD	aminoactinomycin D
AML	Acute Myeloid Leukemia
AML-M6	Acute Myeloid Leukemia subtype M6 (erythroleukemia)
AmpR	Ampicillin Resistance
ARE	Antioxidant Response Element
ASXL1	Additional Sex Combs Like 1
AZA	5-Azacytidine
AZA-R	5-Azacytidine Resistant
AZA-S	5-Azacytidine Sensitive
BCA	Bicinchoninic Acid assay
BCOR	BCL6 Corepressor
BF	Bafilomycin
BSA	Bovine Serum Albumin
CAPN2	Calpain-2
CAST	Calpastatin
CEBPA	CCAAT Enhancer Binding Protein Alpha
CQ	Chloroquine
Ctrl	Control group
Cul	Cullin
Cys	Cysteine
D-2-HG	D-2-hydroxyglutarate
DMSO	Dimethyl Sulfoxide
DNMT	DNA Methyltransferase
dNTPs	Deoxynucleotide triphosphates
Dox	Doxycycline
DTT	Dithiothreitol
ETC	Electron Transport Chain
EZH2	Enhancer of Zeste Homolog 2
FACS	Fluorescence-Activated Cell Sorting

FBS	Fetal Bovine Serum
FLT3	FMS-like Tyrosine Kinase 3
FMO	Fluorescence Minus One
FOXO	Forkhead Box O
GAPDH	Glyceraldehyde 3-Phosphate Dehydrogenase
GATA2	GATA Binding Protein 2
GO	Gene Ontology
GPX	Glutathione Peroxidase
GR	Glutathione Reductase
GRX	Glutaredoxin
GSH	Reduced Glutathione
GSSG	Oxidised Glutathione
HIF	Hypoxia-Inducible Factor
HMA	Hypomethylating Agent
HSC	Hematopoietic Stem Cell
IAM	Iodoacetamide
IC50	Half Maximal Inhibitory Concentration
IDH	Isocitrate Dehydrogenase
iNRF2	NRF2 inhibitor
iodoTMT	Iodoacetyl Tandem Mass Tag
IPSS-R	Revised International Prognostic Scoring System
IκB	Inhibitor of NF-κB
KEAP1	Kelch-like ECH-associated Protein 1
LC3	Microtubule-associated Protein 1 Light Chain 3
LC3-I	Non-lipidated form of LC3
LC3-II	Lipidated form of LC3
LPB	Low Protein Binding
LSC	Leukemic Stem Cell
MAF	Musculoaponeurotic Fibrosarcoma
MDS	Myelodysplastic Syndrome
MFI	Median Fluorescence Intensity

mutIDH1/2	Mutant Isocitrate Dehydrogenase 1/2
NAD	Nicotinamide Adenine Dinucleotide
NADH	Reduced Nicotinamide Adenine Dinucleotide
NADP	Nicotinamide Adenine Dinucleotide Phosphate
NADPH	Reduced Nicotinamide Adenine Dinucleotide Phosphate
NAE	NEDD8-activating Enzyme
Neh	NRF2-ECH Homology domains
NF-κB	Nuclear factor-κB
NOXs	NADPH Oxidases
NPM1	Nucleophosmin 1
NQO1	NAD(P)H Quinone Dehydrogenase 1
NRF2	Nuclear Factor Erythroid 2-Related Factor 2
OXPHOS	Oxidative Phosphorylation
PBS	Phosphate-Buffered Saline
PCR	Polymerase Chain Reaction
Pevo	Pevonedistat
PEVO-PR	Cells resistant to AZA and partially resistant to Pevo
PEVO-R	Cells resistant to AZA and Pevo
PI	Propidium Iodide
pKa	Ionisation constant
PMAIP1	Phorbol-12-myristate-13-acetate-induced protein 1
PPI	Protein-Protein Interaction
PRX	Peroxiredoxin
pSBtet	Sleeping beauty system with tetracycline-inducible expression
PTPN11	Protein Tyrosine Phosphatase Non-receptor Type 11
PuroR	Puromycin Resistance
PVDF	Polyvinylidene Difluoride
Rbx1	RING-box protein 1
Redox	Reduction-oxidation
RING	really interesting new gene
ROS	Reactive Oxygen Species

RUNX1	Runt-related Transcription Factor 1
s-AML	Secondary Acute Myeloid Leukemia
SDC	Sodium Deoxycholate
SDS	Sodium Dodecyl Sulfate
SDS-PAGE	Sodium Dodecyl Sulphate Polyacrylamide Gel Electrophoresis
SEER	Surveillance, Epidemiology, and End Results Program
SF3B1	Splicing Factor 3b Subunit 1
SFN	Sulforaphane
sMaf	Small Maf
SQSTM1	Sequestosome 1
SRSF2	Serine and Arginine Rich Splicing Factor 2
STAG2	Stromal Antigen 2
TCA	Tricarboxylic acid
TCEP	Tris(2-carboxyethyl)phosphine
TEAB	Triethylammonium Bicarbonate
TET2	Tet Methylcytosine Dioxygenase 2
TFA	Trifluoroacetic Acid
TLCK	N-alpha-tosyl-L-lysine chloromethyl ketone (protease inhibitor)
TPCK	Tosyl phenylalanyl chloromethyl ketone (protease inhibitor)
TRX, TXN	Thioredoxin
TRXR	Thioredoxin Reductase
U2AF1	U2 Auxiliary Factor 1
UAE	Ubiquitin activation enzyme
Ub	Ubiquitin
UPS	Ubiquitin-Proteasome System
Ven	Venetoclax
WST	Water-Soluble Tetrazolium
WT, wt	Wild Type
WT1	Wilms Tumor 1
ZRSR2	Zinc Finger (CCCH Type), RNA Binding Motif and Serine/Arginine Rich 2

1 Introduction

Myelodysplastic syndrome (MDS) is a clonal hematopoietic disorder characterised by ineffective haematopoiesis and a significant risk of progression to acute myeloid leukaemia (AML). The primary treatment of MDS patients progressing to AML involves the use of 5-azacytidine (AZA), a DNA methylation inhibitor that has significantly improved patient survival. Despite its benefits, primary resistance to AZA is observed in approximately one-third of patients, creating a challenge for treatment. To overcome this issue, therapies combining AZA with drugs such as venetoclax or pevonedistat (Pevo) have been explored, showing promising results. However, resistance to these drug combinations has also been observed, highlighting the need for a deeper understanding of the underlying mechanisms of resistance.

Drug resistance is a multi-step process that involves an interplay of genetic and metabolic reprogramming of the cell. As a consequence of metabolic abnormalities, tumour cells can undergo significant changes in redox homeostasis. The action of chemotherapeutic agents is often accompanied by excessive production of reactive oxygen species (ROS). Thus, to avoid oxidative damage, ROS must be eliminated, which is achieved by increased activity of the antioxidant system. This often prevents cell death and promotes tumour development, while making cancer cells more resilient to chemotherapy and therefore causing resistance.

The KEAP1-NRF2 pathway, the master regulator of the antioxidant system, plays a key role in this context. KEAP1 is a redox sensor that binds to NRF2 under physiological conditions, leading to its ubiquitination and subsequent degradation. However, oxidative stress can modify cysteine residues in KEAP1, impairing its ability to bind NRF2. This disruption allows newly synthesised NRF2 to translocate to the nucleus, where it acts as a transcription factor that induces the expression of genes critical for the antioxidant response of cells. Aberrant activation of NRF2 has been linked to cancer progression and resistance to therapy. Our previous data showed that redox reprogramming and NRF2 dysregulation play an important role in resistance to AZA.

This thesis explores the contributions of NRF2 and redox state to resistance against the combined treatment of AZA and Pevo in MDS and AML. We focus on alterations in redox homeostasis and NRF2 activity in the context of dual drug resistance, investigating the impact of these changes on key pathways and processes through redox signalling. We explore changes in the oxidative post-translational modifications of proteins and their roles in adapting to therapeutic resistance. Moreover, we address the direct connections between leukaemia-driving mutations in isocitrate dehydrogenase 1 (IDH1) and 2 (IDH2) enzymes, redox homeostasis and therapy sensitivity.

2 Literature review

2.1 Myelodysplastic syndrome and secondary acute myeloid leukaemia

Haemato-oncological diseases arise from malignant transformation of hematopoietic cells by losing the ability to differentiate and gaining the potential to undergo uncontrolled proliferation. Haemato-oncological diseases affect the blood, lymph nodes, and bone marrow tissues. These diseases are typically categorised as lymphoid or myeloid malignancies. This thesis focuses on myeloid disorders, namely myelodysplastic syndromes (MDS) and secondary acute myeloid leukaemia (s-AML).

The National Cancer Institute Surveillance, Epidemiology and End Results (SEER) database estimates that the annual incidence of MDS is approximately 4 cases per 100,000 individuals, with an increasing trend with age, as the annual incidence of MDS is estimated to be 27.3 per 100,000 individuals over the age 65. The median age at diagnosis is 76 years, and men are affected at a higher rate than women, with incidence rates of 5.5 and 3 per 100,000 per year, respectively. (SEER Explorer 2023). Common symptoms of MDS include excessive fatigue, bruising and bleeding, night sweats, and bone pain (Steensma, Heptinstall et al. 2008).

2.1.1 Pathophysiology

MDS represent a heterogeneous group of clonal disorders characterised by ineffective haematopoiesis and bone marrow failure. MDS are caused by impaired proliferation and differentiation of hematopoietic cells, resulting in peripheral-blood cytopenia. MDS may progress to s-AML, with MDS defined by the presence of less than 20% of immature myeloid blood cells (myeloblasts) in bone marrow and peripheral blood, while AML cases display 20% or more myeloblasts (Vardiman, Harris et al. 2002).

The growth and spreading of a somatically mutated clone are considered to be the cause of MDS. Although the identification of the cell of origin that gives rise to the malignant clone has been a challenge in understanding the pathophysiology of MDS, it is now accepted that

the MDS-associated genetic mutations are initiated in a hematopoietic stem cell (HSC) (Sperling, Gibson et al. 2017).

The acquisition of somatic mutations in HSCs can lead to clonal haematopoiesis which occurs over time as individual HSCs branch into distinct clones. Some mutations can influence the survival and function of HSCs, like the ability to proliferate and differentiate properly. Each year, an HSC acquires approximately 0.07-0.9 mutations, subtly changing their behaviour (Welch, Ley et al. 2012). Under normal circumstances, HSCs undergo asymmetrical division, generating one identical HSC and one differentiated progenitor cell. However, certain mutations confer advantageous traits, shifting the balance towards excessive self-renewal. This imbalance can lead to the emergence of blasts as a consequence of overgrown HSC clones (Fig. 1) (Challen and Goodell 2020). Nevertheless, the presence of MDS-specific mutations does not necessarily predispose to dysplasia, nor does the absence of mutations key to the pathophysiology of MDS exclude a diagnosis of MDS (Sperling, Gibson et al. 2017).

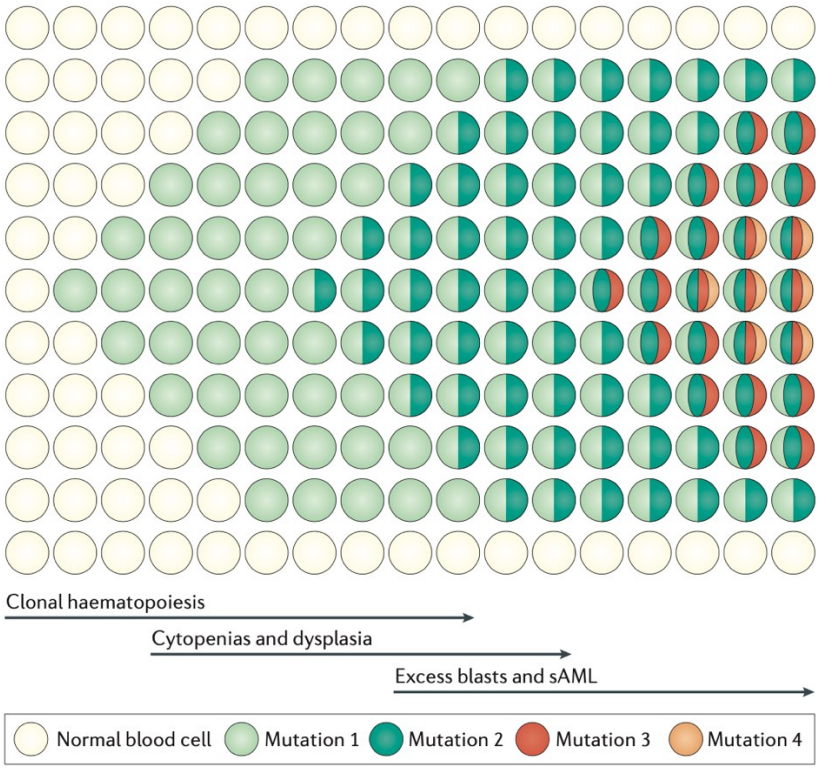

Fig. 1: Clonal expansion of HSCs in MDS and s-AML

Mutations initiated in hematopoietic stem cells (HSCs) can disrupt normal function, leading to increased self-renewal and clonal expansion. This process, known as clonal haematopoiesis, can manifest as cytopenia. As the HSCs acquire additional mutations, the clonal population can give rise to myelodysplastic syndrome (MDS).

In some cases, MDS can further evolve into secondary acute myeloid leukaemia (s-AML) (Adapted from Sperling, Gibson et al. 2017).

Typically, MDS patients carry three driver mutations (Haferlach, Nagata et al. 2014). These mutations are distributed across various biological pathways, including DNA methylation, RNA splicing, chromatin modification, transcription, signal transduction, cohesion regulation, and DNA repair. The most frequent mutations were identified in genes *tet methylcytosine dioxygenase 2* (*TET2*), *splicing factor 3b subunit 1* (*SF3B1*), *serine and arginine rich splicing factor 2* (*SRSF2*), *DNA methyltransferase 3 alpha* (*DNMT3A*), *additional sex combs like 1* (*ASXL1*), and *runt-related transcription factor 1* (*RUNX1*) and are present in at least 10% of patients (Haferlach, Nagata et al. 2014). Most patients harbour combinations of mutations from different pathways, thus highlighting the heterogeneity of MDS pathogenesis.

Evidence suggests that progression of MDS to s-AML is accompanied by the acquisition of additional mutations. Lindsley, Mar et al. identified mutations specific to s-AML compared to de novo AML, including mutations in genes *SRSF2*, *SF3B1*, *zinc finger CCCH-type, RNA binding motif and serine/arginine rich 2* (*ZRSR2*), *U2 small nuclear RNA auxiliary factor binding protein* (*U2AF1*), *BCL6 corepressor* (*BCOR*), *enhancer of zeste 2 polycomb repressive complex 2 subunit* (*EZH2*), and *stromal antigen 2* (*STAG2*), which are also common in MDS. Furthermore, through sequencing of paired MDS and s-AML samples, they observed that mutations in transcription factors *RUNX1*, *CCAAT enhancer binding protein alpha* (*CEBPA*), and *GATA-binding factor 2* (*GATA2*) were the most frequent mutations acquired during the disease progression from MDS to s-AML (Lindsley, Mar et al. 2015). Mutations in these genes are highly specific for s-AML, highlighting that s-AML is biologically distinct from *de novo* AML and reflects its evolution from MDS. Mutations in other genes with a significant impact on s-AML progression displaying higher occurrence in s-AML compared to high-risk MDS have been identified and are represented by *FMS-like tyrosine kinase 3* (*FLT3*), *protein tyrosine phosphatase non-receptor type 11* (*PTPN11*), *Wilms tumor 1* (*WT1*), *nucleophosmin 1* (*NPM1*), *NRAS* and *isocitrate dehydrogenase 1* (*IDH1*) and 2 (*IDH2*) (Makishima, Yoshizato et al. 2017). These studies demonstrate the

diverse impact of genetic mutations on disease onset and progression, revealing potential targets for therapies aimed at blocking disease evolution.

2.1.2 Therapy of high-risk MDS and s-AML

Due to the heterogeneity of MDS, multiple prognostic classification models have been developed in order to assess and effectively select the treatment (Garcia-Manero 2023). The most commonly used system is the Revised International Prognostic Scoring System (IPSS-R), which calculates a risk score based on cytogenetic abnormalities, bone marrow blast percentage, and cytopenias, and categorises MDS into five groups: very low, low, intermediate, high, and very high-risk MDS (Greenberg, Tuechler et al. 2012). In the management of MDS, several factors play a role such as transfusion needs, cytogenetic and mutational profiles, percentage of bone marrow blasts, comorbidities, potential for allogeneic stem cell transplantation, and prior exposure to hypomethylating agents (HMA) (Garcia-Manero 2023). We are focusing on the therapy of intermediate, high, and very high-risk MDS, collectively termed higher-risk MDS. For higher-risk MDS, hematopoietic stem cell transplantation remains the only curative therapy. However, given the relatively high median age of MDS diagnosis, which is approximately 70 years, this form of therapy is not suitable for most patients. Therefore, hypomethylating agents such as 5-azacytidine (AZA) and 2‘-deoxy-5-azacytidine (decitabine) are the preferred option for these patients (Sekeres and Taylor 2022). Early initiation of treatment of high-risk MDS patients is crucial to avoid the disease progression to s-AML. Conventional therapy for AML primarily involves chemotherapy with cytarabine and anthracycline, along with supportive care (Winer and Stone 2019). However, some patients may not be eligible for standard therapy due to an advanced age, the presence of comorbidities or other factors (Etienne, Esterni et al. 2007, Kantarjian, Ravandi et al. 2010). In such cases, hypomethylating agents like AZA or decitabine may be more suitable options.

Despite continuous development and implementation of new drugs, the emergence of therapy resistance often hampers the efficiency of treatment. Resistance can manifest as either primary, where patients do not respond to initial treatment, or secondary, where patients initially respond but later develop resistance (Asić 2016). The molecular mechanisms driving

resistance development are complex and involve a multi-step process, including metabolic reprogramming (Song, Li et al. 2014, Castro, Sampaio-Marques et al. 2019, Gu, Tohme et al. 2021). Given the frequent onset of resistance in MDS and AML, new drug combinations are being investigated to overcome it. Rodriguez-Sevilla, Adema et al. (2023) classified emerging therapies for MDS patients unresponsive to hypomethylation therapy into six categories based on their target cellular pathways: Isocitrate dehydrogenase (IDH) 1/2 inhibitors, immune checkpoint inhibitors, inflammation pathway inhibitors, anti-apoptotic inhibitors, NEDDylation inhibitors and multikinase inhibitors (Fig. 2) (Rodriguez-Sevilla, Adema et al. 2023). Three of these groups, which have demonstrated efficacy in combined treatment with AZA, are described below. Among these, Venetoclax (Ven), a potent Bcl-2 inhibitor, stands out for its ability to selectively induce apoptosis in leukemic cells, offering a targeted approach to therapy (Souers, Leverson et al. 2013). Combined with AZA, Ven has demonstrated efficacy in previously untreated AML and proven safety in MDS therapy (DiNardo, Pratz et al. 2019, Ball, Famulare et al. 2020, DiNardo, Jonas et al. 2020). This combination is currently the subject of clinical studies (Ball, Famulare et al. 2020, Zeidan, Borate et al. 2023). Another category includes inhibitors of IDH 1 and 2, as mutations in these genes occur in approximately 20% of AML cases and are known to contribute to leukemogenesis (Chaturvedi, Araujo Cruz et al. 2013, Medeiros, Fathi et al. 2017). Promising results have been observed in clinical trials with IDH1 and IDH2 inhibitors, ivosidenib and enasidenib, respectively, particularly when combined with hypomethylating agents like AZA (Strati, Kantarjian et al. 2015, DiNardo and Wei 2020, DiNardo, Schuh et al. 2021, Montesinos, Recher et al. 2022, Wang, Montesinos et al. 2022). Lastly, NEDDylation inhibitors targeting the proteasome system, such as pevonedistat (Pevo), have shown enhanced response rates when combined with AZA compared to AZA monotherapy (Sekeres, Watts et al. 2021, Adès, Girshova et al. 2022). Studies on the triplet combination of AZA, Ven and Pevo have demonstrated efficacy in MDS patients (Short, Muftuoglu et al. 2023).

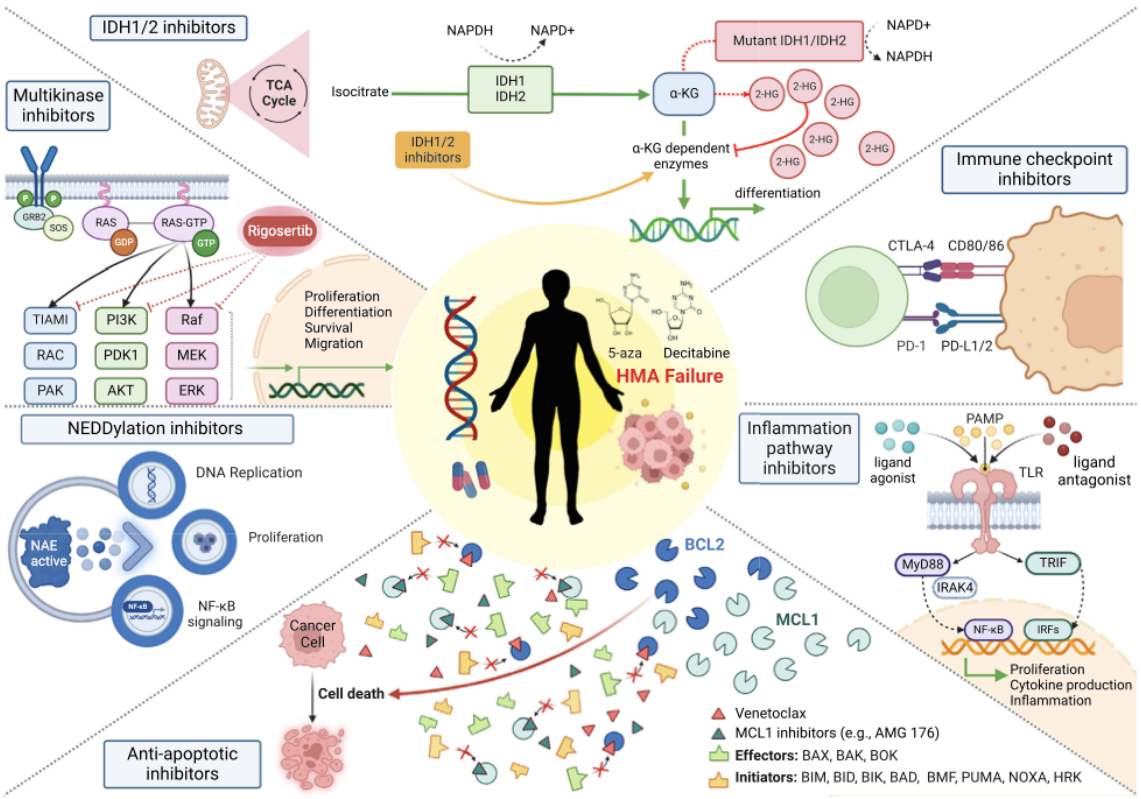

Fig. 2: Emerging therapies for MDS patients unresponsive to hypomethylation therapy (Adapted from Rodriguez-Sevilla, Adema et al. 2023).

2.1.2.1 5-azacytidine

AZA is a cytidine analogue primarily known for its mechanism of action involving DNA hypomethylation, which can reactivate the expression of silenced genes. At higher concentrations, AZA induces cytotoxicity by incorporation into RNA and DNA (Kaminskas, Farrell et al. 2005).AZA incorporates into RNA in its phosphorylated form as 5-azacytidine triphosphate. Incorporation into DNA is preceded by AZA's conversion to 5-AZAdeoxycitidine (decitabine) and by its phosphorylation to 5-AZAdeoxycitidine triphosphate. Approximately 80-90% of AZA is incorporated into RNA, while 10-20% is converted to decitabine triphosphate and incorporated into DNA (Li, Olin et al. 1970). Incorporation into RNA can disrupt RNA methylation and stability (Schaefer, Hagemann et al. 2009, Aimiuwu, Wang et al. 2012). When incorporated into DNA, AZA covalently binds to and inhibits the activity of DNA methyltransferase 1 (DNMT1), affecting DNA methylation (Schermelleh, Spada et al. 2005). This results in hypomethylation, which can reactivate the expression of previously silenced genes. Hypomethylation has been shown to

influence cellular differentiation (Jones and Taylor 1980, Creusot, Acs et al. 1982, Tsuji-Takayama, Inoue et al. 2004). However, at higher doses, AZA incorporation into DNA can induce significant DNA damage (Palii, Van Emburgh et al. 2008). This damage can lead to reactive oxygen species (ROS) production and oxidative damage, although this effect is less well-described (Montes, Guerra-Librero et al. 2022). Despite the therapeutic potential of hypomethylating agents such as AZA or decitabine, only 30-60% of higher-risk MDS patients respond to treatment (Silverman, Demakos et al. 2002, Steensma, Baer et al. 2009, Prébet, Gore et al. 2011). The exact mechanisms behind the resistance remain unclear, although several hypotheses have been proposed.

2.1.2.2 Pevonedistat

Pevo targets the ubiquitin-proteasome system (UPS) which is an essential part of cellular protein regulation. The system functions through the polyubiquitination of substrates by E3 ubiquitin ligases, targeting the substrates for degradation in the proteasome. Pevo is a small molecular inhibitor of the NEDD8-activating enzyme E1 regulatory subunit (NAE1), impairing the NEDDylation cascade that is crucial for the activation of cullin-RING E3 ubiquitin ligases (Fig. 3). These ligases are essential in regulating protein turnover by initiating the ubiquitination of their substrates, ultimately leading to their proteasomal degradation (Nawrocki, Griffin et al. 2012). The substrates affected by Pevo inhibition include important regulators of cell cycle regulation, apoptosis and antioxidative defence, such as p53, c-Myc, hypoxia-inducible factor (HIF)-1alfa and nuclear factor erythroid 2-related factor 2 (NRF2). Some of these substrates showed anti-proliferative effects in AML. Therefore, Pevo has been proposed as a treatment option in AML patients and has been shown effective in inducing cell death and disrupting the redox state in leukemic cells (Swords, Kelly et al. 2010, Swords, Erba et al. 2015).

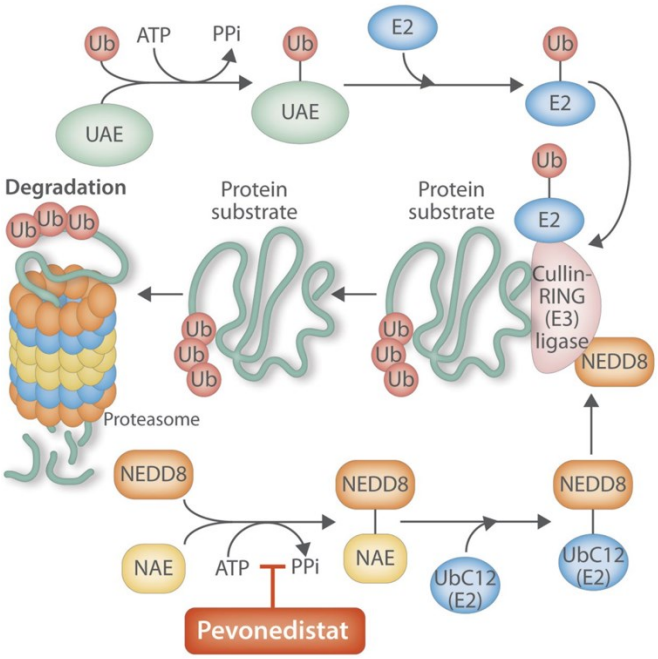

Fig. 3: The mechanism of action of pevonedistat

Pevonedistat inhibits NEDD8-activating enzyme (NAE), impairing the activation of NEDD8, which is an essential component of Cullin-RING ligases. Pevonedistat-mediated inhibition disrupts the degradation of polyubiquitylated proteins, a key process maintaining cellular homeostasis, and leads to the accumulation of the ligase‘s substrates. Ub – ubiquitin; UAE – ubiquitin activation enzyme (Adapted from Fathi 2018).

2.2 Redox metabolism

Increasing evidence points to redox homeostasis as a critical factor in leukemogenesis, progression, cell survival and disease relapse (Trombetti, Cesaro et al. 2021). Redox homeostasis represents the balance between oxidative and antioxidative processes within biological systems. Leukemic stem cells (LSCs) put increased demands on their energy metabolism and metabolic reprogramming is therefore essential for their survival and proliferation. These cells exhibit increased demands for biosynthesis and energy production, necessitating a rewiring of their energy metabolism toward oxidative phosphorylation (OXPHOS) (Castro, Sampaio-Marques et al. 2019, Trombetti, Cesaro et al. 2021). Modulation of redox homeostasis is tightly associated with energy metabolism. Unlike proliferating leukaemia cells, which manifest an increased oxidative state, LSCs are characterised by lower levels of ROS, which are important for maintaining their quiescent state. Hence, targeting redox homeostasis holds promise for eradicating LSCs. However, LSCs have a high capacity to adapt to changes in redox metabolism by enhancing their

antioxidant defence system (Trombetti, Cesaro et al. 2021). These shifts in the redox balance may thus trigger adaptive mechanisms and lead to the survival of these resistant cells.

2.2.1 Sources of reactive oxygen species in leukemic cells

Redox metabolism embodies a dynamic interplay between ROS and their scavengers. ROS are derivatives of molecular oxygen that are highly reactive due to the presence of a single unpaired electron in their outer electron shell. Superoxide (O_2^-), hydroxyl radical (HO•), hydrogen peroxide (H_2O_2), singlet oxygen ($^1O_2$), peroxyl radicals (ROO•) and nitric oxide (•NO) belong among the most abundant ROS (Sies and Jones 2020). ROS are the natural by-products of various cellular processes and environmental exposures. Mitochondrial respiration is a major endogenous source of ROS in leukemic cells (Prieto-Bermejo, Romo-González et al. 2018). During the mitochondrial electron transport chain, mainly at complexes I and III, an electron can be prematurely leaked and can interact with molecular oxygen generating a superoxide radical (Turrens and Boveris 1980, Barja and Herrero 1998, Turrens 2003). Leukemic cells in contrast to normal HSCs rely on mitochondrial OXPHOS and are sensitive to the disruption of electron transport chain (ETC) (Jones, Stevens et al. 2019). Moreover, mitochondrial DNA is commonly mutated in leukaemia, potentially contributing to ETC alterations and increased production of ROS (Silkjaer, Nørgaard et al. 2013). Therefore, mitochondrial function is critical in maintaining the redox homeostasis of leukemic cells.

Other important endogenous producers of ROS in leukemic cells are reduced nicotinamide adenine dinucleotide phosphate (NADPH) oxidases (NOXs) (Hole, Zabkiewicz et al. 2013). NOXs are intermembrane enzymes that deliberately generate superoxide radicals through a series of reactions facilitating the transfer of an electron from cytosolic NADPH to extracellular molecular oxygen. In leukemic cells, NOX2-mediated production of ROS has been associated with a worse prognosis in AML patients (Paolillo, Boulanger et al. 2022). Other sources of ROS include cytochrome P450 enzymes, xanthine oxidases, cyclooxygenases, and lipoxygenases (Sies and Jones 2020). Alterations in these pathways have been observed in AML (Trombetti, Cesaro et al. 2021).

2.2.2 Antioxidative defence systems in leukemic cells

At high concentrations, ROS can be harmful to the cell due to their reactivity. To prevent ROS-induced oxidative damage, cells have developed multiple antioxidative systems. Antioxidative systems are crucial for maintaining cellular redox homeostasis by keeping ROS at physiological levels. However, altered antioxidative systems are often described in leukaemia, contributing to impaired redox homeostasis. Both upregulation and downregulation of antioxidants have been found in leukaemia, reflecting the complexity of the redox environment in leukemic cells (Al-Gayyar, Eissa et al. 2007, Er, Tsai et al. 2007, Battisti, Maders et al. 2008).

Antioxidants can be divided into two groups: enzymatic and non-enzymatic systems. Enzymatic antioxidants include catalase, superoxide dismutase, glutathione peroxidase and peroxiredoxin (Liou and Storz 2010). Superoxide dismutases catalyse the conversion of superoxide radicals to less reactive hydrogen peroxide and oxygen. Subsequently, hydrogen peroxide can be converted to water and oxygen through reactions catalysed by catalase, glutathione peroxidase or peroxiredoxin (Fig. 4) (Panieri and Santoro 2016). To reduce hydrogen peroxide, glutathione peroxidase and peroxiredoxin utilise cysteine thiol groups which can undergo a reversible oxidation. Glutathione peroxidase uses a low molecular weight cysteine-containing molecule – reduced glutathione (GSH) – as a cofactor, converting it to oxidised glutathione (GSSG). GSSG is then reduced back to GSH in a reaction with $NADP^+$ catalysed by glutathione reductase. Peroxiredoxin is a part of a thioredoxin antioxidative system and it utilises a cysteine residue in its active site to reduce hydrogen peroxide. Peroxiredoxin is then reduced by thioredoxin, which is subsequently reduced by thioredoxin reductase in a reaction with NADPH (Liou and Storz 2010).

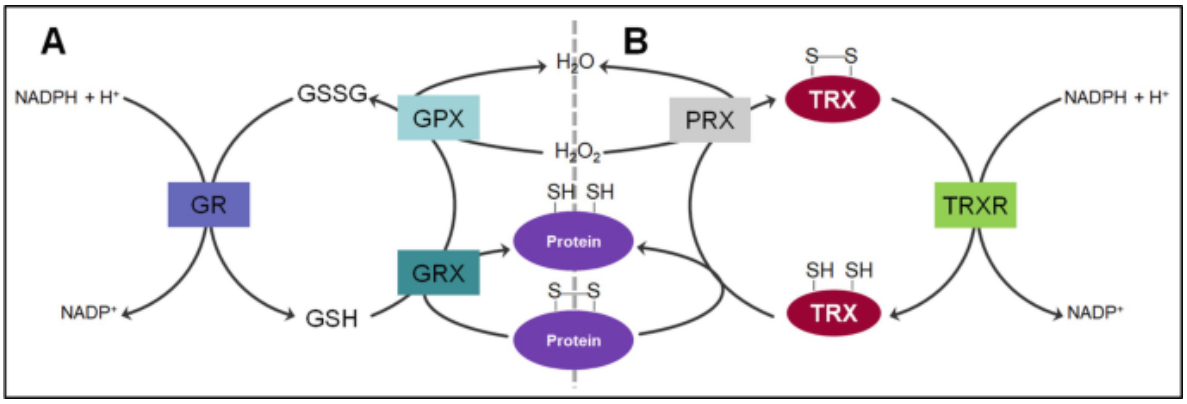

Fig. 4: The thioredoxin and glutathione antioxidant system overview

Thioredoxin and glutathione antioxidative systems protect cells from oxidative stress through reducing hydrogen peroxide (H_2O_2) to water (H_2O) and reducing oxidised protein thiols (-S-S- to -SH). Glutathione system consists of glutathione peroxidase (GPX), glutathione reductase (GR), glutaredoxin (GRX), reduced glutathione (GSH), oxidised glutathione (GSSG) and reduced nicotinamide adenine dinucleotide phosphate (NADPH). Thioredoxin system comprises peroxiredoin (PRX), thioredoxin (TRX), TRX reductase (TRXR) and NADPH. (Adapted from Yu, Di et al. 2022)

Non-enzymatic systems include vitamins A, C and E and GSH (Liou and Storz 2010). GSH, a tripeptide consisting of a glutamate, a cysteine, and a glycine molecule, serves multiple functions. Apart from its role as a cofactor of glutathione peroxidase, GSH can directly scavenge specific ROS. Additionally, GSH is important in the elimination of xenobiotics or electrophiles from cells by conjugating with them, followed by secretion through specific membrane transporters. This conjugation process can occur spontaneously or be catalysed by glutathione-S transferase (Forman, Zhang et al. 2009). Furthermore, GSH can modify proteins by forming disulphide bonds with free thiols on proteins, a process known as S-glutathionylation. This modification can influence the function, activity and stability of proteins, indicating its important regulatory role (Ghezzi 2013). Dysregulation of GSH metabolism has been observed in various cancer types, including haematological malignancies (Al-Gayyar, Eissa et al. 2007).

NADPH is an important reducing equivalent in cells. Apart from its role as a cofactor in lipid and nucleotide biosynthesis, it plays a pivotal role in maintaining redox homeostasis and supporting antioxidative defence mechanisms. NADPH is essential for the regeneration of antioxidant enzymes and molecules necessary to protect against elevated levels of ROS, thereby preventing oxidative damage. As a high-energy molecule, NADPH acts as an

electron donor for the reduction of GSSG and thioredoxin. Various cellular pathways contribute to the generation of NADPH. These include the pentose phosphate pathway, activity of isocitrate dehydrogenase 1 (IDH1) and 2 (IDH2), malic enzyme 1 and 3 activity and one-carbon metabolism (Chandel 2021). Each of these sources contributes to the pool of NADPH necessary for maintaining redox balance through supporting antioxidative defence mechanisms. However, defects and mutations in these enzymes and pathways have been described in haematological malignancies. They can lead to the disruption of NADPH balance influencing the overall redox homeostasis, possibly contributing to the pathogenesis of the disease and therapy resistance (Al-Khallaf 2017)..

2.2.3 KEAP1-NRF2 antioxidative pathway

The primary regulatory system for cellular defence against stress, is the Kelch-like ECH-associated protein 1 (KEAP1)-NRF2 pathway. KEAP1, a component of a Cullin (Cul)3-based E3 ubiquitin ligase complex, functions as a negative regulator of NRF2. Under normal conditions, KEAP1 binds NRF2 in the cytoplasm and induces its ubiquitination and subsequent degradation in the proteasome (Itoh, Wakabayashi et al. 1999, Kobayashi, Kang et al. 2004). However, under stress conditions, KEAP1's association with NRF2 is disrupted, allowing NRF2 to translocate to the nucleus. In the nucleus, NRF2 functions as a transcription factor, activating the expression of its target genes important in anti-stress defence (Itoh, Chiba et al. 1997, Kobayashi, Kang et al. 2006). Overexpression of NRF2 has been found in patients with AML and correlated with poor prognosis (Jalali, Mahmoudi et al. 2021, Yu, Wang et al. 2024).

NRF2 is a basic leucine zipper transcription factor comprising seven NRF2-ECH homology (Neh) domains: Neh1-7. KEAP1, a member of the BTB-Kelch protein family, possesses three domains: BTB, intervening region and Kelch domain (Canning, Sorrell et al. 2015). Interaction between KEAP1 and the N-terminal Neh2 domain of NRF2 occurs via the Kelch domain of KEAP1 (Itoh, Wakabayashi et al. 1999). The Neh2 domain features two binding sites for KEAP1 with varying affinities: the high-affinity ETGE motif and the low-affinity DLGex motif, each binding one KEAP1 molecule of a KEAP1 dimer (Tong, Katoh et al. 2006). KEAP1 dimerisation, mediated by the N-terminal BTB/POZ domain, is essential for

NRF2 binding, as the binding of both ETGE and DLGex motifs by KEAP1 is needed for the ubiquitination of NRF2 (Zipper and Mulcahy 2002, McMahon, Thomas et al. 2006). The identification of the different affinities between the two NRF2 sites interacting with KEAP1 gave rise to the hinge and latch binding model. The hinge represents the constant, high-affinity binding of the ETGE motif with KEAP1, while the latch indicates the low-affinity binding of the DLGex motif with KEAP1, whose dissociation can be triggered by various NRF2 inducers, affecting KEAP1's ability to ubiquitinate NRF2 (Tong, Kobayashi et al. 2006). It is important to note that NRF2 inducers can be divided into three categories: electrophilic inducers including hydrogen peroxide or sulforaphane (SFN), non-electrophilic inducers including KEAP1-NRF2 protein-protein interaction (PPI) inhibitors, mostly pharmaceutics, and non-canonical activation of NRF2 by p62/Sequestosome-1 (SQSTM-1) (Suzuki, Takahashi et al. 2023). It was later discovered that the hinge and latch mechanism is only applicable to NRF2 activation by non-electrophilic NFR2 inducers and by p62. NRF2 activation by electrophilic inducers mediated by the modification of cysteine thiols on KEAP1 does not trigger DLGex-KEAP1 dissociation, probably utilizing a different mechanism (Fig. 5) (Horie, Suzuki et al. 2021, Suzuki, Takahashi et al. 2023).

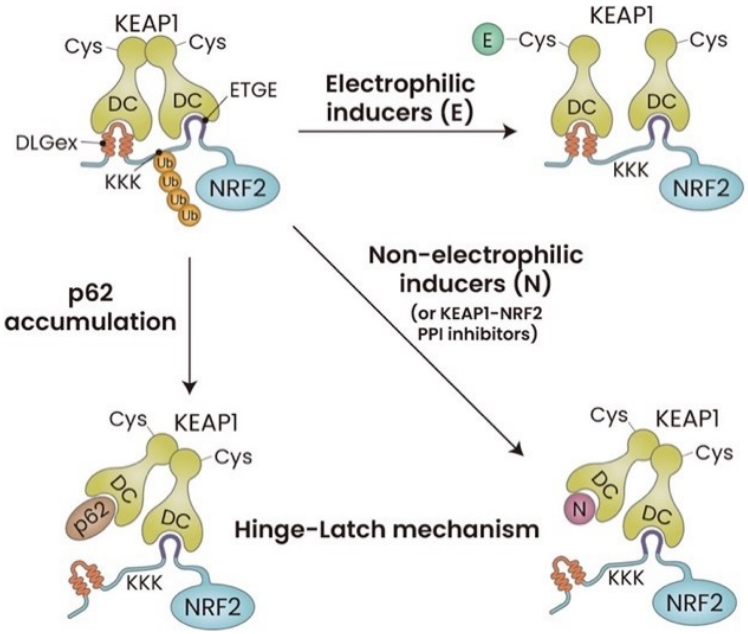

Fig. 5: Updated hinge and latch binding model

Hinge and latch binding mechanism is utilised by p62 and non-electrophilic inducers when mediating nuclear factor erythroid 2-related factor 2 (NRF2) activation. When accumulated, autophagy receptor p62 disrupts the interaction of DLGex of NRF2 with Kelch-like ECH-associated protein 1 (KEAP1), while the ETGE motif of NRF2 remains bound to KEAP1. This disruption impairs the ability of KEAP1 to ubiquitinate NRF2. Non-

electrophilic inducers function similarly. Electrophilic inducers, however, activate NRF2 without disrupting its interaction with KEAP1. They work through the modification of KEAP1 cysteine (Cys) thiols. PPI – protein-protein interaction (Adapted from Suzuki, Takahashi et al. 2023).

KEAP1 serves as an adaptor subunit of a Cul3-based E3 ubiquitin ligase complex, facilitating the binding of the N-terminal part of Cul3 via its intervening region domain (Kobayashi, Kang et al. 2004). Together with really interesting new gene (RING)-box protein 1 (Rbx1), KEAP1 and Cul3 form a Cullin-RING ubiquitin ligase complex. The complex promotes the ubiquitination of an α-helix within the Neh2 domain of NRF2, comprising seven lysine residues (Zhang, Lo et al. 2004). This ubiquitination triggers a rapid degradation of NRF2 in the proteasome (Itoh, Wakabayashi et al. 2003). However, upon exposure to electrophilic or oxidative stressors, thiol groups of cysteine residues of KEAP1 become modified (Kobayashi, Kang et al. 2006). Importantly, this pattern of cysteine modifications varies depending on the specific stressor encountered, leading to the activation of distinct NRF2-mediated programs. This highlights the role of KEAP1 as a redox sensor. Yamamoto et al. named this phenomenon the "cysteine code" hypothesis (Yamamoto, Suzuki et al. 2008). Suzuki et al. categorized NRF2 inducers into five classes based on which cysteine residues on KEAP1 they modify (Suzuki, Takahashi, and Yamamoto 2023). These modifications impair the ability of KEAP1-Cul3-based E3 ubiquitin ligase complex to ubiquitinate NRF2, while not releasing the NRF2 already bound to KEAP1. However, newly synthesized NRF2 becomes liberated to translocate to the nucleus, utilising its nuclear localisation signal (Kobayashi, Kang et al. 2006, Theodore, Kawai et al. 2008). In the nucleus, NRF2 dimerizes with small musculoaponeurotic fibrosarcoma (sMAF) proteins and together they bind antioxidant (ARE)/electrophile response elements in the upstream regulatory regions of NRF2's target genes, thereby activating their transcription (Fig. 6) (Itoh, Chiba et al. 1997). Otsuki et al. named the sequences recognised by NRF2 and MAF protein heterodimer the CNC-sMaf binding element (Otsuki, Suzuki et al. 2016).

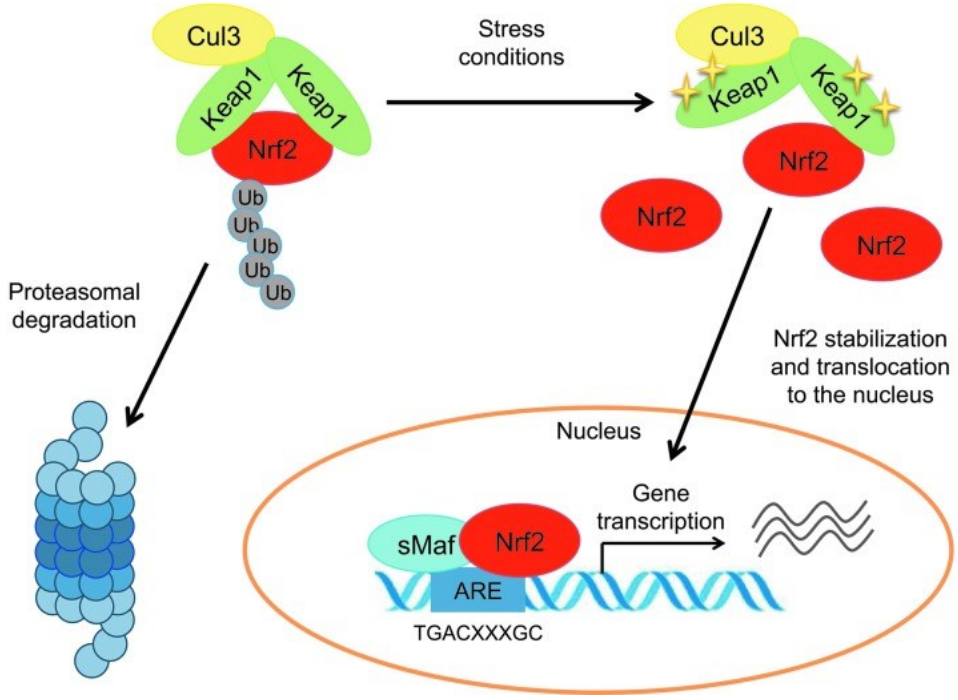

Fig. 6: NRF2 regulation by KEAP1 and its activation under stress conditions

Under physiological conditions, nuclear factor erythroid 2-related factor 2 (NRF2) is bound to Kelch-like ECH-associated protein 1 (KEAP1), while constantly being ubiquitinated by the Cullin (Cul)3 ubiquitin ligase and degraded in the proteasome. However, in response to stress, KEAP1 is inactivated and NRF2 is stabilised and free to translocate to the nucleus, where it forms heterodimers with small Maf proteins (sMaf) and binds the antioxidant response element (ARE), activating transcription of its target genes (Adapted from Tonelli, Chio et al. 2018).

The major group of NRF2-regulated genes are the cytoprotective genes with function in cellular antioxidative responses, metabolic reprogramming, or detoxification (Suzuki, Takahashi, and Yamamoto 2023). Selected cytoprotective genes regulated by NRF2 are shown in Fig. 7. Apart from the cytoprotective genes, NRF2 also regulates genes involved in unfolded protein response, proteostasis, autophagy, mitochondrial biogenesis and physiology, inflammation and immunity, as reviewed by He, Ru and Wen in 2020 (He, Ru et al. 2020). Furthermore, the NRF2 promoter contains an ARE-like sequence, AREL2, which can be bound by NRF2, thereby creating a positive feedback loop that activates its expression (Kwak, Itoh et al. 2002). On the other hand, ARE sequences are found in the promoters of KEAP1, CUL3 and RBX1, contributing to a negative regulatory effect by promoting NRF2 degradation (Lee, Jain et al. 2007, Kaspar and Jaiswal 2010). This dual regulatory mechanism highlights the complex control of NRF2 expression and activity.

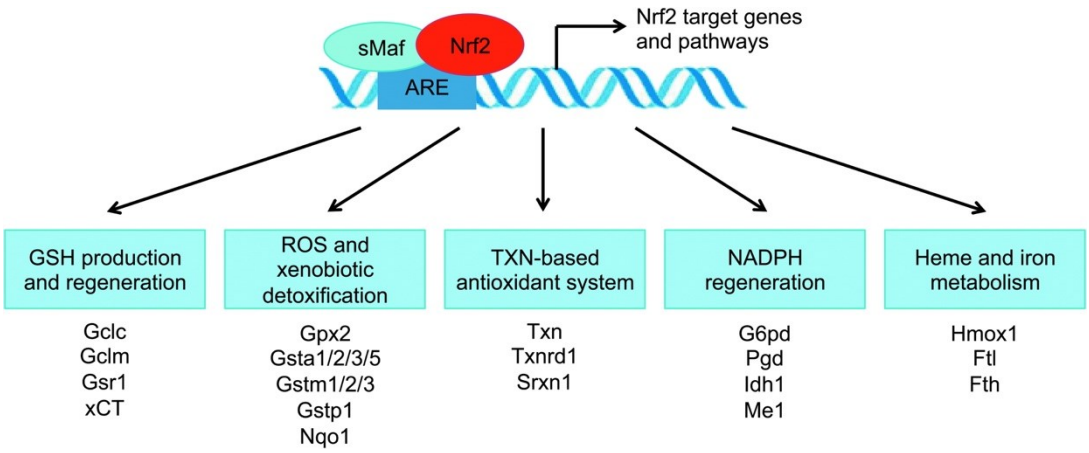

Fig. 7: The NRF2-regulated cytoprotective genes

NRF2 activates cytoprotective genes with roles in glutathione (GSH) production and regeneration, reactive oxidative species (ROS) detoxification, thioredoxin (TXN) antioxidant system, nicotinamide adenine dinucleotide phosphate (NADPH) regeneration or iron metabolism. Gclc – glutamate—cysteine ligase catalytic subunit; Gclm – glutamate—cysteine ligase modifier subunit; Gsr1 – glutathione reductase 1; xCT – cystine/glutamate transporter; Gpx2 – glutathione peroxidase 2; Gst – glutathione S-transferase; Nqo1 – NAD(P)H dehydrogenase [quinone] 1; Txn – thioredoin; Txnrd1 – thioredoxin reductaes 1; Srxn1 – sulfiredoxin 1; G6pd – glucose-6-phosphate 1-dehydrogenase; Pgd – 6-phosphogluconate dehydrogenase; Idh1 – isocitrate dehydrogenase 1; Me1 – malic enzyme 1; Hmox1 – heme oxygenase 1; Ftl – ferritin light chain; Fth – ferritin heavy chain (Adapted from Tonelli, Chio et al. 2018).

2.2.4 The role of protein redox signalling

It has long been known that at highly elevated levels, ROS can cause oxidative damage to macromolecules in cells, such as fatty acids, proteins, and DNA. This pathological state is called oxidative stress. Two forms of oxidative stress based on the concentration of hydrogen peroxide exist. These forms include pathological oxidative distress, marked by impaired redox signalling and susceptibility to oxidative damage, and oxidative eustress, crucial for physiological redox signalling (Sies 2017). At physiological levels, ROS, mainly hydrogen peroxide, oxidatively modify protein cysteines and act as second messengers in various redox signalling pathways (Schreck, Rieber et al. 1991, Sies and Jones 2020).

Thiols of cysteine residues are the key players of redox signalling. Redox signalling is mediated by post-translational modifications of these thiols primarily by hydrogen peroxide (Sies and Jones 2020). Cysteines are amino acids that are present in proteins in low abundance and only 10-20% of all 214,000 cysteine thiols present in proteins are redox-sensitive and therefore susceptible to oxidation (Jones 2008). This susceptibility is influenced

by the ionisation constants (pK_a) of the thiols which depend on the protein environment and their accessibility (Nelson and Creighton 1994, Winterbourn and Metodiewa 1999).

The reaction of hydrogen peroxide with a cysteine thiol group (-SH) initiates the formation of sulfenic acid (-SO), which is susceptible to further modification. Sulfenic acid can form intermolecular or intramolecular disulphide bridges (-SS-) (Sies and Jones 2020). To prevent further oxidative modifications of sulfenic acid, a cysteine residue on GSH forms a disulphide bridge, resulting in S-glutathionylation (Fig. 8). Additionally, other reversible modifications occur (see Fig. 9 for an overview of detectable modifications of cysteine thiols on proteins). These modifications can be reversed by glutathione or thioredoxin systems (Jung and Thomas 1996, Dalle-Donne, Rossi et al. 2007). Yet, in cases when sulfenic acid is not reversed, it can undergo additional oxidation to sulfinic acid or sulfonic acid, both originally considered irreversible modifications. However, the discovery of an enzyme with the ability to reduce sulfinic acid in mammals, named sulfiredoxin, has contradicted this view (Biteau, Labarre et al. 2003). Nevertheless, sulfonic acid, once formed, cannot be reversed (Fig. 8).

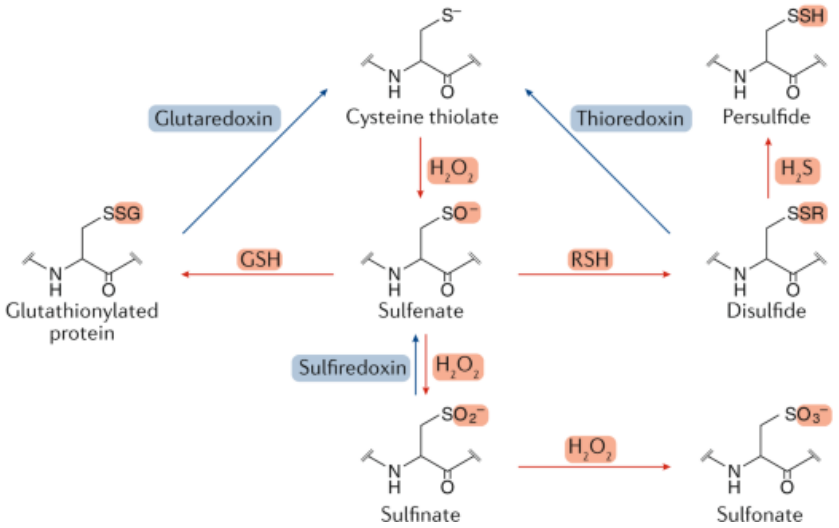

Fig. 8: Overview of posttranslational modifications of cysteine thiols of proteins mediated by ROS, and the enzymes regulating their reverse reaction (Adapted from Sies and Jones 2020).

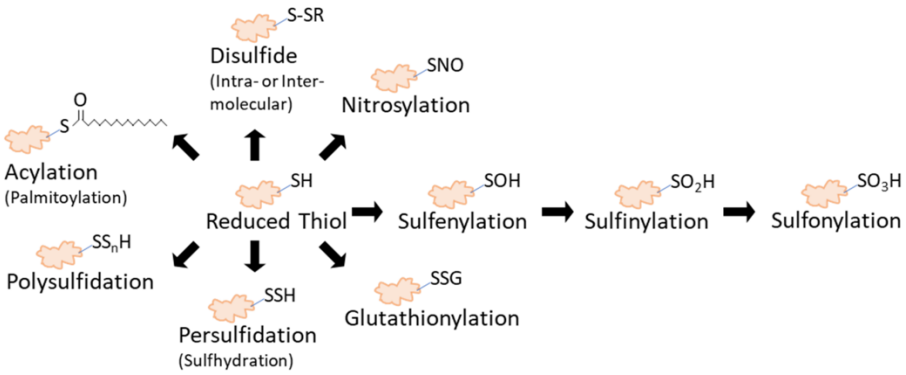

Fig. 9: Cysteine thiol modifications (Adapted from Day, Gaffrey et al. 2021).

These reversible modifications, which can be transferred from one cysteine to another, are also known as "redox switches", forming the base of redox signalling. Oxidation can impact the function, activity, or localisation of proteins (Sies and Jones 2020).

The targets of redox signalling comprise many transcription factors, enzymes, and membrane receptors, each playing a crucial role in cellular processes. One of the examples is nuclear factor-κB (NF-κB), which mediates inflammatory responses. Hydrogen peroxide activates the inhibitor of NF-κB (IκB) kinases through oxidation of their cysteines, which leads to the release and activation of NF-κB (Schreck, Rieber et al. 1991). Conversely, NF-κB can also be negatively regulated by hydrogen peroxide through the direct oxidation of thiols on the DNA-binding domain of the transcription factor. Other redox-regulated transcription factors include forkhead box protein O (FOXO) family regulating cellular homeostasis, and the tumour suppressor protein p53 (Sies and Jones 2020). A model example of a redox-regulated transcription factor crucial for defence against oxidative stress is NRF2. NRF2 is directly activated by oxidative modifications of its inhibitor, highlighting its important role in mediating cellular antioxidant responses. These transcription factors play a critical role in cellular function, and their diminished expression in target genes has been linked to leukemogenesis and disease progression (Trombetti, Cesaro et al. 2021).

2.2.5 Redox metabolism in anti-leukemic therapy

The alterations in redox metabolism observed in cancer cells present potential targets for therapy. Pro-oxidant therapy focusing on increasing intracellular oxidative stress is based on

the presence of a shifted redox balance and elevated ROS levels found in AML cells. This impaired balance makes these cells more susceptible to further increases in oxidative stress (Iacobini, Menichelli et al. 2001, Prieto-Bermejo, Romo-González et al. 2018). For instance, various drugs used in the treatment of MDS and AML have demonstrated the ability to elevate oxidative stress, potentially sensitising leukemic cells to treatment (Fandy, Jiemjit et al. 2014, Montes, Guerra-Librero et al. 2022, Chiou, Hsu et al. 2023). Additionally, targeting the synthesis and metabolism of antioxidants increases oxidative stress, as seen in buthionine sulfoximine targeting GSH, or auranofin aimed at thioredoxin inhibition (Hedley, McCulloch et al. 1998, Karsa, Kosciolek et al. 2021). However, it is recognised that ROS play a crucial role in the initiation and progression of MDS and AML, potentially making leukemic cells dependent on these elevated ROS levels. Therefore, an alternative approach targeting the elimination of ROS, primarily by increasing antioxidative activities, is also under investigation, though without any conducted clinical trials yet (Trombetti, Cesaro et al. 2021).

As mentioned earlier, NRF2 plays a crucial role in the protection of cells against oxidative and electrophilic stress, thereby significantly protecting against carcinogenesis. Therefore, strategies targeting NRF2 have emerged as promising in cancer therapy. One of the NRF2 activators is sulforaphane, functioning through the modification of KEAP1's cysteine thiols and inhibiting KEAP1's binding of NRF2 (Hong, Freeman et al. 2005). In contrast, numerous studies over the past decades have discovered that increased NRF2 activation is prevalent across various types of cancer, including AML, and can promote cancer progression and resistance to therapy. This phenomenon, often termed "the dark side of NRF2", has been documented extensively (Stacy, Ely et al. 2006, Shibata, Kokubu et al. 2008, Wang, Sun et al. 2008, Zhang, Singh et al. 2010, Rushworth, Bowles et al. 2011). Multiple studies describe the role of NRF2 in increasing chemotherapy resistance in AML and MDS (Karathedath, Rajamani et al. 2017, Lin, Ren et al. 2019, Hu, Pan et al. 2022). Thus, inhibiting NRF2, for instance through ML385 or brusatol, presents itself as a promising strategy to increase the efficacy of cancer therapy, particularly in patients with NRF2 overexpression (Wang, Sun et al. 2008). Notably, Ven has been shown to inhibit the nuclear translocation of NRF2 by dissociating NRF2 from Bcl-2, which likely protects NRF2 from KEAP1 binding (Nguyen,

Troadec et al. 2019) Ven-mediated inhibition of NRF2 could therefore be one of the mechanisms lying behind the higher efficacy of combined AZA and Ven therapy. Both activation and inhibition of NRF2 appear to be effective strategies in cancer treatment. Activators have demonstrated efficacy in preventing cancer initiation, while inhibitors could potentially help overcome therapy resistance in more advanced stages of cancer (Milkovic, Zarkovic et al. 2017). In conclusion, achieving the optimal balance between inducing oxidative stress and activating antioxidative pathways is still a subject of research and depends on the specific characteristics of the case. Understanding the specific metabolic and redox dependencies and alterations is key for selecting the most suitable therapeutic strategy.

2.3 IDH mutations and redox reprogramming

MDS patients with IDH1 and IDH2 mutations are an example of a direct link between leukemogenesis, changes in redox metabolism and response to treatment. These mutations are associated with the progression of MDS to s-AML, significantly impact cellular metabolism, including redox homeostasis, and their presence is linked to positive outcomes in response to Ven therapy (Chaturvedi, Araujo Cruz et al. 2013, Chen, Liu et al. 2013, DiNardo, Rausch et al. 2018, Mugoni, Panella et al. 2019, Lou, Shao et al. 2020).

2.3.1 Function of wild-type and mutant IDH1 and IDH2 enzymes

Isocitrate dehydrogenases (IDHs) are enzymes found in three isoforms with distinct subcellular localizations: IDH1 is primarily located in the cytoplasm and peroxisomes, while IDH2 and isocitrate dehydrogenase 3 (IDH3) are situated in the mitochondria, where they participate in the tricarboxylic acid cycle. These enzymes are encoded by five genes in the human genome: *IDH3A*, *IDH3B*, and *IDH3G* encode IDH3, and *IDH1* and *IDH2* encode IDH1 and IDH2, respectively (Testa, Castelli et al. 2020). IDH3 catalyses an irreversible conversion of isocitrate to α-ketoglutarate (α-KG), while reducing nicotinamide adenine dinucleotide (NAD) to reduced NAD (NADH). In contrast, IDH1 and IDH2, each found in separate cellular compartments, catalyse the oxidative decarboxylation of isocitrate to α-KG, while reducing nicotinamide adenine dinucleotide phosphate (NADP) to reduced NADP (NADPH), as well as its reverse reaction (Fig.10). IDH1/2 function as homodimers (Testa, Castelli et al. 2020).

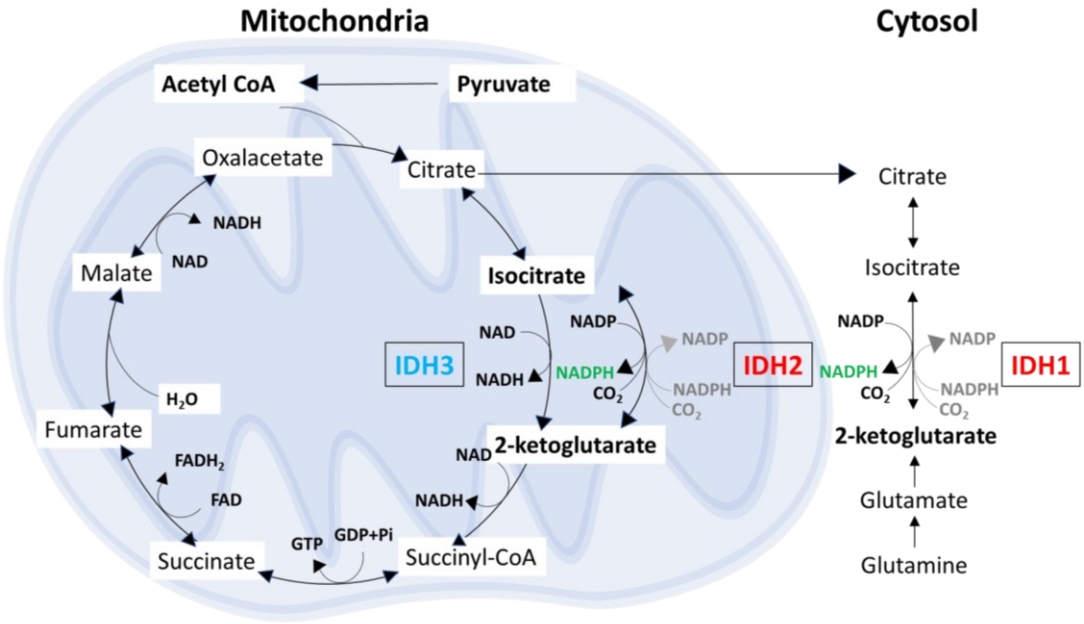

Fig. 10: The physiological function of IDH1, IDH2 and IDH3

IDH – isocitrate dehydrogenase; NADH – nicotinamide adenine dinucleotide; GTP – guanosine triphosphate; GDP – guanosine diphosphate; FAD – flavin adenine dinucleotide (Modified from Al-Khallaf 2017).

IDH1/2 play a pivotal role in cellular processes. However, point mutations in their genes have been identified in multiple cancers, having diverse effects on cellular functions. Mutations in IDH1 and IDH2 were initially discovered in gliomas in 2008 and 2009, respectively (Parsons, Jones et al. 2008, Yan, Parsons et al. 2009). Subsequently, these mutations were also identified in AML shortly after (Mardis, Ding et al. 2009, Ward, Patel et al. 2010). Notably, IDH1/2 mutations are present in approximately 20% of AML and 5% of MDS patients (Medeiros, Fathi et al. 2017). Mutations in *IDH1* and *IDH2* are manifested by specific substitutions of arginine residues in the active site with other amino acids. Specifically, arginine R132 in IDH1 and R140 and R172 in IDH2 are commonly affected. The most frequently observed mutations involve the substitution of arginine R132 in IDH1 by histidine or cysteine ($IDH1^{R13H}$ or $IDH1^{R132C}$, respectively). In IDH2, the most common mutations are the substitution of arginine R140 by glutamine ($IDH2^{R140Q}$) and arginine R172 by lysine ($IDH2^{R172K}$) (Marcucci, Maharry et al. 2010). This alteration in the key amino acid residue reduces the affinity of IDH for its natural substrate, isocitrate, making mutant IDH1/2 (mutIDH1/2) incapable of catalysing the physiological reaction while acquiring a

neomorphic enzymatic activity. MutIDH1/2 gain the ability to convert α-KG to D-2-hydroxyglutarate (D-2-HG), concomitantly oxidising NADPH to NADP (Fig. 11) (Dang, White et al. 2009, Zhao, Lin et al. 2009, Ward, Patel et al. 2010). Somatic mutations in *IDH1* and *IDH2* have been found in various cancer types, with the highest occurrence in gliomas and haematological malignancies.

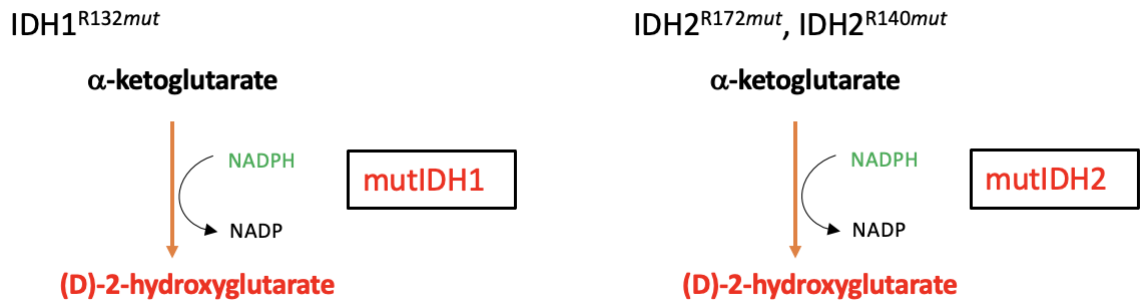

Fig. 11: Neomorphic activity of mutated IDH1 and IDH2.

As previously mentioned, IDH1/2 function in the form of homodimers. Except for one study that identified a case of homozygosity, IDH mutations are mostly heterozygous (Ward, Patel et al. 2010, Singh, Gurav et al. 2017). Unlike mutIDH2, mutIDH1 heavily relies on the activity of wild-type (wt) IDH1 to provide the required α-KG and NADPH in the cytosol. Consequently, they operate in the form of wt/mut IDH1 heterodimers. MutIDH2, on the other hand, does not exhibit this dependency on its wt counterpart, likely due to the supplying of mitochondrial α-KG and NADPH by other enzymes (Ward, Lu et al. 2013).

2.3.2 IDH mutations and redox homeostasis

The leukemogenic effect of IDH1/2 mutations is mainly attributed to the oncometabolite D-2-HG. Due to its structural similarities with α-KG, D-2-HG competitively inhibits α-KG-dependent dioxygenases which leads to epigenetic alterations in cells, potentially suppressing the expression of genes critical for physiological functions (Xu, Yang et al. 2011). Recently, however, there has been increasing evidence for its key role in leukemogenesis in the context of metabolic reprogramming and its effects on redox homeostasis (Chen, Liu et al. 2013, Mugoni, Panella et al. 2019). WtIDH1/2 are important producers of NADPH in both the cytosol and mitochondria. As previously described, NADPH plays a significant role as a reducing agent in cells, essential for the regeneration of antioxidative enzymes of the GSH

and thioredoxin system. Conversely, mutIDH1/2, consume NADPH, with IDH1 mutations specifically associated with reduced NADPH levels (Bleeker, Atai et al. 2010, Shi, Sun et al. 2015, Gelman, Naser et al. 2018, Tang, Fu et al. 2020). This altered balance between NADPH production and consumption disrupts redox homeostasis, prompting cells to shift their metabolism to favour NADPH production (Gelman, Naser et al. 2018). In gliomas, the $IDH1^{R132H}$ mutation has been associated with increased activity of the pentose phosphate pathway, an important producer of NADPH, by approximately 40%. Despite this heightened activity, cells with this mutation still exhibit decreased levels of available NADPH, leading to a deficiency in critical cellular functions such as fatty acids biosynthesis and regeneration of antioxidant enzymes. This deficiency contributes to increased sensitivity to oxidative stress induced by treatments with oxidants such as hydrogen peroxide. Interestingly, the cells prioritised D-2-HG synthesis even at the expanse of NADPH depletion (Gelman, Naser et al. 2018).

$IDH1^{R132H}$ was associated with increased hydrogen peroxide levels and lipid peroxidation indicating oxidative stress. Conversely, inhibition of $IDH1^{R132H}$ led to decreased ROS levels. Silencing of glutamate-cysteine ligase, an enzyme crucial for GSH synthesis, resulted in increased apoptosis specifically in IDH1-mutated cells, indicating the dependency of these cells on GSH metabolism. Moreover, increased NRF2 activity has been observed in response to IDH1 mutation, with NRF2 inhibition through brusatol leading to decreased GSH/GSSG ratio, increased oxidative damage and increased rate of apoptosis. Brusatol-treated cells showed a significant decrease in tumour growth, suggesting a significant role of NRF2 in the protection of IDH-mutated cells. Targeting NRF2 and GSH metabolism has thus been suggested as a potential therapeutic strategy (Tang, Fu et al. 2020). As evidenced by these studies, $IDH1^{R132H}$ mutated glioma cells undergo redox reprogramming to maintain the $NADPH/NADP^+$ balance. This reprogramming involves increased activation of the pentose phosphate pathway and NRF2, coupled with increased dependency on glutamate and GSH metabolism. Despite these adaptations, the reprogramming is insufficient to fully compensate for the NADPH consumption, leading to decreased NADPH levels in these cells. In the context of AML, the $IDH2^{R140Q}$ mutation has been linked to an altered redox state, characterised by increased mitochondrial ROS levels and DNA damage (Mugoni, Panella et

al. 2019). However, most research on the redox reprogramming associated with IDH mutations has been conducted in gliomas, highlighting the need for further investigation in AML.

2.3.3 Role of IDH mutations in the response to anti-leukemic therapy

The impact of IDH mutations on AML prognosis remains unclear. However, they have been shown to influence therapy outcomes due to their altered metabolism. Studies have indicated that patients with IDH1/2 mutations show a more favourable response to combined therapy with AZA and Ven, resulting in higher overall survival and response rates (DiNardo, Rausch et al. 2018, Lou, Shao et al. 2020). As mentioned above, Ven inhibits the activity of NRF2 through the dissociation from Bcl-2, enabling the degradation of NRF2 by KEAP1 (Nguyen, Troadec et al. 2019). These findings along with other studies previously mentioned suggest a potential dependency of IDH mutated cells on NRF2, making them more sensitive to its inhibition through Ven, therefore increasing their sensitivity to AZA and Ven therapy. However, the role of IDH1/2 mutations in the development of resistance is still a subject of intensive research. To fully understand the redox metabolic adaptations observed in IDH1/2 mutant AML patients, further research is needed. Elucidating the redox reprogramming strategies that are key for MDS/AML pathogenesis represents a significant step towards a more effective therapy. By clarifying the molecular mechanisms underlying these metabolic alterations, we can not only improve our understanding of cancer biology but also identify novel therapeutic targets and strategies to enhance patient outcomes and quality of life.

3 Hypothesis and aims of thesis

We hypothesise that activation of NRF2 and enhanced cellular redox state help confer resistance of leukemic cells to selected anti-leukemic therapy.

To answer this question, we set ourselves the following aims:

1. To characterise the role of redox homeostasis in the response of leukemic cells to therapy
    a. To characterise the impact of selected therapy on redox homeostasis
    b. To characterise the redox state in OCI-M2 cells sensitive and resistant to therapy
2. To characterise the role of the KEAP1-NRF2 pathway activity in the response of leukemic cells to therapy
    a. To characterise the impact of selected therapy on the KEAP1-NRF2 pathway
    b. To measure the activity of the KEAP1-NRF2 pathway in OCI-M2 cells sensitive and resistant to therapy
3. To identify protein targets of changes in redox homeostasis and activity of NRF2 in the context of therapy resistance and treatment
4. To analyse the impact of IDH1/2 mutations on the redox homeostasis of leukemic cells
    a. To prepare and validate a biological model expressing IDH1 WT, IDH1 R132H, IDH2 WT, IDH2 R172K enzymes in OCI-M2 cells
    b. To determine the impact of IDH1 R132H and IDH2 R172K mutations on the redox state of OCI-M2 cells

4 Material and methods

4.1 Material

4.1.1 Equipment

Agar plate
Analytical scale ALJ 220-4 (KERN)
Automated cell imaging system Incucyte® SX1 (Sartorius)
Automatic pipettes BioPette autoclavable (Labnet)
BD FACS Aria Fusion (BD Bioscience)
BioPette Plus Multichannel Pipette (Gilson)
Centrifugal OrTubes 15/50 ml (Orange Scientific)
Centrifuge 5415R (Eppendorf)
Centrifuge 5810R (Eppendorf)
ChemiDocTM MP Imaging system (Bio-Rad)
Counting chamber, Bürker-Türk (Karl Hecht)
CytoFLEX LX Flow Cytometer (Beckman Coulter)
Cytometer BD LSRFortessa (BD Bioscience)
Dionex liquid chromatography (Thermo Fisher Scientific)
Elektrophoretic system PowerPac Basic Power Supply + Mini-PROTEAN Tetra Cell (BioRad)
Flowtubes for Flow Cytometry Instruments (VWR)
Falcon® 40µm Cell Strainer, Sterile, Individually Packaged, 50/Case 4x (VWR)
FastPette™ Pro Pipet Controller (Labnet)
Filtered pipette tips (VWR)
Immun-Blot® Low Fluorescence PVDF Membrane (Bio-Rad)
Invitrogen™ Neon™ Transfection System (Invitrogen)
4–15% Mini-PROTEAN® TGX™ Precast Protein Gels (Bio-Rad)
MR-1Mini-Rocker Shaker (BioSan)
Multifunctional modular reader Infinite M200 PRO (Tecan)
MyTemp™ mini digital incubator (Merck)
NextSeq 500 (Illumina)
Orbitrap Fusion Tribrid MS instrument (Thermo Fisher Scientific)
PCR 0,2 ml Thin Wall PCR 8-Strip Tubes (BioCentrix)
Pipette, serological (VWR)
Prism Mini Centrifuge (Sigma-Aldrich)
Protein LoBind Tube 0,5ml/1,5ml/2ml (Eppendorf)
Safe-lock tubes 1,5 ml (Eppendorf)
Shaking incubator Bench Top (N-Biotek)
Spektrophotometer NanoDrop ND-1000 (Thermo Fisher Science)
T100TM Thermal Cycler (Bio-Rad)
Termoblok AccuBlock Digital Dry Bath (Labnet)
Tissue Culture Plates 96 wells-flat (VWR)
Tissue Culture Plates 96 wells-flat (VWR)
Tissue Culture Plates 96 wells-U (VWR)

TPP® tissue culture 96 well plate (Merck)
Trans-Blot Turbo Transfer Systém (Bio-Rad)
Transiluminator (P-LAB)
Ultra-micro-spin columns (Thermo Fisher Scientific)
Vertical electrophoresis (Bio-Rad)
Vortex WIZARD IR Infrared Vortex Mixer (Velp Scientifica)
Water bath NB 20 (NUVE)

4.1.2 Software:

DAVID
FlowJo software (BD Life Sciences, Becton, Dickinson & Company)
GraphPad Prism
i-controlTM Microplate Reader Software from Tecan
ImageJ
Image Lab
Incucyte® Software (v2020C) for Live-Cell Analysis (Sartorius)
Proteome Discoverer (Software Version 2.5) (Thermo Fisher Scientific)
Perseus (Software Version 2.0.11)

4.1.3 Facilities

BIOCEV OMICS Proteomics and Metabolomics
BIOCEV OMICS Genomics Next Generation Sequencing
BIOCEV Imaging Methods Core Facility

4.1.4 List of chemicals

10x cut smart buffer (New England Biolabs)
1M Triethylammonium bicarbonate buffer (Thermo Fisher Scientific)
4–15% Mini-PROTEAN® TGX™ Precast Protein Gels (Bio-Rad)
4x Laemmli sample buffer (Bio-Rad)
5x Q5 reaction buffer (BioTech)
Acetone (Fisher Scientific)
Acetonitrile OPTIMA LC-MS Grade (Thermo Fisher Scientific)
Agarose (VWR)
Albumin, from bovine serum (BSA) (Sigma Aldrich)
Amonium bicarbonate, 500g (Sigma Aldrich)
Calcium chloride 1M sterile (CaCl2) (Amresco)
CELL PROLIFERATION REAGENT WST-1, sufficient for ≤2,500 tests (Sigma Aldrich)
ddH2O
Deoxycholate (Sigma Aldrich)
Dimethyl sulfoxide 99.9% (Sigma Aldrich)
Dithiolthreitol (DTT) (Sigma Aldrich)

dNTP Mix 10mM (Biogen)
EDTA disodium salt dehydrate (VWR)
EGTA, Ethylene glycol-bis(2-aminoethylether)-N,N,N′,N′-tetraacetic acid (Sigma Aldrich)
Ethanol absolute (Penta)
Ethidium bromide (Invitrogen)
Fetal Bovine Serum (Biosera)
Glycerol (Sigma Aldrich)
Halt™ Protease Inhibitor Cocktail (Thermo Fisher Scientific)
IMDM (Thermo Fisher Scientific)
Inhibitory fosfatáz (PhosSTOP; Roche) a proteáz (cOmplete ULTRA; Roche)
Iodoacetamide (IAM) (Sigma Aldrich)
Liquid Nitrogen
Loading dye elfo (Sigma Aldrich)
Magnesium chloride (MgCl2) (Sigma Aldrich)
Methanol OPTIMA LC-MS (Thermo Fisher Scientific)
Milk powder (Sigma Aldrich)
Na_3VO_4 (Sigma Aldrich)
NP-40 Detergent (10%) (Sigma Aldrich)
Nuclease-free Water (Sigma Aldrich)
Phosphate Buffered Saline (Cat. No. 20012050)
PMSF (1 mM) (Sigma Aldrich)
Precision Plus ProteinTM Dual Color Standards (Bio-Rad)
Q5® High-Fidelity DNA Polymerase, 100 units (Biotech)
RapiGest SF surfactant (Waters)
S.O.C. recovery medium (Invitrogen)
SDS (Sodium Dodecyl Sulfate) (Amresco)
Sep-Pak C18 1 cc Vac Cartridge, 50 mg Sorbent per Cartridge, 55 - 105 µm, 100/pk (Waters)
Sequencing Grade Modified Trypsin,5x20 ug (Eastport)
Sodium chloride (NaCl) (VWR)
Sodium deoxy cholate (SDC)
Sodium fluoride (NaF)
Sterile ddH_2O
SuperSignal™ West Atto Ultimate Sensitivity Substrate (Thermo Fisher Scientific)
Thermo Scientific SuperSignal West Femto Maximum Sensitivity Substrate (Fisher Scientific)
Thermo Scientific™ GeneRuler 1 kb Plus DNA Ladder (Fisher Scientific)
TLCK (Sigma Aldrich)
TPCK (Sigma Aldrich)
Trichluoroacetic acid (TCA) (Sigma Aldrich)
Triethylammonium bicarbonate buffer (TEAB) (Thermo Fisher Scientific, 90114)
Trifluoroacetic acid (TFA) (Honeywell Fluka)
Tris-HCl, pH 7.4 (Sigma Aldrich)
Tris(2-carboxyethyl)phosphine hydrochloride (TCEP) (Sigma Aldrich, C4706-10G)
Triton X-100 (Sigma Aldrich)
Trypan Blue solution (0,4% liquid) (Sigma Aldrich)
Trypsin (0,25%) EDTA 1x (Sigma Aldrich)
Tween 20 reagent (VWR)

Water Optima TM (LC/MS grade) (Fisher Chemical)

4.1.4.1 Drugs and inhibitors

5-azacytidine (Vidaza) (Cell Gene)
Bafilomycin (Sigma Aldrich)
Bortezomib (Velcade®) (Janssen-Cilag International N.V., Beerse)
Chloroquine diphosphate salt (Sigma Aldrich)
ML385 (Merck)
Pevonedistat (MLN4924) (Takeda Pharmaceuticals)

4.1.4.2 Antibiotics

Ampicilin (Sigma Aldrich)
Doxycycline (Sigma Aldrich)
Puromycin (Serva)
Spectinomycin (Sigma Aldrich)
Penicillin/Streptomycin Solution (BioTech)

4.1.4.3 Enzymes

AscI endonuclease (Thermo Fisher Scientific)
Bensonase (Thermo Fisher Scientific)
Trypsin/P (Promega)

4.1.4.4 Commercial kits

Pierce™ BCA Protein Assay Kit (Thermo Fisher Scientific)
SepPak columns (Waters)
Genaid columns (Genaid)
Miniprep kit (Sigma Aldrich)
NEON™ transfection system (Thermo Fisher Scientific)
Iodoacetyl Tandem Mass Tag (iodoTMT) sixplex™ Isobaric Label Reagents and Kits (Thermo Fisher Scientific)
NEBuilder® HiFi DNA Assembly Master Mix (New England Biolabs)

4.1.5 Flow cytometry probes

Probe	**Manufacturer**	**Catalogue number**	**Fluorochrome**
7-Aminoactinomycin D	Invitrogen	A1310	PE-Texas Red
CellROX™ Orange Reagent	Invitrogen	C10443	PE
CM-H_2DCFDA	Invitrogen	C6827	FITC
Propidium iodide	Invitrogen	P1304MP	PE-Texas Red
ThiolTracker™ Violet	Invitrogen	T10096	AmCyan

4.1.6 Primary and secondary antibodies for Western Blot immunodetection

Primary antibody	Type	Manufacturer	Catalogue number	Dilution
Anti-Actin	Goat polyclonal	Santa Cruz Biotechnology	Sc-1616	1:1000
Anti-FLAG	Rabbit polyclonal	Cell Signaling Technology	2368S	1:1000
Anti-GAPDH	Rabbit polyclonal	Sigma Aldrich	15810	1: 2500
Anti-Histone H3	Rabbit polyclonal	Abcam	Ab1791	1:80000
Anti-LC3	Mouse polyclonal	Santa Cruz	376404	1:1000
Anti-KEAP1	Rabbit polyclonal	Sigma Aldrich	HPA005558	1:500
Anti-NRF2	Rabbit monoclonal	Cell Signaling Technology	12721T	1:1000
Anti-NQO1	Rabbit polyclonal		HDA007308	1:1000
Anti-SQSTM1	Rabbit polyclonal	Cell Signaling Technology	5114	1:1000

Secondary antibody	Manufacturer	Catalogue number	Dilution
Anti-Rabbit	Jackson Immuno Research	7074	1:10000
Anti-Goat	Thermo Fisher Scientific	13-4113-85	1:10000

4.1.7 Plasmids

Plasmids with IDH genes purchased from Addgene:

plasmid	gene	Manufacturer	Catalogue number	Resistance
pDONR223	IDH1 WT	Addgene	81921	Spectinomycin
pDONR223	IDH1 R132H	Addgene	81686	Spectinomycin
pDONR223	IDH2 WT	Addgene	81800	Spectinomycin
pDONR223	IDH2 R172K	Addgene	81432	Spectinomycin

plasmid	Manufacturer
Transponase SB100	AddGene
pSB Tet transposon vector	Thermo Fisher Scientific

4.1.8 Primers

PCR primers

IDH1 forward	tcgaaaagggtggaggcgggcgcgcctccaaaaaaatcagtggc
IDH1 reverse	agtagctccgcttcccgcggcgcgcccaagtttggcctgagctag
IDH2 forward	tcgaaaagggtggaggcgggcgcgccgccggctacctgcgggtc
IDH2 reverse	agtagctccgcttcccgcggcgcgcccctgcctgcccagggctctg

Sequencing primers

IDH1 forward 1	accaaatggcaccatacg
IDH1 forward 2	gcccaagctatgaaatcagag
IDH2 forward 1	cagaagtacagtgtggctgtc
IDH2 forward 2	ttgacaagcactataagaccgac

4.1.9 Cell lines

OCI-M2 cell line
E. cloni competent cells

4.1.10 Media and solutions

Complete IMDM medium

IMDM
20% FBS
1% Penicillin/Streptomycin solution

Freezing IMDM medium

IMDM
20% FBS
10% DMSO

FACS buffer

PBS
0.5% BSA
0.4% 0.5 M EDTA

NaCl lysis buffer

150 mM NaCl
50 mM Tris (pH 7.5)
0.4% Triton X-100
2 mM CaCl2

2 mM MgCl2
1 mM EDTA
0.1% DTT
0.1% TLCK
0.1% TPCK
0.1% PMSF
0.1% Bensonase
1% Na_3VO_4

Hypotonic buffer solution

20 mM Tris-HCl (pH 7.52)
10 mM NaCl
3 mM $MgCl_2$

Cell Extraction Buffer

10 mM Tris, pH 7.52
2 mM Na_3VO_4
100 mM NaCl
1% Triton X-100
1 mM EDTA
10% glycerol
1 mM EGTA
0.1% SDS
1 mM NaF
0.5% sodium deoxycholate
1 mM PMSF (added right before use)
1% Protease Inhibitor Cocktail (added right before use)

Lysis/blocking buffer

3% SDC
200 mM TEAB
1 mM EDTA

Digestion buffer

0.1% Rapigest
50 mM ammonium bicarbonate

Probe mix

PBS
4 µM CM-H2DCFDA
10 µM ThiolTracker violet
5 µM CellROX orange
1:1000 1 µg/ml PI/1 µM 7-AAD

Solution for primary antibodies
PBS
3% BSA
5% NaN_3
Primary antibody according to dilution

4.2 Methods

4.2.1 Cell handling

4.2.1.1 Cultivation of OCI-M2 cells

We worked with OCI-M2 cell line, that was established from the leukemic cells of a 56-year-old patient with erythroleukemia (AML-M6), representing the end stage of a previously identified myelodysplastic syndrome.

OCI-M2 cells were cultured in flasks containing complete IMDM medium (IMDM supplemented with 20% [v/v] fetal bovine serum (FBS) and 1% [v/v] antibiotic mix (penicillin and streptomycin) and maintained in an incubator with 5% carbon dioxide (CO_2) and a temperature set at 37 °C. The medium was additionally supplemented with 2 µl/ml of puromycin for transfected cells carrying the pSBtet vector, which includes IDH genes and genes conferring puromycin resistance. Cells were passaged three times per week and were maintained at an optimal confluence of 0.5-1.5 x 10^6 cells/ml.

4.2.1.2 Thawing of cells

OCI-M2 cells were cryopreserved in a freezing IMDM solution consisting of 70% [v/v] IMDM medium, 20% [v/v] FBS, and 10% [v/v] dimethyl sulfoxide (DMSO) and stored at -80 °C. During thawing, the tube containing the cells was immersed in a water bath set at 37 °C for 1 minute. Subsequently, the cells were transferred to a 15 ml Falcon tube containing 10 ml of phosphate-buffered saline (PBS) and centrifuged at 350x g for 5 minutes at 24 °C. The resulting cell pellet was then resuspended in 6 ml of complete IMDM medium and transferred to a flask, which was then placed in an incubator set at 37 °C with 5% carbon dioxide (CO_2).

4.2.1.3 Cell counting

For cell counting, a Bürker chamber was used. 10 µl of the cells mixed at a 1:1 ratio with trypan blue to stain dead cells were pipetted into the chamber and the cells in three squares were counted. The concentration of cells (number of cells per ml) was calculated by multiplying the average calculated number of cells per square by 20,000.

4.2.1.4 Cell treatment

For treatment, the required number of cells for the experiment was transferred either into a 6-well plate (for cell quantities ranging from 400,000 to 2,000,000) or into a flask for larger amounts. The treating agent was then added at the desired concentration, and the cells were subsequently incubated in the incubator maintained at 37 °C with 5% CO_2 for the designated treatment duration.

4.2.1.5 Development of resistant cell clones

The clones of OCI-M2 cells resistant to 5-azacytidine (AZA-R) were developed in our laboratory by treating cells sensitive to 5-azacytidine (AZA-S) with an increasing concentration of 5-azacytidine and by a selection of the surviving clones (Minařík, Pimková et al. 2022). Clones resistant to 5-azacytidine and partially (PEVO-PR) and completely (PEVO-R) resistant to pevonedistat were then developed by treating AZA-R clone with an increasing concentration of pevonedistat and by subsequent selection of the surviving clones.

4.2.2 Flow cytometry

Flow cytometry is a technique used to analyse and quantify the characteristics of individual cells within a heterogeneous population. By passing cells through a laser beam, it measures various parameters such as size, granularity, and fluorescence intensity. Fluorogenic probes can be used to detect cellular components or processes. They work by emitting fluorescence after binding its substrate or after undergoing a specific reaction.

For the flow cytometry experiments detecting the cellular redox state, we utilised following probes:

300,000 cells per replicate was used. In the initial experiment, we prepared unstained controls, single stained control samples (stained with only one fluorogenic probe), and fluorescence minus one (FMO) samples (stained with all probes except one). Cells were collected into 10 ml of pre-cooled PBS in 15 ml Falcon tubes and washed twice by centrifugation (350x g, 5 min, 4 °C) with subsequent discarding of the supernatant, all while maintaining them on ice. The pellet was then resuspended in 200 µl of probe mix or in a single probe solution for the single stained control. Probes were appropriately diluted with PBS according to recommended concentrations. The cells in the probe cocktail were incubated for 30 minutes in a water bath at 37 °C. Following incubation, the cells were washed with 10 ml of pre-cooled PBS and centrifuged (350x g, 5 min, 4 °C). The resulting pellet was resuspended in 200 µl of PBS and transferred to a FACS tube. Propidium iodide (PI) or 7-aminoactinomycin D (7-AAD), when used for viability detection, were added immediately before analysis. Subsequently, the samples were analysed using a BD LSRFortessa flow cytometer with compensations for the signals of the probes pre-set for the experiment. The acquired data were then analysed using FlowJo software, with visual graphs and statistical analysis performed using GraphPad software.

4.2.3 Fluorescence-activated cell sorting

Fluorescence-activated cell sorting (FACS) is a technique combining flow cytometry with cell sorting, enabling a precise separation of cells based on their fluorescence characteristics.

5,000,000 cells were incubated in a complete IMDM medium supplemented with 0.6 µg/ml of Doxycycline (Dox) for 24 hours in an incubator set at 37 °C and 5% CO_2. Following the treatment, the cells were transferred to 15 ml Falcon tubes and washed with 10 ml of PBS through centrifugation (350x g, 5 min, 4 °C), with subsequent removal of the supernatant. The resulting pellet was resuspended in 1 ml of FACS buffer and transferred into FACS tubes. All these procedures were conducted within a laminar flow hood to minimize the risk of cell contamination. Subsequently, the dsRED-positive cells were sorted into 15 ml Falcon Tubes containing 1 ml of PBS using a BD FACS Aria Fusion sorting machine.

4.2.4 Nuclear and cytosolic fractionation

To perform nuclear fractionation, 5,000,000 cells were required per condition. The cells were collected into 15 ml Falcon tubes and washed with pre-cooled PBS by centrifugation (350x g, 5 min, 4 °C). The cells were maintained on ice during subsequent steps. They were then transferred into microcentrifuge tubes and centrifuged again (350x g, 5 min, 4 °C). After removing the supernatant, the pellet was gently resuspended by pipetting in 250 µl of pre-prepared hypotonic buffer, as described in the Materials chapter. The mixture was incubated on ice for 15 minutes. Following the incubation, 12.5 µl of detergent (10% NP-40) was added and vortexed for 10 seconds at the highest setting. The homogenate was then centrifuged for 10 minutes at 3,000 rpm at 4 °C. The resulting supernatant, containing the cytoplasmic fraction, was transferred into a low-protein binding (LPB) microcentrifuge tube. The pellet obtained after centrifugation represented the nuclear fraction. The nuclear pellet was resuspended in 25 µl of complete Cell Extraction Buffer, prepared in advance as described in the Materials chapter, and incubated on ice with vortexing at 10-minute intervals for 30 minutes. Subsequently, the sample was sonicated for 5 minutes and 0.05 µl of bensonase (1:1000) was added. Next, the samples were centrifuged for 30 minutes at 14,000x g at 4 °C. The resulting supernatant was carefully transferred to a clean microcentrifuge tube, representing the nuclear fraction.

4.2.5 Cell lysis using NaCl lysis buffer

To perform cell lysis, $1x10^6$ cells were collected per condition. The cells were washed with 10 ml of pre-cooled PBS by centrifugation (350x g, 5 min, 4 °C), and the supernatant was discarded. The pellet was then resuspended in approximately 50 µl of NaCl lysis buffer containing protease inhibitors, as described in the Materials chapter, and incubated on ice for 30 minutes. Following the incubation, 50 µl of 50 mM Tris (pH 8.8)/2% SDS solution in water was added in a 1:1 ratio (50 µl). The sample was then incubated for 10 minutes at 95 °C. Subsequently, the sample was centrifuged for 10 minutes at maximal speed, at 4 °C, to remove debris. The supernatant containing the lysed cells was transferred to a new microcentrifuge tube.

4.2.6 Bicinchoninic Acid assay

The Bicinchoninic Acid (BCA) assay is a method used for quantifying total protein concentration in a sample. It relies on the reduction of Cu^{2+} ions to Cu^{1+} ions by proteins in an alkaline environment, forming a purple-coloured complex that can be quantified spectrophotometrically.

The samples were diluted fourfold in ddH_2O (6 µl of the sample with 18 µl of ddH_2O), and then 10 µl of the diluted sample was pipetted in duplicates into a 96-well flat bottom plate, alongside 10 µl of pre-prepared bovine serum albumin standards at concentrations 0-2 mg/ml. Subsequently, BCA detection reagent was prepared by mixing solution A and B at a ratio of 50:1, and 190 µl of the BCA detection reagent was pipetted to the standards and samples. The plate was incubated in an incubator for 30 minutes at 37 °C. The absorbance was read using a TECAN spectrophotometer, at 560 nm at 25 °C, and the protein concentrations were calculated based on a calibration curve of the standards using linear regression.

4.2.7 SDS-page electrophoresis and Western blot

SDS-PAGE (Sodium Dodecyl Sulphate Polyacrylamide Gel Electrophoresis) is a technique used to separate proteins based on their molecular weight. Proteins are denatured and coated with SDS, then electrophoresed through a polyacrylamide gel. Western blot is a method used to transfer separated proteins to a polyvinylidene difluoride (PVDF) membranes. Transferred proteins are immunodetected with specific antibodies, allowing their visualisation and quantification.

4.2.7.1 SDS-PAGE electrophoresis

The specific amount of each sample, containing 10-20 µg of proteins and consistent across all samples, was pipetted into a PCR microtube along with a 1:10 [v/v] ratio of DTT (Dithiothreitol) and a 1:4 [v/v] ratio of 4x Laemmli sample buffer (Bio-Rad). DdH_2O was added to bring the total volume to 50 µl. Subsequently, the samples were denatured in a

thermal cycler at 95 °C (with the lid at 105 °C) for 5 minutes. Next, 50 µl of the denatured samples were loaded into a pre-purchased 4-15% SDS-PAGE gel assembled into a cassette, with 5 µl of Precision Plus Protein Dual Color Standard (BioRad) added. The gel was run at 65 V for 10 minutes, followed by an increase to 130 V for approximately 1 hour, until the samples had migrated to the bottom of the gel.

4.2.7.2 Western blot

The cassette was then disassembled, and the gel was transferred to a PVDF membrane via a Western blot Trans-Blot Turbo Transfer System (Bio-Rad) at 25 V, 1 A for 30 minutes. Subsequently, the membrane was washed in PBS with 0.1% [v/v] Tween for 5 minutes on a shaker at room temperature, followed by a 1-hour incubation in PBS/0.1% [v/v] Tween/5% [w/v] milk on a shaker at room temperature. The membrane was then washed again three times for 8 minutes, and then cut at specific protein sizes according to the marker and incubated with the desired primary antibodies overnight at 4 °C on a shaker. The following day, the membrane was washed 3 times in PBS/0.1% [v/v] Tween for 10 minutes each, and then incubated for 1 hour in secondary antibody in PBS/0.1% [v/v] Tween/3% [w/v] milk. After another 3 washes for 10 minutes each on a shaker, the membrane was incubated with chemiluminescent substrate (Thermo Scientific SuperSignal West Femto Maximum Sensitivity Substrate) pre-mixed in a 1:1 ratio and incubated for 1 minute and imaged using Illumina imaging system. The bands were quantified using Image Lab software, and graphs were generated using GraphPad.

4.2.8 WST proliferation assay

WST (Water-Soluble Tetrazolium) is a colorimetric assay reagent employed to detect cell viability and proliferation. Upon reduction by metabolically active cells, WST forms a soluble formazan product, the intensity of which is directly proportional to the number of viable cells, enabling quantitative measurement of cell viability.

The analysis was conducted in 96-well flat-bottom plates, with 1,000,000 cells per plate collected in PBS and centrifuged (350x g, 5 min, 24 °C). After discarding the supernatant,

the pellet was resuspended in 5 ml of pre-warmed complete IMDM medium at 37 °C. According to the table, PBS was pipetted into the side wells, while 50 µl of complete IMDM medium containing the tested drug/inhibitor was pipetted into the appropriate wells. Additionally, 100 µl of complete IMDM medium was pipetted into the blank wells. Subsequently, 10,000 cells/50 µl of cells were pipetted into the corresponding wells, and the plate was incubated in the incubator at 37 °C for 72 hours. After the incubation, 10 µl of WST-1 agent was pipetted into all wells (except the sides containing PBS) and incubated for 1 hour at 37 °C. Finally, the plate was analysed using a TECAN spectrophotometer at 430 nm at 37 °C, and the data was visualised in GraphPad, where statistical analysis was performed.

4.2.9 Incucyte

Incucyte is a live-cell analysis system that enables real-time monitoring of cellular proliferation directly inside a cell culture incubator. By capturing continuous images of cells over time, Incucyte allows the precise measurement of cell proliferation.

For Incucyte analysis, TPP 96-well plates were used. The initial preparation procedure was identical with that of the WST assay, with the exception that no blank was required for Incucyte analysis. After pipetting the cells into the plate along with the medium containing the tested agent, the plate was inserted into the Incucyte machine, and analysis was conducted for the desired duration (3-7 days) with measurements taken every 4 hours. Subsequently, the data were analysed using the Incucyte software and GraphPad for visualization, including statistical analysis.

4.2.10 Redox proteomics analysis using mass spectrometry

Redox proteomics is a specialised type of proteomic analysis that allows the studying of redox regulation of proteins. It involves a comprehensive analysis of oxidative post-translational modifications of proteins' cysteines using a liquid chromatography separation with mass spectrometry-based identification. Quantitative approach with isobaric tagging using iodoTMT allows site-specific identification and quantification of thiols redox state.

4.2.10.1 Sample preparation

We analysed three conditions: cells resistant to 5-azacytidine (AZA-R), AZA-R cells treated with 0.5 µM pevonedistat for 24 hours, and cells resistant to both 5-azacytidine and pevonedistat (PEVO-R). Three replicates of 400'000 cells (app. 20 µg of protein) per condition (after treatment or without treatment) were transferred to a 15 ml Falcon tube and washed with 10 ml PBS through centrifugation (350x g, 5 minutes, 4 °C). Cell were transferred into lLPB microcentrifuge tubes and centrifuged again under the same conditions. In a new LPB microcentrifuge tube, 150 µl of lysis/blocking buffer (consisting of 3% [v/w] SDC/200mM TEAB/1mM EDTA) was prepared, and 2 µl of appropriate iodoTMT label resuspended in 10 µl of methanol (4 mM iodoTMT) was added to prevent oxidation of free thiols during sample preparation. The cell pellet was resuspended in 50 µl of the lysis/blocking buffer mixture and sonicated for 15 minutes. Subsequently, 4 µl of the same iodoTMT label was added to further block free thiols, and the sample was incubated at 37 °C on a shaker in darkness for 2 hours. The samples were then precipitated with 200 µl of ice-cold acetone (1:4 [v/v]) overnight at -20 °C to remove the excess of iodoTMT. Following this, the samples were centrifuged at 15,000x g, 4 °C for 10 minutes. The resulting pellet was washed with 100 µl of cold acetone by centrifugation at 15,000x g, 4 °C for 5 minutes, with the supernatant discarded. This washing step was repeated, and the microcentrifuge tubes were left uncapped for 20-30 minutes until the acetone evaporated. The pellet was dissolved in 50 µl of loading buffer with 5 mM TCEP and incubated for 1 hour at 50 °C to reduce reversibly oxidised thiols. Next, 5 µl of the second iodoTMT was added to the sample and incubated at 37 °C for 2 hours on a shaker in darkness to block newly generated free thiols. The samples were precipitated again with 200 µl of ice-cold acetone (1:4) overnight at -20 °C. Subsequent centrifugation and two washing steps were conducted, followed by evaporation of the acetone as already described. The samples were then resuspended in digestion buffer (45 µl of 0.1% Rapigest in 50 mM ammonium bicarbonate) and let for 10 minutes at room temperature to allow complete resuspension of the pellet. After centrifugation at 15,000x g at 24 °C to remove debris, the supernatant from each condition (AZA-R, AZA-R/Pevo, PEVO-R) was combined into an LPB microcentrifuge tube for each replicate, resulting in three replicates, each containing the three analysed conditions. 0.26 µg/µl of Trypsin was added (1:50 [w/w] enzyme:protein) to the samples and incubated

overnight at 37 °C. The following day, 2 µl of 50% TFA was added to the samples to precipitate Rapigest for 45 minutes at 37 °C, followed by centrifugation at 17,000x g for 20 minutes at 24 °C. The supernatant was collected and cleaned with SepPak columns according to provided protocol. The samples were then transported to the Proteomics facility in Biocev, where they were dried in a vacuum concentrator and measured.

4.2.10.2 Mass spectrometry analysis

The analyses were performed using an Orbitrap Fusion Tribrid MS instrument (Thermo Scientific) equipped with a Dionex liquid chromatography system, employing a 120-minute linear gradient separation followed by an MS^2 method. Mass spectrometry raw data were analyzed with Proteome Discoverer software (version 2.5). For protein identification, an FDR of 1% was set, with methionine oxidation and N-terminal acetylation designated as dynamic modifications. Trypsin/P was selected as the enzyme with a specific digestion mode, allowing for two missed cleavages. The dataset underwent filtration for contaminants, proteins identified by site, and non-cysteine peptides. Hits lacking quantitative information were excluded. The minimum count for protein oxidation quantification was set to two. Reporter ion intensities from the iodoTMT labels were $\log_2$ transformed and then normalised by adjusting the median of each channel to the mean of either free (SH) or oxidised (Sox) thiols. Normalised $\log_2$ data were unlogged, and the oxidation level (% oxidation) was calculated as $\frac{\mathrm{Sox}}{\mathrm{SH}+\mathrm{Sox}} * 100$. Following confirmation of the normal distribution of the data, p-values for each peptide were calculated using a two-sided t-test in Perseus software (version 2.0.11). Changes in oxidation level exceeding 10% with a p-value < 0.05 were considered differential. For data visualization, Perseus and GraphPad Prism were utilised, while David software was employed for Gene Ontology analysis of biological processes.

4.2.11 Cloning

To generate OCI-M2 cells with overexpression of IDH proteins (including IDH1 WT, IDH1 R132H, IDH2 WT, and IDH2 R172K variants), we cloned the *IDH* gene into a Sleeping Beauty (SB) transposon system (Geurts, Yang et al. 2003). This vector system encompassed genes conferring resistance to ampicillin and puromycin, along with a Tetracycline-inducible promoter. This promoter controlled the expression of genes encoding a dsRED fluorescent

protein, the desired IDH protein variants, and additional sequences encoding 3xFLAG and Twin-Strep-tag peptides.

4.2.11.1 Plasmid DNA isolation

Pre-purchased plasmids in the form of bacterial stabs were spread onto agar plates containing 50 µg/ml Spectinomycin and allowed to grow for 24 hours at room temperature. Colonies were then selected and grown in 6 ml of media supplemented with 50 µg/ml Spectinomycin overnight at 37 °C while shaking at 220 rpm. The following day, 1.5 ml of the culture was transferred into a microcentrifuge tube and centrifuged for 1 minute at 14,000x g at 24 °C to remove the medium. Another 1.5 ml of the culture was then added to the pellet, and the mixture was centrifuged again under the same conditions. The plasmid DNA was subsequently isolated using the Miniprep kit according to the provided protocol. After the isolation of plasmid DNA, the DNA concentration was measured using a Nanodrop spectrophotometer which also provided information about DNA purity (A_{260}/A_{280} and A_{260}/A_{230}).

4.2.11.2 Polymerase chain reaction

The polymerase chain reaction (PCR) was conducted using primers specific to the sequence of the *IDH* gene of interest, targeting the amplification of the desired DNA fragment from the isolated plasmid DNA. The reaction components were as follows:

Reagents	Volume [µl] /reaction
5x Q5 reaction buffer	10
2.5 mM dNTPs	5
10 µM primer	2.5
DMSO	2.5
Q5 polymerase	0.5
H2O	28.5
DNA	1 (50 ng)

The PCR program steps were set as follows (shown as temperature and time [minutes:seconds]):

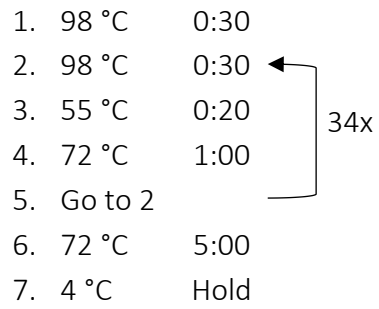

4.2.11.3 DNA electrophoresis and DNA isolation

For the isolation of our gene of interest, DNA electrophoresis was performed.
A 0.8% agarose gel was prepared by dissolving 0.8 g of agarose in 100 ml of 0.5% TBE buffer supplemented with 0.5 µl of ethidium bromide. The gel was poured into a mold and combs were placed into the gel to create the wells for sample loading. The samples were mixed with loading dye at a ratio of 1:5 [v/v] (10 µl into 50 µl of PCR product). Subsequently, 5 µl of DNA ladder 1 kb marker was loaded alongside 50 µl of the samples onto the gel. The gel was electrophoresed at 100 V for approximately 1 hour. Post-electrophoresis, the gel was visualized under a UV lamp, and the bands corresponding to the size of the target gene were excised and purified using Genaid columns according to the manufacturer's protocol. The DNA was then eluted in nuclease-free water.

4.2.11.4 Gibson assembly

The DNA fragments were assembled into the desired vector backbone using the Gibson assembly method. The vector backbone and DNA fragments were combined in a PCR microtube at a molar ratio of 1:2, with nuclease-free water added to reach a final volume of 5 µl. Subsequently, 5 µl of NEBuilder HiFi assembly master mix was added to the tube, and the mixture was incubated at 50 °C for 15 minutes in a thermocycler.

4.2.11.5 Transformation of a plasmid DNA into E. cloni

The assembly mixture was added to 40 µl of competent E. cloni cells and incubated on ice for 30 minutes. Subsequently, the bacteria were transformed using the heat-shock method by

incubating in a water bath at 42 °C for 45 seconds, followed by a 2-minute incubation on ice. After heat shock, 250 µl of SOC recovery media was added to the transformed bacteria, and the mixture was incubated for 1 hour at 37 °C in a shaker. The bacteria were then spread onto agar plates supplemented with Ampicillin and incubated at 37 °C in an incubator for 24 hours or until visible and adequately sized colonies formed. Colonies were then selected and grown in 6 ml of media supplemented with 100 mg/ml Ampicilin overnight at 37 °C while shaking at 220 rpm. The following day, 1.5 ml of the culture was transferred into a microcentrifuge tube and centrifuged for 1 minute at 14,000x g at 24 °C to remove the medium. Another 1.5 ml of the culture was then added to the pellet, and the mixture was centrifuged again under the same conditions. The plasmid DNA was subsequently isolated using the Miniprep kit according to the provided protocol. After the isolation of plasmid DNA, the DNA concentration was measured using a Nanodrop spectrophotometer.

To verify the newly cloned gene into the desired vector, PCR, DNA electrophoresis and DNA isolation were performed.

4.2.11.6 Plasmid restriction

The digested agarose gel DNA was pipetted into a PCR microtube along with the appropriate endonuclease, which recognizes a restriction site present in our plasmid, as outlined in the following table:

	Volume [µl]
DNA	10
10x Cut Smart Buffer	1.5
AscI (endonuclease)	0.5
H_2O	3
Total volume	**15**

The mixture was incubated for 1 hour at 37°C. Following incubation, DNA electrophoresis was performed, and the gel was visualized to confirm the presence of the correct plasmid DNA.

4.2.11.7 Sequencing

DNA isolated from the agarose gel was purified and volume containing 300 ng of DNA was added into PCR microtubes, along with 2 µl of 2.5 µM sequencing primers and nuclease-free water to achieve the final volume of 8 µl. Subsequently, the mixture was submitted for sequencing at the Biocev Sequencing facility.

4.2.11.8 Electroporation transfection of a plasmid into a cell line

After verification of the plasmid through sequencing, electroporation was used to introduce the plasmid DNA into OCI-M2 cells. Electroporation is a transfection technique that utilises a brief electrical pulse to create transient pores in the cell membrane, allowing the plasmid DNA to enter the cell. Once inside, the DNA can be integrated into the host genome.

1.2 x 10^6 cells were prepared per condition and washed in 10 ml PBS through centrifugation at 350x g for 5 min at 24 °C. A mixture of 10 µg plasmid DNA and a 6.4 µg transposase SB100 in nuclease-free water was prepared to a final volume of 10 µl. Electroporation was performed using the NEON^{TM} transfection system (ThermoFisher) according to the protocol. The cell pellet was resuspended in 100 µl of NEON buffer R per condition. The 100 µl cell suspension was combined with the plasmid and transposase mixture in a microcentrifuge tube. The entire volume was transferred into the electroporation chamber of the NEON device in a pipette, and the cells were transfected using specific conditions for the cell line optimised in our laboratory (1400 V, 20 ms, 1 pulse for OCI-M2). After electroporation, the transfected cells were transferred into a 6-well plate containing 2 ml of IMDM medium with 20% [v/v] FBS without antibiotics and incubated for 48 hours at 37 °C in an incubator. Following the incubation period, antibiotics (penicilin, streptomycin and puromycin) were added to the transfected cells.

5 Results

Our laboratory is dedicated to elucidating the role of redox homeostasis in the context of resistance to therapy of acute myeloid leukaemia (AML) and myelodysplastic syndrome (MDS). Working with cell clones resistant to 5-azacytidine (AZA-R), which were developed in our laboratory, my colleagues have discovered evidence showing the important role of redox homeostasis alterations in conferring resistance to the hypomethylating agent – 5-azacytidine (AZA). By modulating the KEAP1-NRF2 pathway, they were able to increase the sensitivity of AZA-R cells to AZA. These findings underscore the important role of redox balance and NRF2 in the sensitivity of AML cells to therapy, prompting us to further investigate this concept.

5.1 Estimation of the sensitivity of OCI-M2 cells to 5-azacytidine and pevonedistat

In our study, we studied the role of redox homeostasis in the response to selected drugs used for the treatment of MDS/AML patients. We worked with 5-azacytidine (AZA), representing hypomethylation therapy, and pevonedistat (Pevo), a NEDDylation inhibitor. Initially, to determine the appropriate dosage for subsequent experiments, we assessed the sensitivity of OCI-M2 cells to Aza and Pevo in the presence of a concentration range of the inhibitors using WST coulorimetric proliferation assay. We estimated half maximal inhibitory concentrations (IC50), which represent the drug concentration needed to reduce cell proliferation by 50%. Our findings revealed that the IC50 of AZA in OCI-M2 cells is 1.3 μM (Fig. 12A), while the IC50 of Pevo is 9 μM (Fig. 12B).

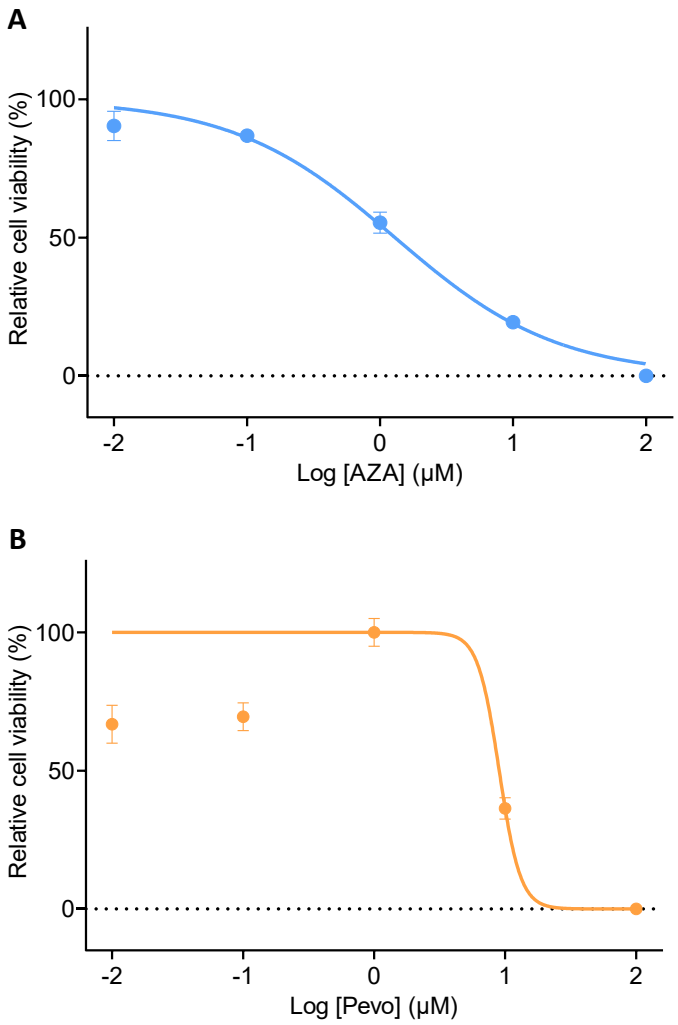

Fig. 12A, B: Relative cell viability of OCI-M2 cells in the presence of various concentrations of AZA (A) and Pevo (B) for 72 hours.

5.2 Both 5-azacytidine and pevonedistat treatment led to alterations in the oxidative state of OCI-M2 cells

First, we aimed to investigate the impact of AZA and Pevo on the reduction-oxidation (redox) homeostasis of OCI-M2 cells. Using flow cytometry, we measured three parameters related to oxidative stress and antioxidative response by employing three fluorogenic probes. CellROX Orange was utilized to detect reactive oxygen species (ROS), as it permeates cell membranes and fluoresces upon oxidation by ROS. We also used CM-H_2DCFDA, which reacts with intracellular thiols including reduced glutathione (GSH) with its chloromethyl group. CM-H_2DCFDA is subsequently oxidised by intracellular oxidants and this reaction

results in the conversion of CM-H_2DCFDA into a fluorescent adduct unable to leave the cell. As the fluorescence-inducing mechanism of CM-H_2DCFDA includes the reaction with thiols, we decided to label the measured parameter “oxidative state”. ThiolTracker Violet Reagent, capable of detecting free thiol groups, was employed for GSH detection, the most abundant free thiol in cells with concentrations ranging at 1-10 mM (Meister 1988). Propidium iodide (PI) was used to filter dead cells.

The median fluorescence intensity (MFI) of each fluorescent probe in the treated samples was compared to that of the control (ctrl). We examined four time points (15 min, 1 hour, 2 hours, and 24 hours) involving both short-term and long-term treatments with concentrations of 1 μM and 2 μM for AZA, and 1.4 μM and 2.9 μM for Pevo. Surprisingly, short-term treatment with 2 μM AZA resulted in slightly decreased ROS levels (Fig. 13C), although the changes were not statistically significant, but the overall oxidative state was not affected (Fig. 13A). Notably, GSH levels significantly increased in OCI-M2 cells treated with 1 μM AZA for 24 hours compared to short-term treatment (Fig. 13B), indicating that only prolonged exposure to AZA induces changes in free thiol levels. In contrast, Pevo treatment exhibited more pronounced effects. Both 1.4 μM and 2.9 μM Pevo treatments for 24 hours led to a significant increase in GSH levels compared to the control (Fig. 14B). Additionally, ROS levels significantly rose more than two-fold in cells treated with 2.9 μM Pevo for 24 hours compared to the control (Fig. 14C). These findings suggest that prolonged exposure to Pevo and AZA is more effective in eliciting redox changes in OCI-M2 cells.

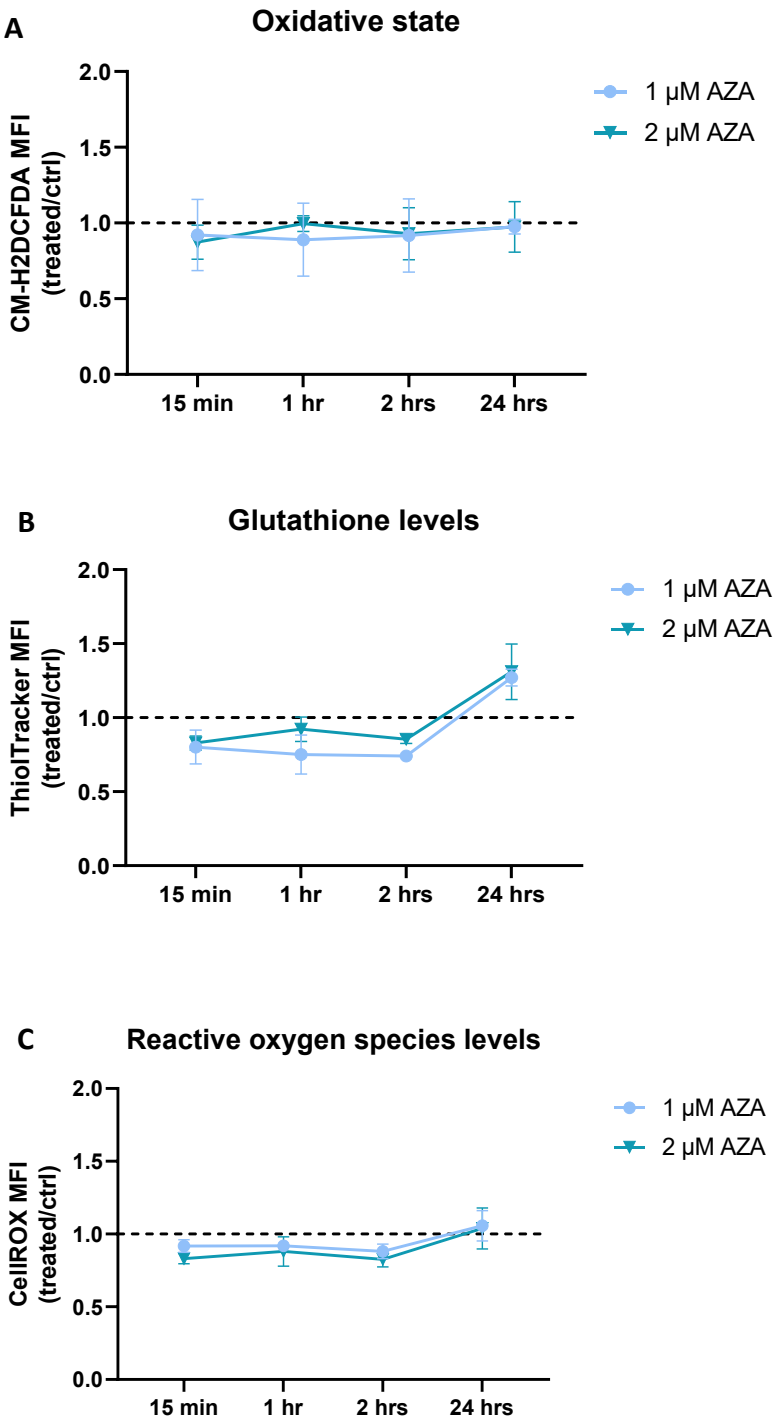

Fig. 13A-C: Intracellular detection of oxidative state (A), glutathione (B) and reactive oxygen species (C) in OCI-M2 cells treated with 1 µM AZA and 2 µM AZA for 24 hours, displayed as mean fluorescence intensity (MFI)

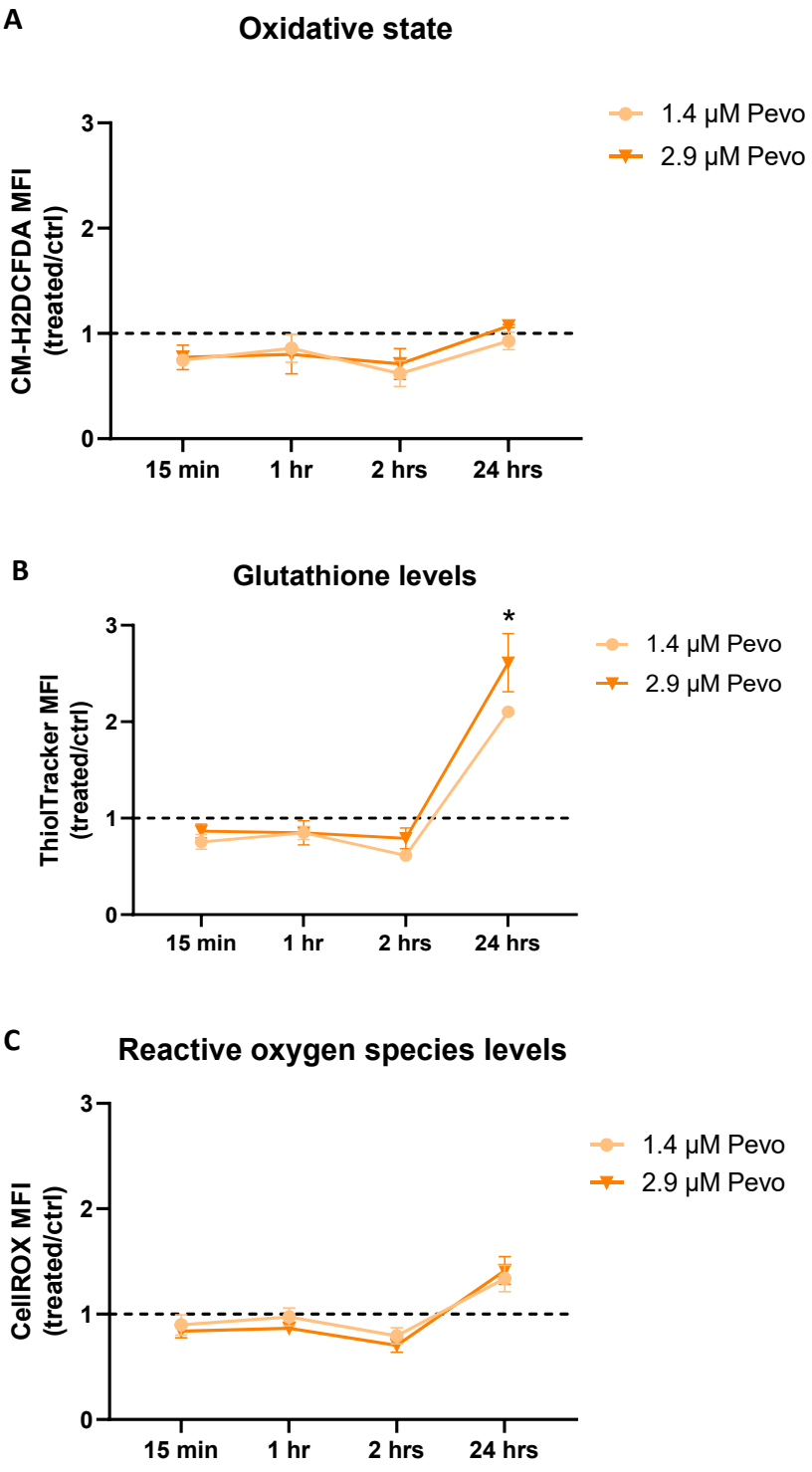

Fig. 14A-C: Intracellular detection of oxidative state (A), glutathione (B) and reactive oxygen species (C) in OCI-M2 cells treated with 1.4 µM Pevo and 2.9 µM Pevo for 24 hours.

5.3 NRF2 plays a crucial role in the response of OCI-M2 cells to 5-azacytidine

We measured cell proliferation using a WST assay administering a dilution series of AZA to untreated cells and cells treated with 10 µM NRF2 inhibitor ML385, 0.5 µM Pevo, and their combination. Our results indicated that 0.5 µM Pevo treatment decreased IC_{50} of AZA in OCI-M2 cells, making them more sensitive to treatment. Conversely, when combined with NRF2 inhibition, Pevo treatment increased the IC_{50} of AZA by approximately six-fold. Our findings suggest that treatment with 0.5 µM Pevo enhanced the sensitivity of AZA-sensitive (AZA-S) cells to AZA via NRF2 activation, as the effect was reversed by NRF2 inhibition (Fig. 15).

A

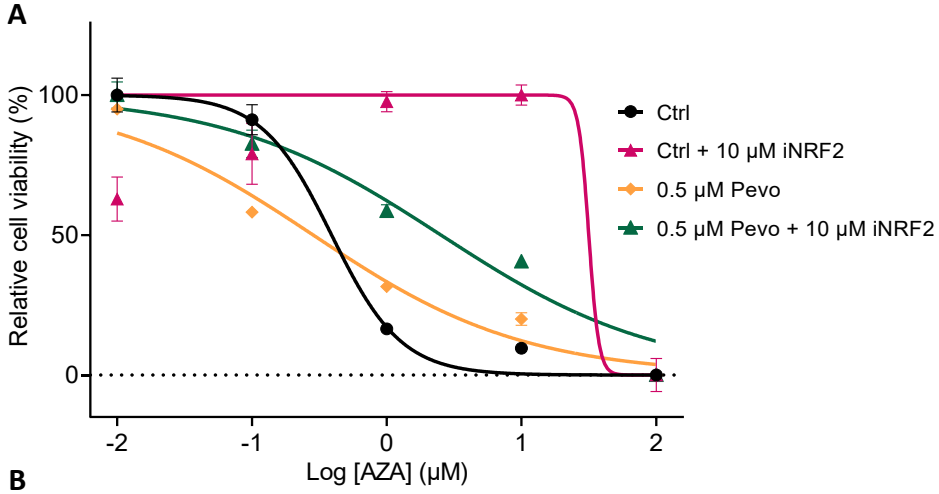

B

OCI-M2 cells	$IC50_{AZA}$ [µM]
Ctrl	0.39
0.5 µM Pevo	0.28
10 µM ML385	31.58
0.5 µM Pevo + 10 µM ML385	2.527

Fig. 15A, B: Relative cell viability of OCI-M2 cells in the presence of various concentrations of AZA for 72 hours with a pre-treatment of 10 µM NRF2 inhibitor (iNRF2), 0.5 µM Pevo, and 0.5 µM Pevo with 10 µM iNRF2 for additional 24 hours (A); IC50 concentrations of AZA for the different pre-treatment conditions are displayed in table (B).

5.4 The acquisition of multidrug resistance to 5-azacytidine and pevonedistat is accompanied by changes in the redox state

Pevo has been proposed as a treatment option for MDS/AML patients who no longer respond to AZA. However, the emergence of resistance to both drugs has introduced further challenges in treatment. Therefore, our research focused on the combined resistance to Pevo and AZA in MDS/AML cells. In our lab, we developed cell clones with dual resistance

derived from AZA-resistant cells. We established one clone partially resistant to Pevo and completely resistant to AZA (PEVO-PR), and a clone that is resistant to both AZA and Pevo (PEVO-R), as illustrated in Fig. 16.

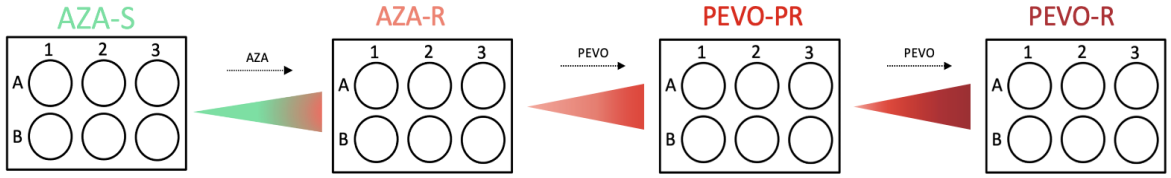

Fig. 16: Cells resistant to 5-azacytidine (AZA-R) were developed by treating cells sensitive to 5-azacytidine (AZA-S) with an increasing concentration of 5-azacytidine and by a selection of the surviving clones. Cells resistant to 5-azacytidine and partially (PEVO-PR) and completely (PEVO-R) resistant to Pevonedistat were then developed by treating AZA-R with an increasing concentration of Pevonedistat and by subsequent selection of the surviving clones.

Since our previous data showed that AZA resistance in MDS/AML cells involves a redox reset, and Pevo, similarly to AZA, alters the cellular redox state, we aimed to reveal if changes in the redox state are also linked to the Pevo resistance. We characterised the redox state of these cells using flow cytometry with CM-H2DCFDA, CellROX Orange and ThiolTracker Violet probes. We observed significant changes in the redox state of PEVO-PR cells (Fig. 17). These data demonstrate that the acquirement of resistance to Pevo is accompanied by a significant decrease in oxidative state and GSH levels (Fig. 17A, B). However, PEVO-R cells showed no alterations compared to AZA-R cells (Fig. 17). These findings suggest, that while the redox states of PEVO-R and AZA-R cells appear the same, the development of resistance involves oxidative changes.

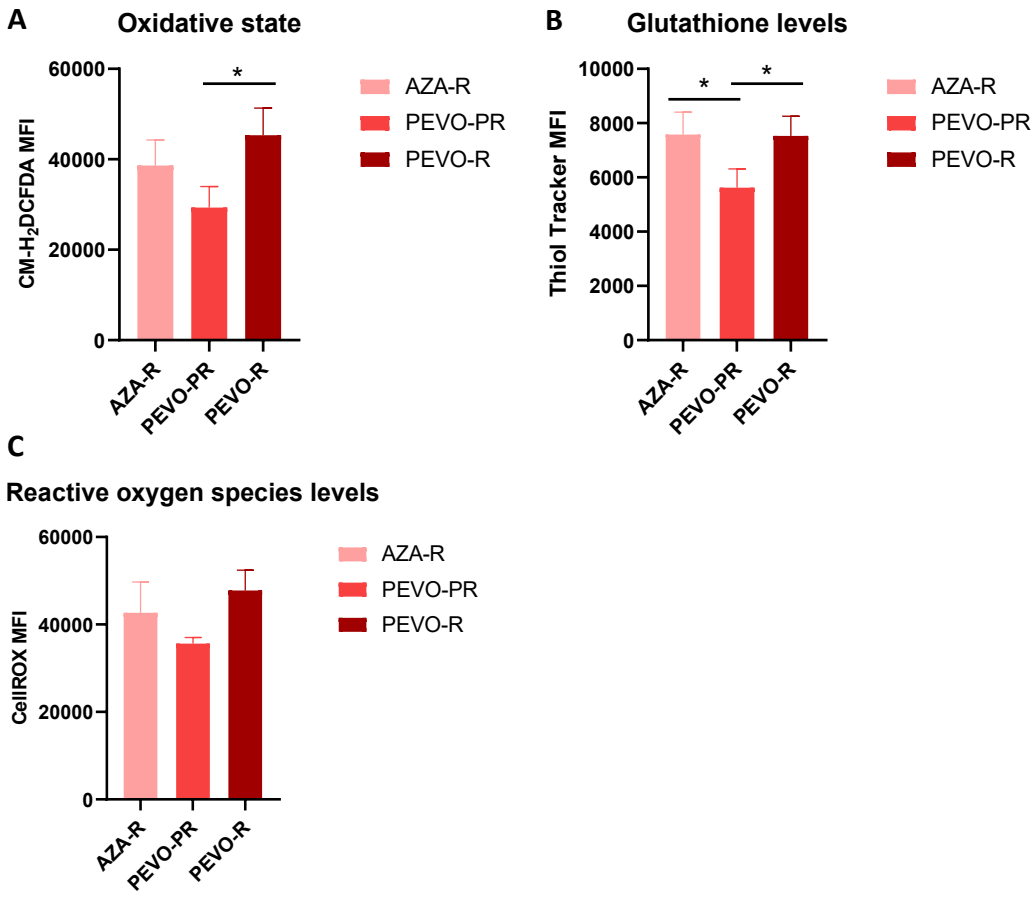

Fig. 17A-C: Intracellular detection of oxidative state (A), glutathione (B) and reactive oxygen species (C) in AZA-R, PEVO-PR and PEVO-R cells, displayed as mean fluorescence intensity (MFI).

5.5 Cells resistant to pevonedistat and 5-azacytidine display activation of NRF2

Considering that the redox system is under control of KEAP1-NRF2 system, the next step in the identification of the oxidative changes in multidrug-resistant cells was the detection of NRF2 activation. Considering the fact that PEVO-R cells did not show significant oxidative changes compared to AZA-R cells, but significant changes did occur in PEVO-PR (Fig. 17), we hypothesised that the activity of the KEAP1-NRF2 system might play a role in establishing the redox state balance. Upon activation of KEAP1-NRF2 pathway, NRF2 is translocated to the nucleus, therefore its nuclear levels reflect its activity.

We performed nuclear fractionation and detected the levels of NRF2 in the cytosolic and nuclear fraction of cell lysates using immunodetection. Using specific primary antibodies,

we detected NRF2, one of the proteins expressed from NRF2 target gene – NAD(P)H Quinone Dehydrogenase 1 (NQO1), and KEAP1, and used Actin and histone H3 as housekeeping genes in the cytosol and nucleus, respectively (Fig. 18A). Actin and histone H3 detection served as a verification of successful nuclear fractionation. We were able to isolate the nuclear fraction with a minimal presence of actin, however, our cytosolic fraction showed a significant amount of histone H3 (Fig. 18A), rendering the cytosolic fraction inaccurate. As we focus on the translocation of NRF2 to the nucleus, our main aim is to have an isolated nuclear fraction, which was achieved. We found no changes in KEAP1 levels (Fig. 18A), however, we detected a significant amount of NRF2 in the nuclear fraction of these cells. We found that the cytosolic levels of NRF2 did not significantly differ in these cells. However, the nuclear fraction showed a significant accumulation of NRF2 in both PEVO-PR and PEVO-R cells compared to AZA-R (Fig. 18B). Additionally, we examined the levels of NQO1, a protein associated with the antioxidative response and produced from NRF2 target genes. We observed increased levels of NQO1 in PEVO-PR and PEVO-R cells (Fig. 18C). These findings indicate a critical role for KEAP1-NRF2 in the regulation of redox homeostasis during the development of resistance.

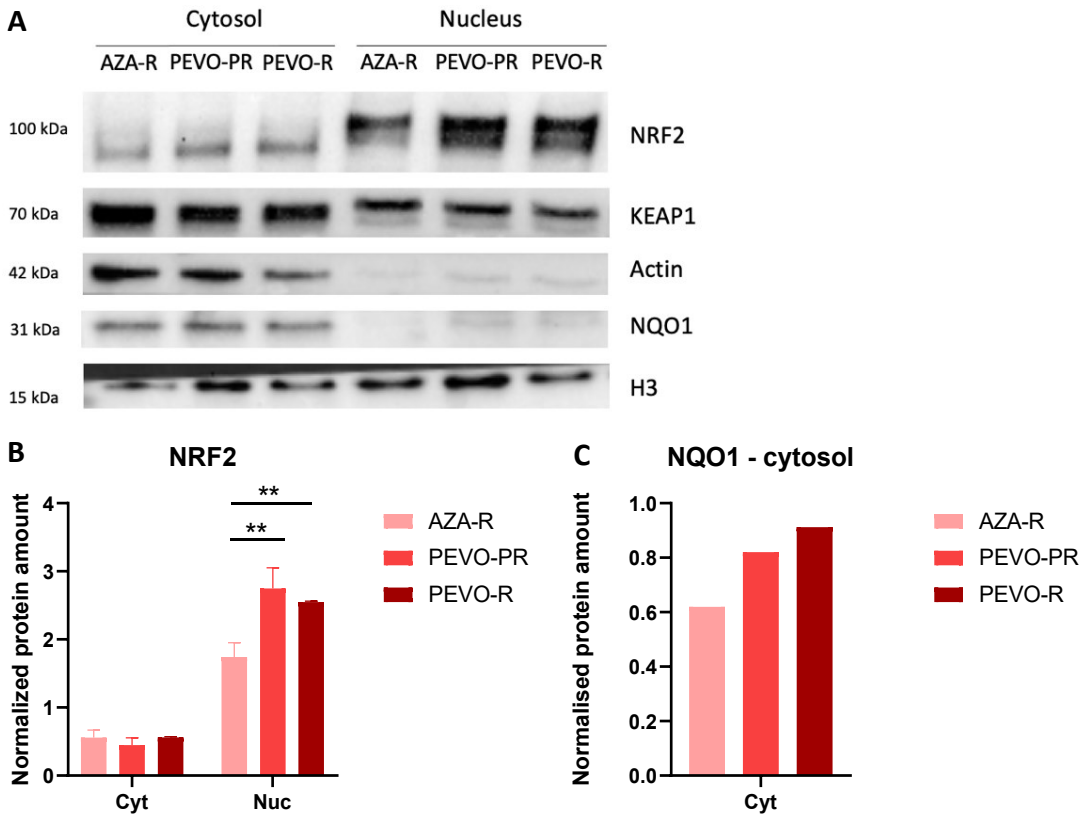

Fig. 18A-C: Relative abundance of NRF2, KEAP1 and NQO1 in the nuclear and cytosolic fraction of AZA-R, PEVO-PR and PEVO-R cells quantified by immunodetection.

5.6 Pevonedistat activates NRF2 in cells with partial resistance to pevonedistat

As KEAP1 is an adaptor protein of E3 ubiquitin ligases whose activity is inhibited by Pevo, we aimed to explore how Pevo treatment impacts the activation of NRF2 and its transcription targets in AZA-R, PEVO-PR and PEVO-R cells. We treated AZA-R, PEVO-PR and PEVO-R cells with 0.5 µM Pevo for 24 hours and then monitored the levels of NRF2 in the nucleus and its transcription targets using immunoblotting. Our findings revealed a significant increase in NRF2 activation in AZA-R cells following Pevo treatment, with expression levels in the nuclear fraction multiple-fold higher (Fig. 19). Notably, the expression of NRF2 in Pevo-treated cells was detected at a significantly shorter exposition (10.9 s for the Pevo-treated vs. 291 s for the untreated samples). This underscores the extent of the observed difference. As expected, PEVO-R cells showed minimal changes in NRF2 level after Pevo treatment, thus confirming the resistance to Pevo (Fig. 19A). Consistent with our NRF2

results, we detected increased NQO1 expression in the cytosolic fraction of AZA-R, while PEVO-R cells showed no changes in NQO1 abundance (Fig. 20). Interestingly, even in cells that are already partially resistant (PEVO-PR) and have a slightly higher Pevo IC50, Pevo significantly activated the KEAP1-NRF2 system even when exposed to only 0.5 µM Pevo (Fig. 19, 20). These results signify that both AZA-R and PEVO-PR cells respond to Pevo treatment with a distinctive increase in NRF2 activation, seemingly activating the expression of its target genes, while PEVO-R cells lose this ability to react to Pevo treatment. Therefore, NRF2 activity might play a role in the establishment of the redox balance during the process of adaptation to Pevo.

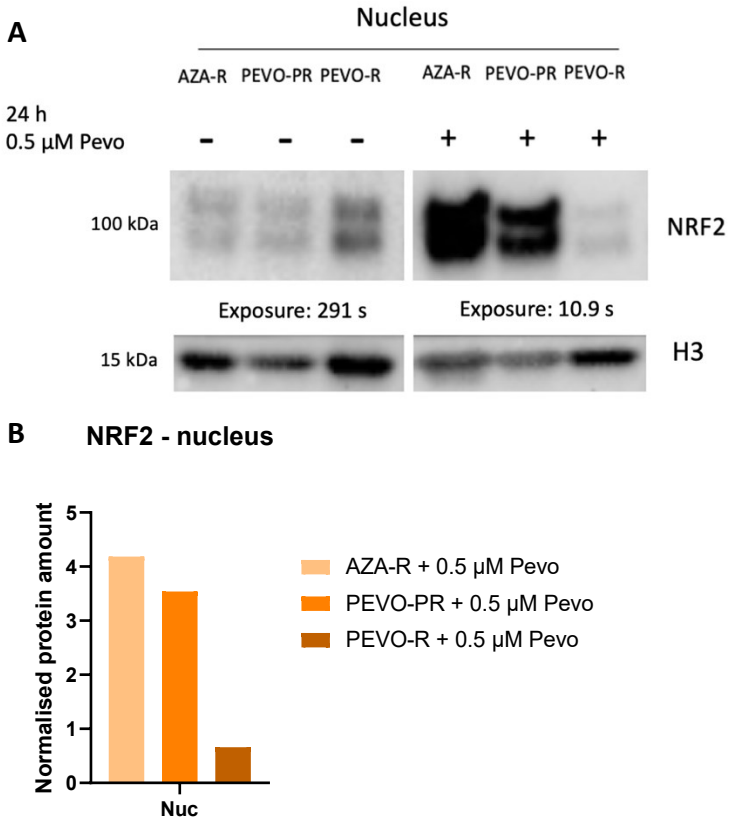

Fig. 19A, B: Relative abundance of NRF2 in the nuclear fraction of AZA-R, PEVO-PR and PEVO-R cells with and without a 24 hours treatment with 0.5 µM Pevo quantified by immunodetection.

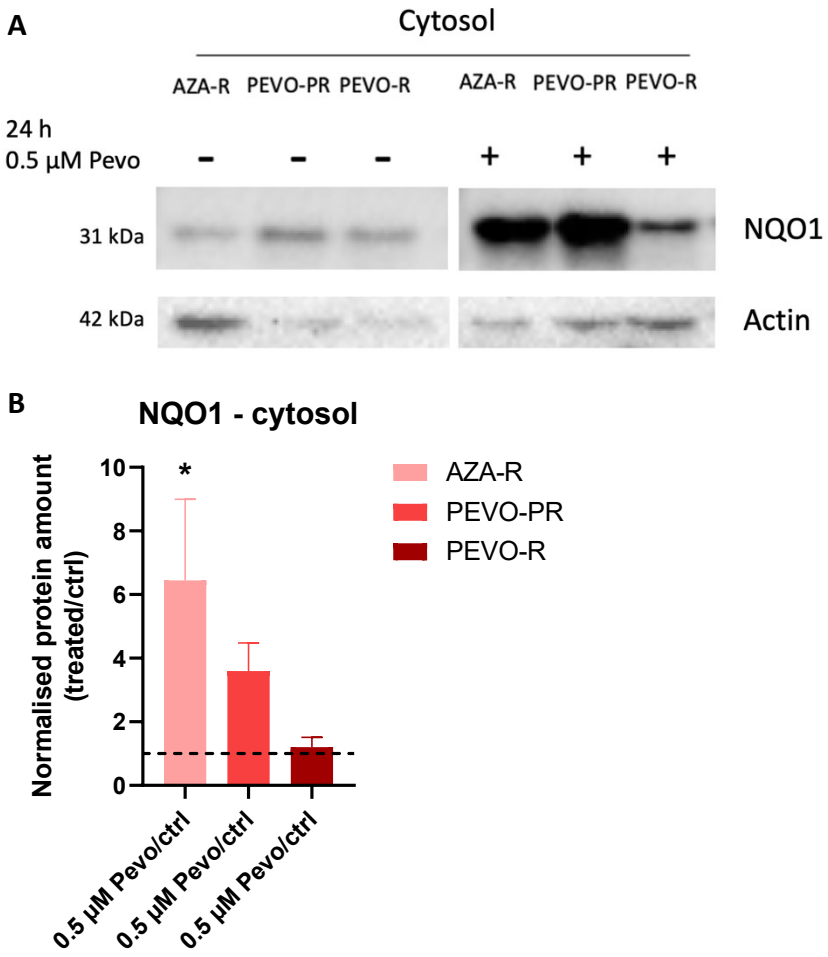

Fig. 20A, B: Relative abundance of NQO1 in the cytosolic fraction of AZA-R, PEVO-PR and PEVO-R cells with and without a 24 hour treatment with 0.5 µM Pevo quantified by immunodetection (A) and displayed as treated/untreated ratio of abundance (B).

5.7 Activation of NRF2 by pevonedistat in pevonedistat-partially resistant cells is associated with an increase in the oxidative state along with antioxidative response

Next, we were interested in how Pevo-mediated NRF2 activation affects the oxidative state of AZA-R, PEVO-PR and PEVO-R cells. We performed flow cytometry analysis of the oxidative state, ROS and GSH levels after a 24-hour treatment with 0.5 µM Pevo. The results, displayed as treated/ctrl ratios, revealed a significant decrease in ROS levels in AZA-R cells after Pevo treatment (Fig. 21C), while GSH levels remained unchanged (Fig. 21B). These findings suggest that the increased activation of NRF2 in response to Pevo treatment increases the antioxidative response, thus eliminating ROS in AZA-R cells. Surprisingly, PEVO-PR cells demonstrated more than two-fold increase in GSH levels (Fig. 21B) and no

changes in ROS levels (Fig. 21C). This distinct response of AZA-R and PEVO-PR cells to NRF2 activation by Pevo treatment suggests an altered mechanism regulating the oxidative state during the development of Pevo resistance. In accordance with the activity of NRF2, Pevo did not induce any changes in the oxidative state, ROS or GSH levels in PEVO-R cells (Fig. 21).

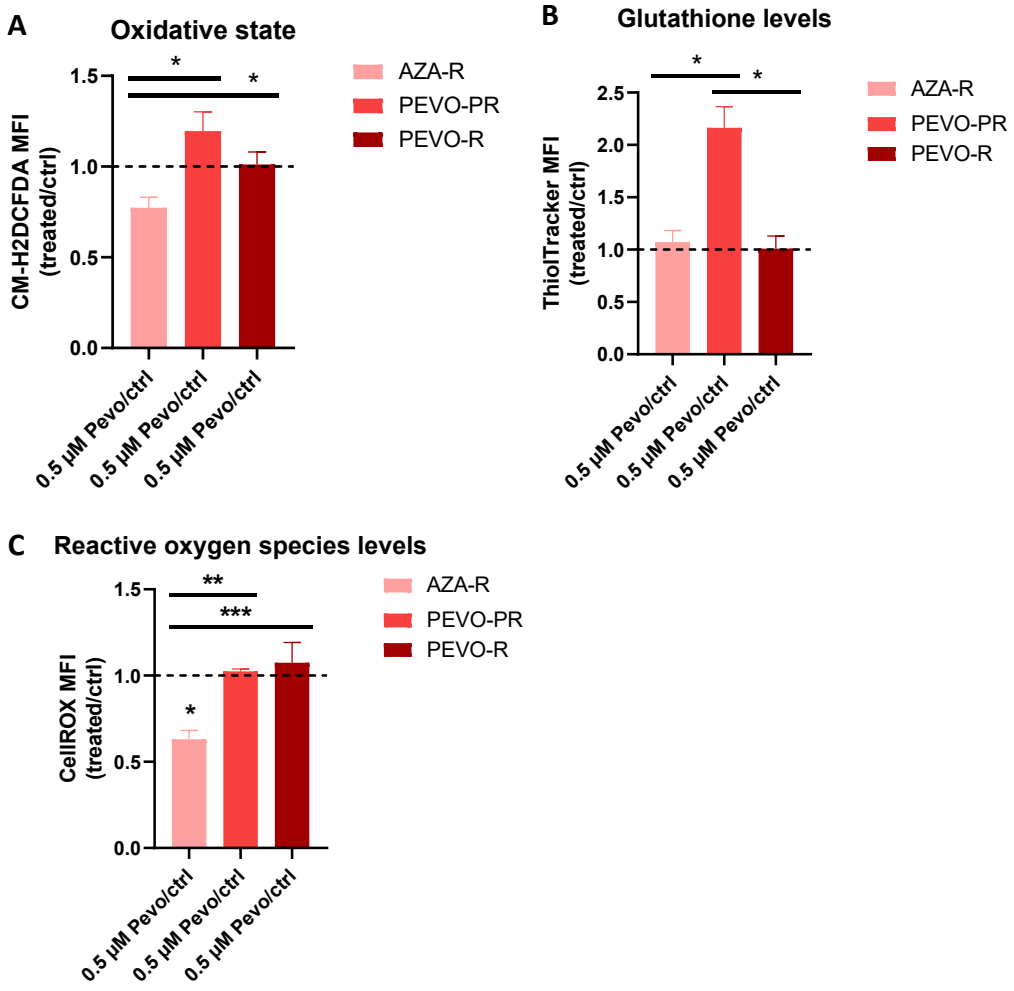

Fig. 21A-C: Intracellular detection of oxidative state (A), glutathione (B) and reactive oxygen species (C) in AZA-R, PEVO-PR and PEVO-R cells treated and untreated with 0.5 µM Pevo for 24 hours, displayed as treated/untreated ratio of mean fluorescent intensity (MFI).

5.8 A redox proteomics analysis identified proteins with significant changes in cysteine oxidation induced by pevonedistat and during pevonedistat resistance

Our findings revealed substantial changes in the cellular redox state following Pevo treatment of AZA-R and PEVO-PR cells, primarily attributed to the increased NRF2 activation. At the same time, Pevo-resistant cells showed increased NRF2 levels at steady state and are resistant to Pevo-induced redox changes. According to these findings, we suppose that NRF2 activity and redox changes induced by Pevo play an important role in the development of resistance to Pevo. To better understand the functional consequences of the different oxidative states associated with Aza and Pevo resistance, we performed a redox proteomic analysis. We used a previously described MS-based proteomic workflow that allows us to identify and quantify reversible oxidative modifications of proteins (Pimkova, Jassinskaja et al. 2022).

We compared three distinct conditions: AZA-R cells, AZA-R cells treated with 0.5 μM Pevo for 24 hours, and PEVO-R cells. In each case, we compared Pevo-treated AZA-R cells and PEVO-R cells against AZA-R cells as the control to reveal the redox-regulated pathways associated with Pevo treatment and Pevo resistance. In total, we identified 25,265 cysteine-containing peptides belonging to 6634 proteins. To be able to estimate the extent of oxidation (% oxidation) meaning to determine how many of these peptides carry oxidative modification on their cysteines and how many of them possess free thiol groups, the equation shown was used (Fig. 22). The calculation is based on the ratio of iodoTMT reporter ion intensity representing oxidised thiol(s) of the peptides and the sum of iodoTMT reporter ion intensity representing oxidised thiol(s) and free thiol(s). We were able to acquire % oxidation values on average in 9127 peptides for AZA-R, 8539 for AZA-R+Pevo and 11,520 in Pevo-R (Fig. 23). These values were used for subsequent comparison between analysed conditions.

$$\%\ \text{oxidation} = \frac{\text{oxidised thiols}}{\text{oxidised thiols} + \text{reduced thiols}} * 100$$

Fig. 22: Calculation of % oxidation.

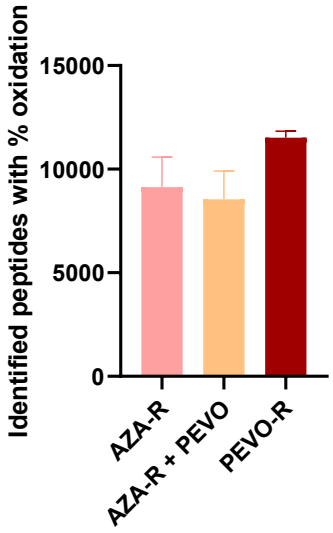

Fig. 23: The mean number of peptides with % oxidation values in AZA-R, AZA-R treated with 0.5 µM Pevo for 24 hours and PEVO-R.

We found that the redox state of the proteome significantly differed between the conditions (ANOVA, $p<0.05$). Post hoc analysis revealed that Pevo treatment increased oxidative modifications on the protein cysteines (5.8% vs. 4.9%) (Fig. 24). This finding is surprising, considering the previous results from flow cytometry analysis that showed a decreased oxidative state and levels of ROS after Pevo treatment (Fig. 21). Resistance to Pevo was not associated with overall changes in the redox state of the proteome (4.8% vs. 4.9%) (Fig. 19C).

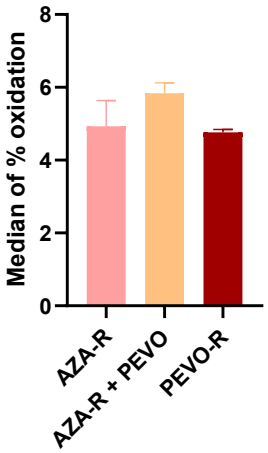

Fig. 24: The median of % oxidation of all quantified cysteine thiols in AZA-R, AZA-R treated with 0.5 µM Pevo for 24 hours and PEVO-R.

Treatment with Pevo changed the oxidation of 328 cysteine peptides of 301 unique proteins (Fig. 25), whereas resistance to Pevo was associated with a different redox state of 241 peptides of 226 unique proteins (Fig. 26). Notably, 30 peptides displayed significant changes in both Pevo-treated and resistant cells compared to AZA-R (Fig. 29).

Heat maps display the peptides with significantly changed % oxidation in PEVO-R cells (Fig. 26) and in Pevo-treated AZA-R cells (Fig. 25) compared to AZA-R. Notably, the replicates of each sample cluster together, affirming the reproducibility among the replicates.

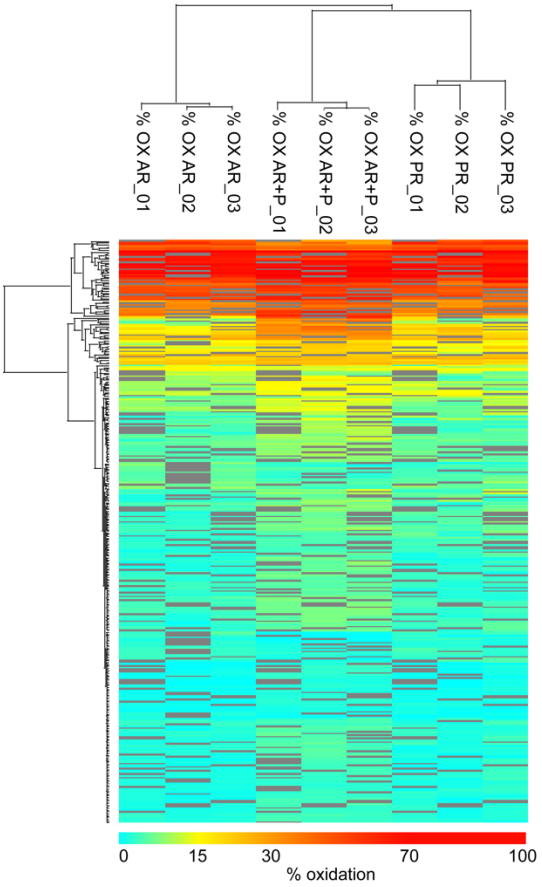

Fig. 25: Heat map showing % oxidation of pepetides with significantly changed oxidation in AZA-R cells treated with 0.5 µM Pevo for 24 hours (AR+P) compared to untreated AZA-R (AR), displayed as individual replicates of AZA-R, AZA-R treated with 0.5 µM Pevo for 24 hours and PEVO-R (PR)

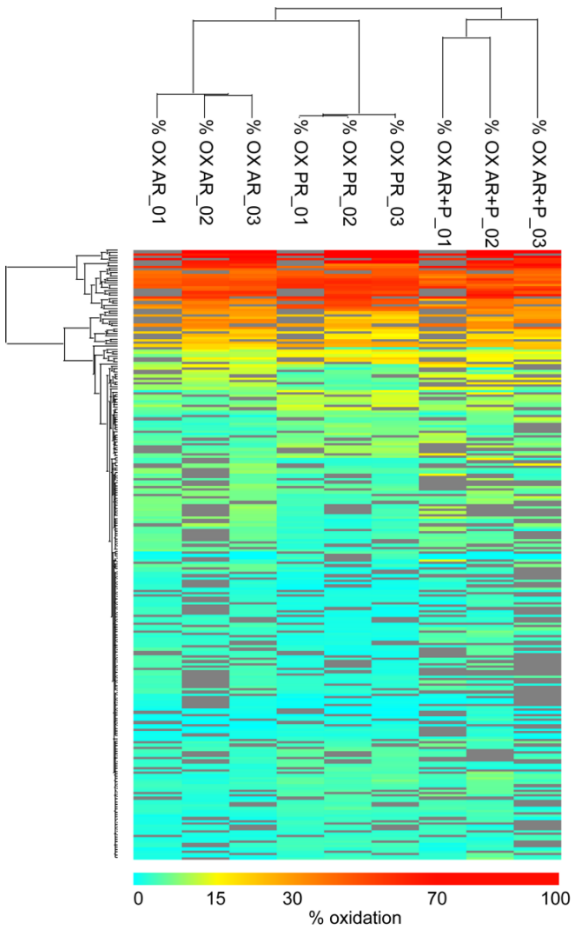

Fig. 26: Heat map showing % oxidation of peptides with significantly changed oxidation in PEVO-R cells (PR) compared to AZA-R (AR), displayed as individual replicates of AZA-R, AZA-R treated with 0.5 µM Pevo for 24 hours (AR+P) and PEVO-R

Volcano plots illustrate the $\log_2$-transformed % oxidation differences between AZA-R cells treated with Pevo and untreated AZA-R cells (Fig. 27), and between PEVO-R cells and AZA-R cells (Fig. 28). Pevo-treated cells exhibit increased oxidation levels, while PEVO-R cells display more evenly distributed changes. Depicted on a heat map are the gene names of proteins with significantly changed oxidation in both Pevo-resistant and Pevo-treated cells (Fig. 29).

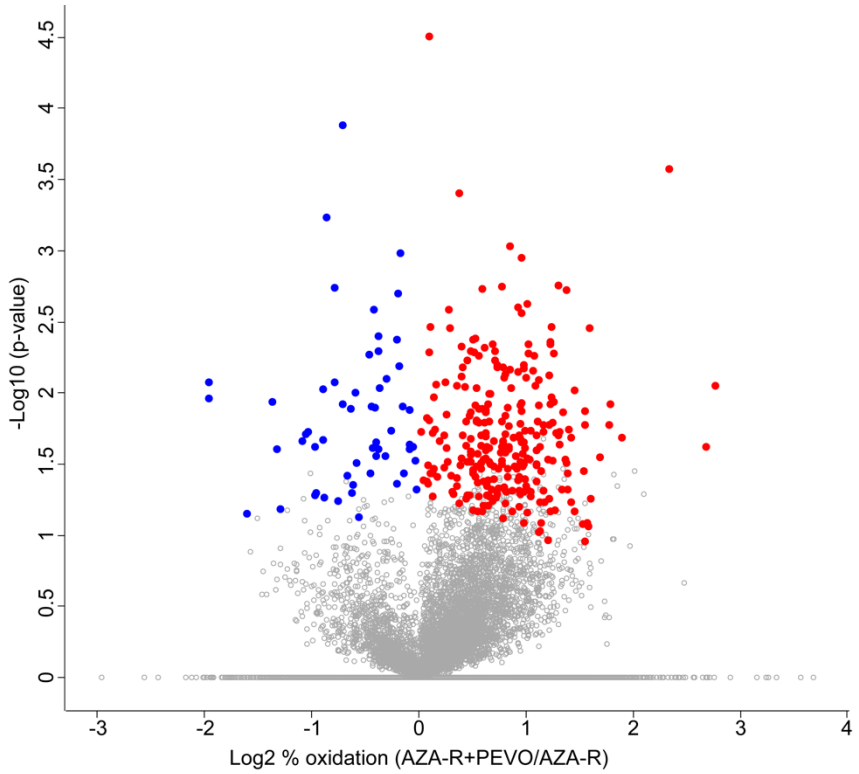

Fig. 27: Volcano plot showing the log_2-transformed % oxidation related to $-log_{10}$ p-value of peptides with significantly increased (red) and decreased (blue) oxidation in AZA-R cells treated with 0.5 µM Pevo for 24 hours compared to untreated AZA-R.

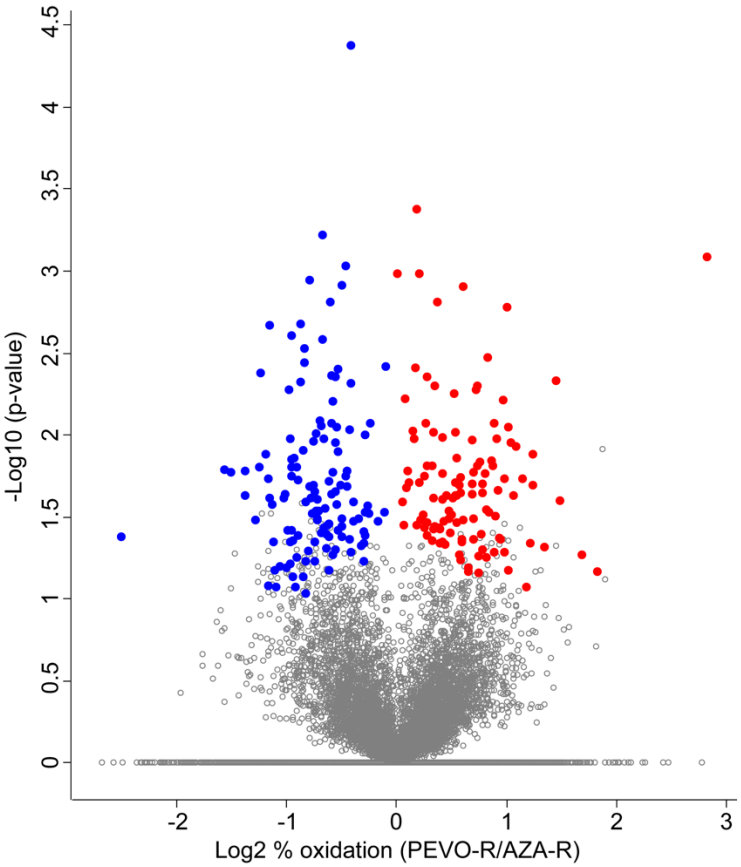

Fig. 28: Volcano plot showing the $\log_2$-transformed % oxidation related to $-\log_{10}$ p-value of peptides with significantly increased (red) and decreased (blue) oxidation in PEVO-R cells compared to untreated AZA-R.

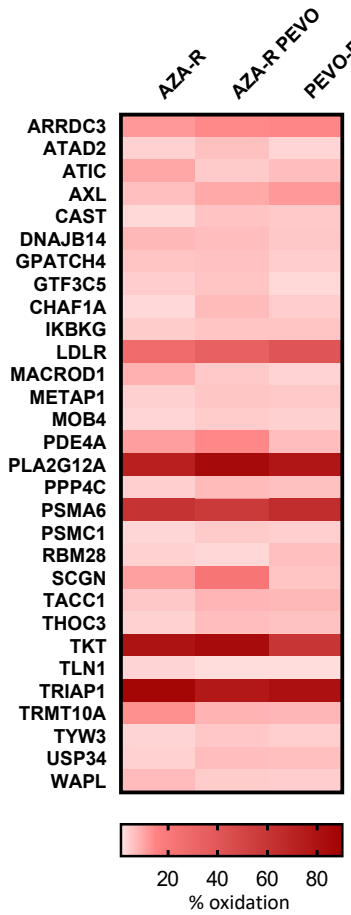

Fig. 29: Heat map showing mean % oxidation of peptides with significantly changed oxidation in both AZA-R cells treated with 0.5 µM Pevo for 24 hours compared to untreated AZA-R and in PEVO-R cells compared to AZA-R.

To understand which biological processes are affected by the changes in the redox state of proteins we performed Gene Ontology (GO) analysis. The DAVID software facilitated GO analysis of biological processes associated with proteins exhibiting significant changes in oxidation. Our investigation revealed that Pevo treatment resulted in increased oxidation of proteins involved in negative regulation of protein metabolic processes, cell cycle, DNA replication, cell signalling, and negative regulation of proteolysis (Fig. 30). Conversely, Pevo resistance was linked to elevated oxidation in proteins associated with cellular signalling, positive regulation of protein metabolic processes, replication, regulation of apoptosis, and protein modification, particularly phosphorylation (Fig. 31). Consequently, both Pevo treatment and Pevo resistance led to increased oxidation in proteins involved in DNA replication and cellular response to chemical stimuli. Notably, Pevo treatment induced

increased oxidation in proteins involved in the negative regulation of protein metabolic processes, while Pevo resistance showed heightened oxidation in proteins with roles in the positive regulation of protein metabolic processes, indicating differential regulation of protein metabolism (Fig. 30, 31). Moreover, PEVO-R cells exhibited significantly increased oxidation of 23 proteins involved in programmed cell death compared to AZA-R cells (Fig. 32). Further analysis revealed that four of these proteins are important in autophagy pathway: Sequestosome 1 (SQSTM1), Calpain-2 catalytic subunit (CAPN2), Calpastatin (CAST) and Phorbol-12-myristate-13-acetate-induced protein 1 (PMAIP1).

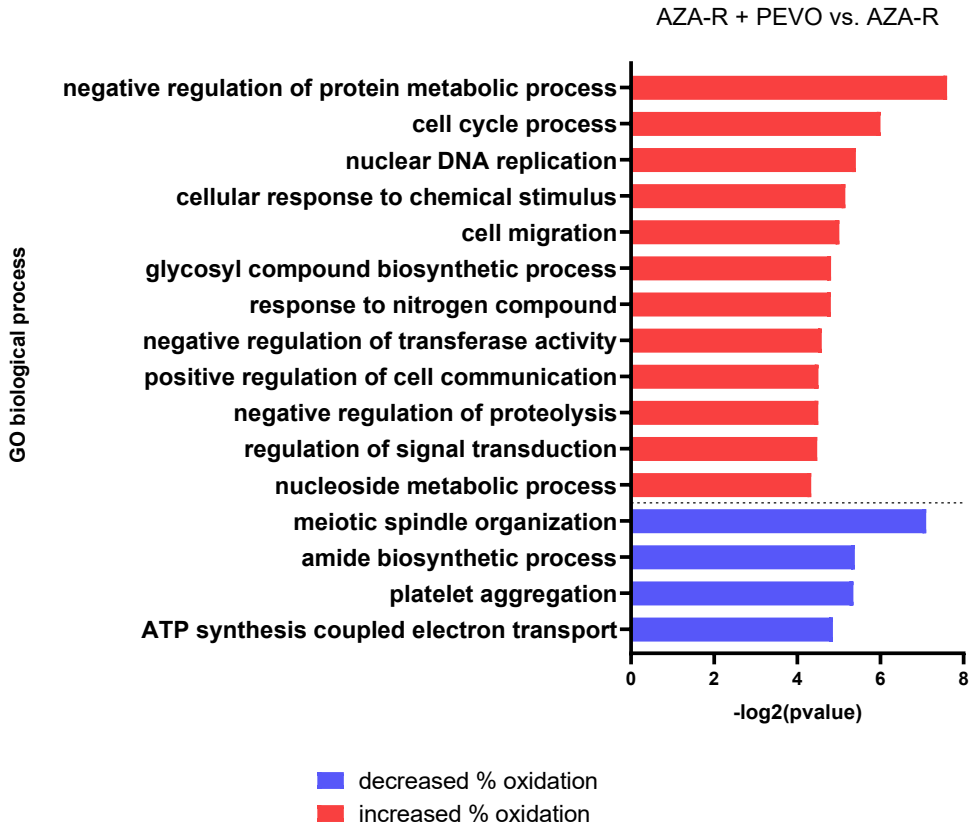

Fig. 30: Graph displaying the -$\log_2$(p-value) of gene oncology (GO) biological processes involving the proteins with significantly changed % oxidation on their cysteines (increased in red, decreased in blue) in AZA-R cells treated with 0.5 µM Pevo for 24 hours compared to untreated AZA-R.

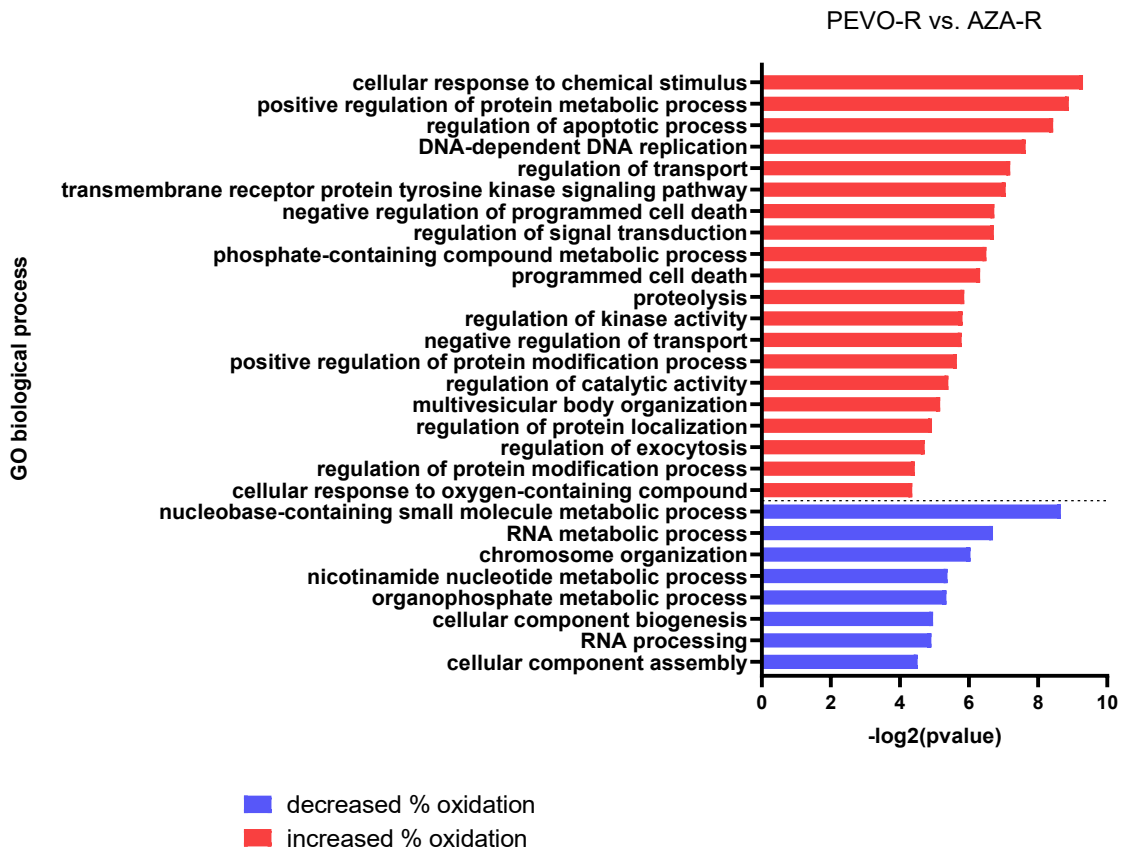

Fig. 31: Graph displaying the -$\log_2$(p-value) of gene oncology (GO) biological processes involving the proteins with significantly changed % oxidation of their cysteines (increased in red, decreased in blue) in PEVO-R cells compared to untreated AZA-R.

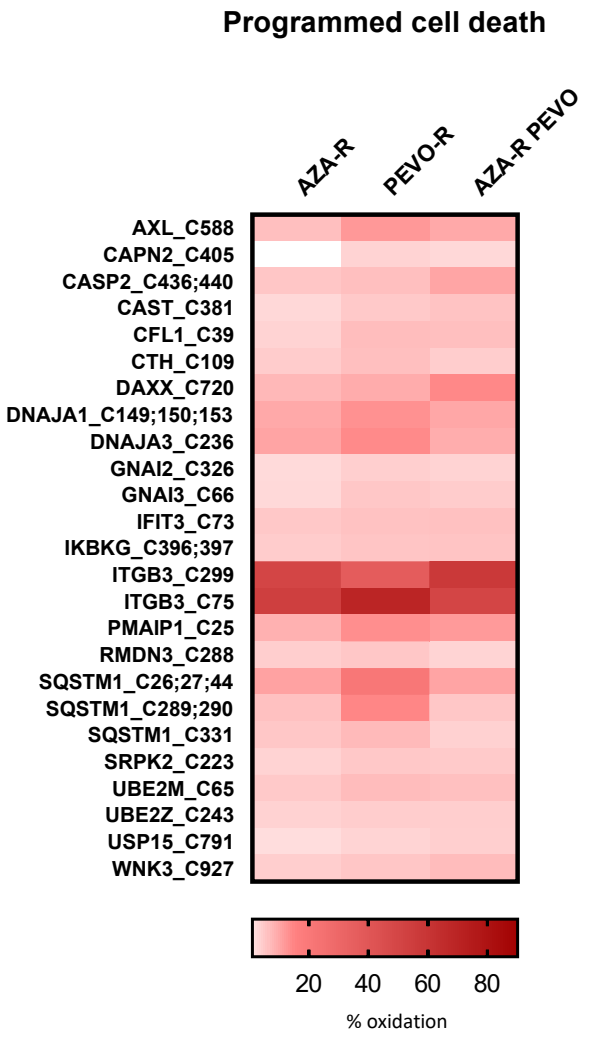

Fig. 32: Heat map showing mean % of cysteine oxidation of proteins with significantly changed oxidation in PEVO-R cells compared to AZA-R, with roles in programmed cell death.

5.9 Pevo-resistant cells display oxidation of SQSTM1 cysteines critical in regulation of autophagy

Next, we aimed to explore the involvement of autophagy in Pevo resistance and response to Pevo treatment. By comparing our results with a gene toolbox for monitoring autophagy (Bordi, De Cegli et al. 2021), we identified 11 proteins associated with autophagy that significantly changed the redox state of their cysteines after treatment with Pevo (Fig. 33) and 11 proteins exhibiting changes in oxidation upon Pevo resistance (Fig. 34).

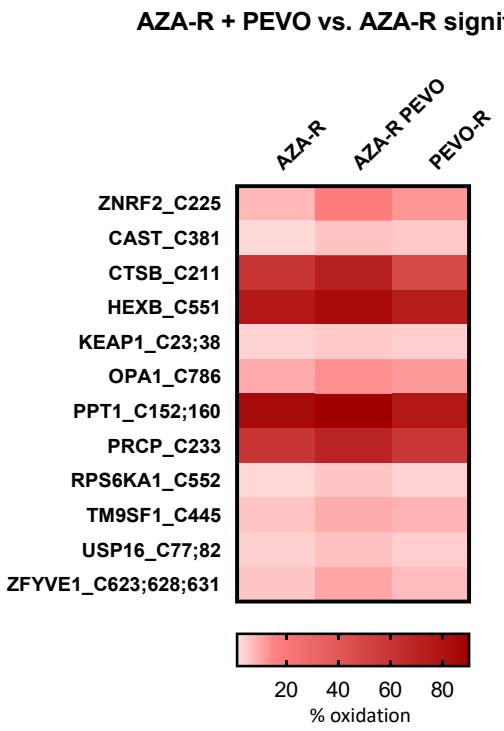

Fig. 33: Heat map showing mean % oxidation of proteins with significantly changed cysteine oxidation in AZA-R cells treated with 0.5 µM Pevo for 24 hours compared to untreated AZA-R, with roles in autophagy.

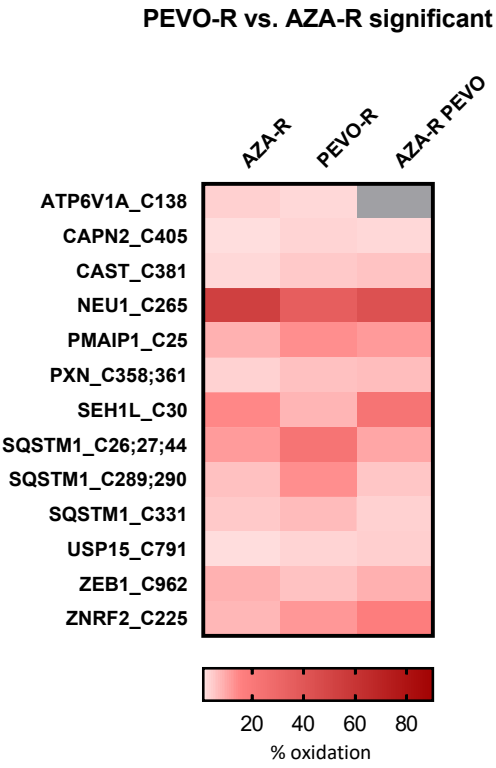

Fig. 34: Heat map showing mean % oxidation of proteins with significantly changed cysteine oxidation in PEVO-R cells compared to AZA-R, with roles in autophagy.

These results led us to investigate the activation of autophagy in resistant clones. To detect the autophagic activity in AZA-R, PEVO-PR, and PEVO-R cells, we first validated the antibodies binding non-lipidated (LC3-I) and lipidated (LC3-II) LC3, and SQSTM1. Glyceraldehyde dehydrogenase (GAPDH) was used for normalisation. We observed that a 72-hour treatment with two concentrations (50 and 100 μM) of an autophagy inhibitor chloroquine (CQ) led to increased levels of LC3-II and slightly increased SQSTM1 in PEVO-PR cells (Fig. 35A). After the validation, we detected autophagy levels in untreated cells. We observed autophagy activity in AZA-R, PEVO-PR and PEVO-R cells and found increased levels of LC3-II in PEVO-R cells along with decreased SQSTM1, which are considered markers of long-term activated autophagy (Fig. 35B).

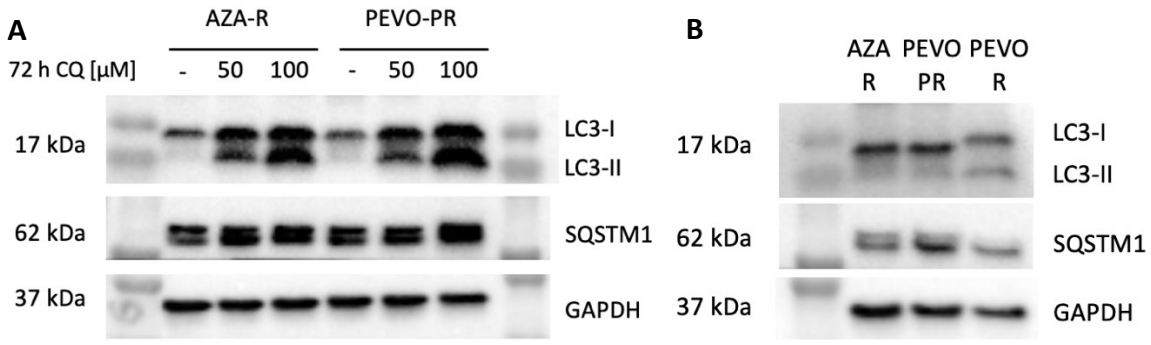

Fig. 35A, B: Relative abundance of LC3-I, LC3-II, SQSTM1 and GAPDH in AZA-R, PEVO-PR and PEVO-R cells with (A) and without (A, B) a 72-hour treatment with 50 and 100 μM chloroquine (CQ) quantified by immunodetection. GAPDH was used as a housekeeping gene for normalisation.

To further explore the role of autophagy in Pevo resistance, we measured the sensitivity of AZA-R, PEVO-PR and PEVO-R cells to autophagy inhibition via Bafilomycin (BF) through a WST proliferation assay with a dilution series of BF. The results revealed a significantly increased sensitivity of PEVO-R cells to BF, suggesting a higher reliance on autophagy in these cells (Fig. 36). Together, these results suggest that PEVO-R cells exhibit increased activation of autophagy, implying an increased dependency on this process.

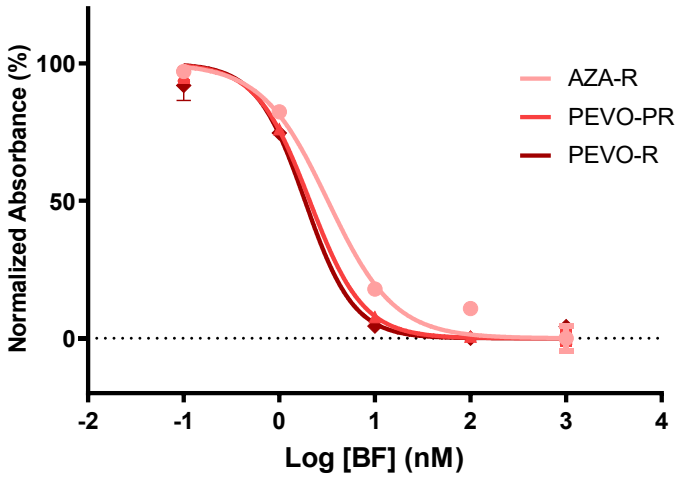

Fig. 36*:* Relative cell viability of AZA-R, PEVO-PR and PEVO-R cells in the presence of concentration range of Bafilomycin (BF) for 72 hours.

5.10 Resistance to pevonedistat is accompanied by an increased sensitivity to proteasomal inhibition

To determine cellular dependency on NRF2 and proteasomal function, we conducted an Incucyte analysis, monitoring the proliferation of AZA-R and PEVO-R cells over seven days with a dilution series of ML385 – an NRF2 inhibitor (iNRF2) ($1x10^{-6}$-$1x10^{2}$ µM), and Bortezomib – a proteasomal inhibitor ($1x10^{-8}$-$1x10^{0}$ µM). We found that PEVO-R cells are less sensitive to NRF2 inhibition, with AZA-R displaying a significant decrease in long-term proliferation at 1 µM iNRF2 concentration with the final confluence normalised to start point at 60% of the control (Fig. 37), while PEVO-R cells showed 70% of the control at 1 µM iNRF2 concentration (Fig. 38). Additionally, the 1 µM iNRF2-treated PEVO-R cells' proliferation slowed down later after approximately 6 days, whereas in AZA-R cells we can see the difference at day 3.

In contrast, treatment with Bortezomib revealed a significant increase in the dependency of PEVO-R cells on proteasomal function (Fig. 40). Surprisingly, the lowest concentration, $1x10^{-8}$ µM, inhibited proliferation in both AZA-R and PEVO-R cells, whereas one order of magnitude higher concentration $1x10^{-7}$ µM showed the final confluence normalised to start point to be at approximately 0.6 of the control in PEVO-R and 0.9 in AZA-R cells (Fig. 39,

40). Additionally, our analysis demonstrates a slowdown in replication following the acquisition of Pevo resistance.

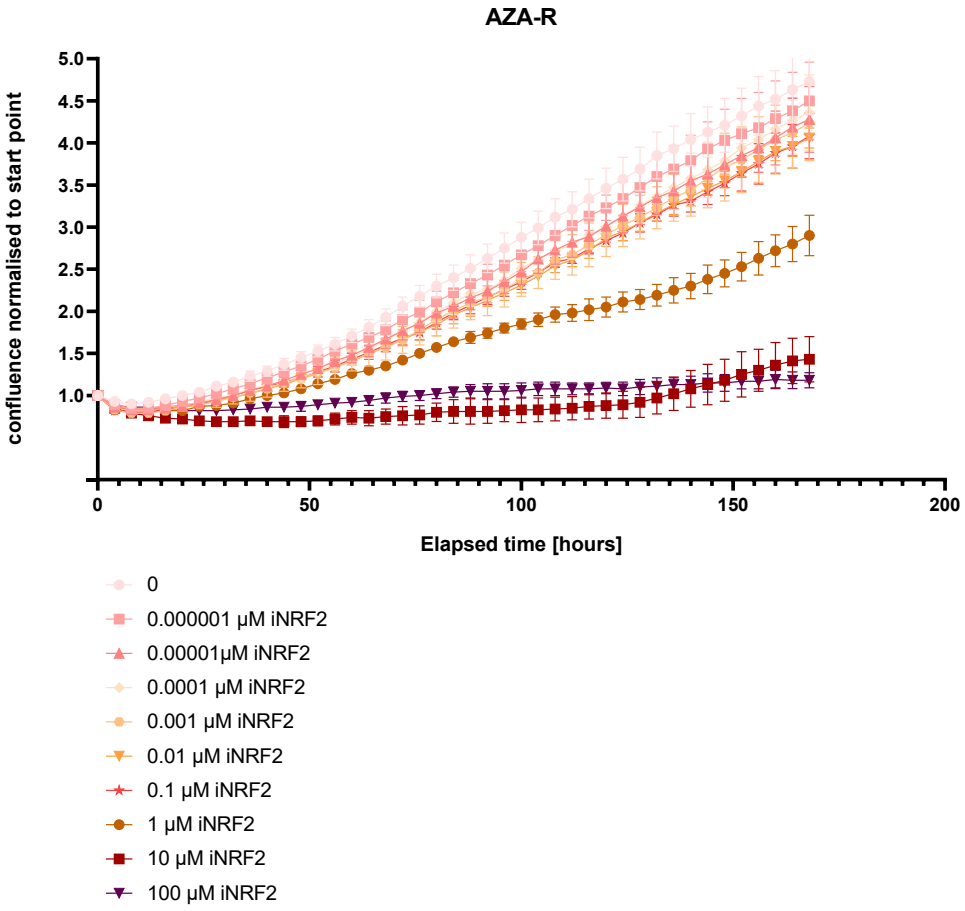

Fig. 37: Relative rate of proliferation of AZA-R cells in the presence of various concentrations of an NRF2 inhibitor ML385 (iNRF2).

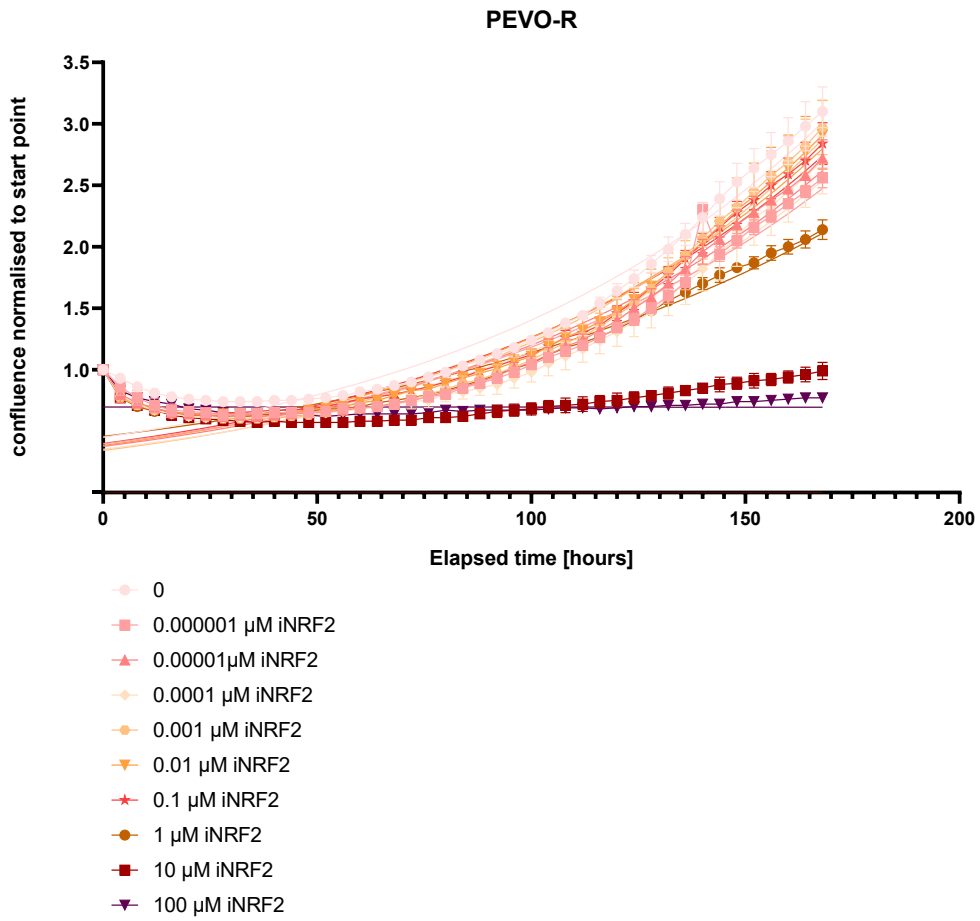

Fig. 38: Relative rate of proliferation of PEVO-R cells in the presence of various concentrations of an NRF2 inhibitor ML385 (iNRF2).

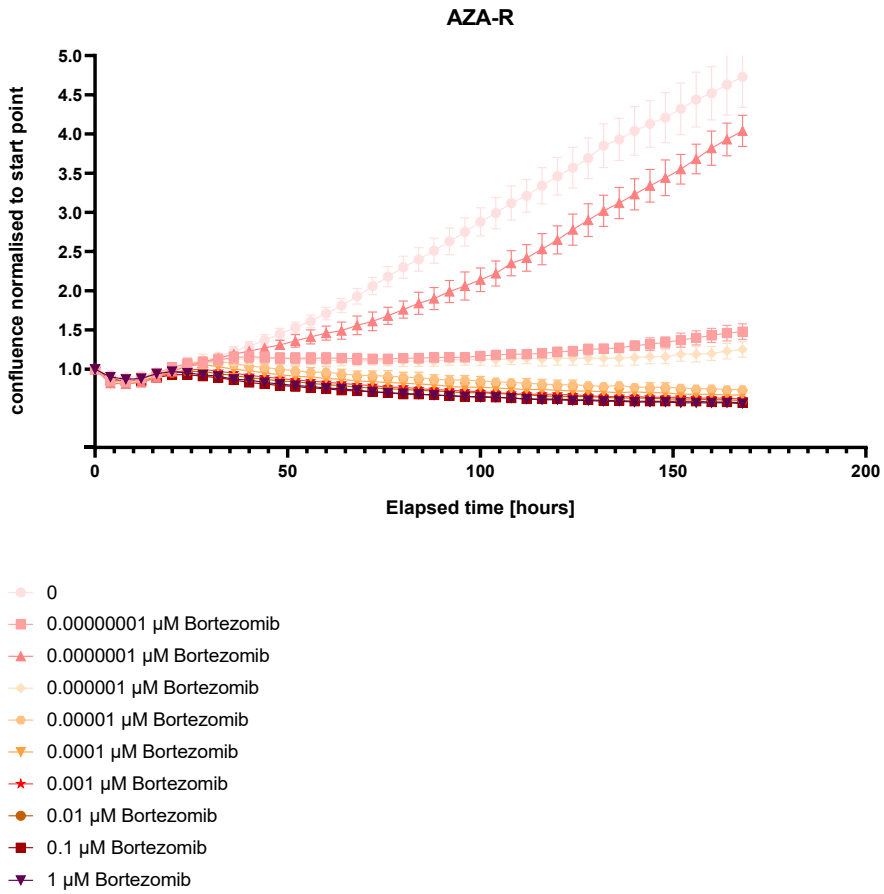

Fig. 39: Relative rate of proliferation of AZA-R cells in the presence of various concentrations of bortezomib.

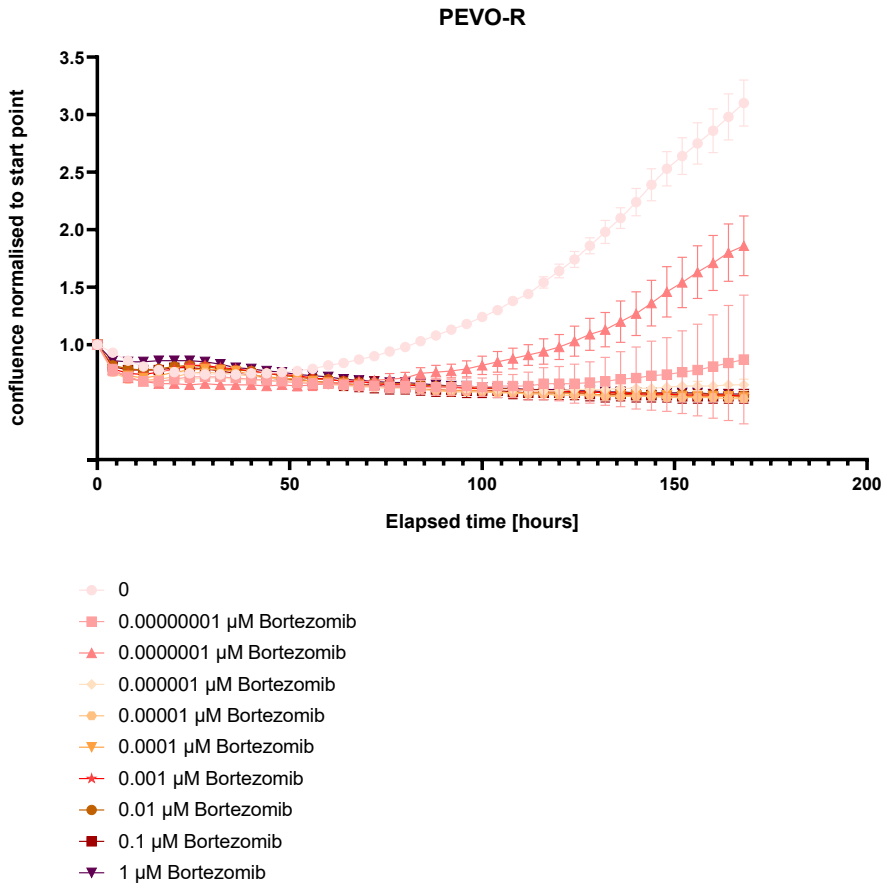

Fig. 40: Relative rate of proliferation of AZA-R cells in the presence of various concentrations of bortezomib.

5.11 Leukemogenic IDH1 and IDH2 mutations are associated with changes in redox homeostasis in MDS/AML cells

Finally, to explore the connection between altered redox homeostasis, leukemogenesis, and changes in therapy sensitivity, we aimed to establish a model featuring overexpression of mutant isocitrate dehydrogenase 1 (IDH1 R132H) and 2 (IDH2 R172K) known to have leukemogenic potential and significant impact on redox homeostasis. To achieve this, we created OCI-M2 cells with a Doxycycline (Dox)-inducible overexpression system for wild-type (WT) and mutant IDH proteins. In this model, we first cloned the *IDH2 R172K* gene into a plasmid sleeping beauty system. This plasmid harboured resistance to both puromycin and ampicillin, and it contained the dsRED protein along with 3x FLAG and Strep-Tag, all under the control of a tetracycline-inducible promoter (pSBtet-Pur-STREP-FLAG-dsRED) (Fig. 41). Subsequently, we verified the genes through sequencing. *IDH1 WT, IDH1 R132H* and *IDH2 WT* genes were already cloned into the pSBtet-Pur-STREP-FLAG-dsRED system

by my colleagues. This system should achieve a stable inducible expression of the gene of interest.

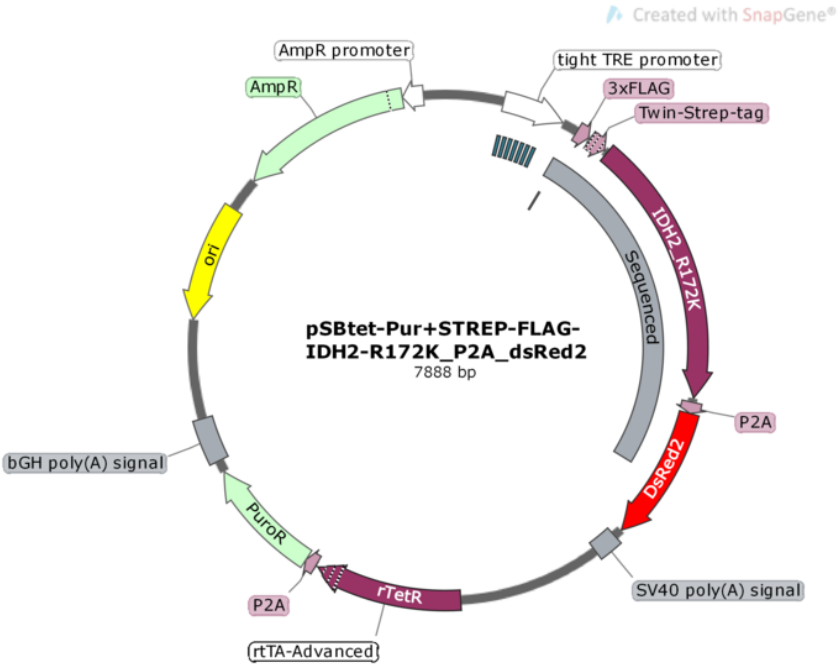

Fig. 41: Plasmid sleeping beauty system with resistance for puromycin (PuroR) and ampicilin (AmpR) and a Doxycycline-inducible promoter controlling the expression of 3xFLAG, Twin-Strep-tag, IDH2 R172K and dsRED gene; TRE – tetracycline-responsive element.

We transfected OCI-M2 cells with the cloned plasmids via electroporation and cultured them for 5-7 days in the presence of Puromycin to select the transfected cells. Subsequently, we induced the expression of *IDH* genes by treating the transfected cells with 0.6 µl/ml Dox for 48 hours. We then measured the expression of IDH by detecting the dsRED fluorescent protein via flow cytometry (Fig. 42A). Since the *dsRED* gene is under the same Dox-inducible promoter as *IDH*, dsRED expression provided us with information about the presence of IDH expression.

After confirming successful transfection through dsRED detection, we proceeded to optimise the concentration and duration of Dox treatment using two different concentrations of Dox and two time points (Fig. 43A-D). Our experiment revealed that treatment with 0.6 µl/ml Dox for 24 hours yielded optimal results. Unfortunately, we observed rapid loss of expression of the transfected protein in the cells following each transfection (Fig. 42B).

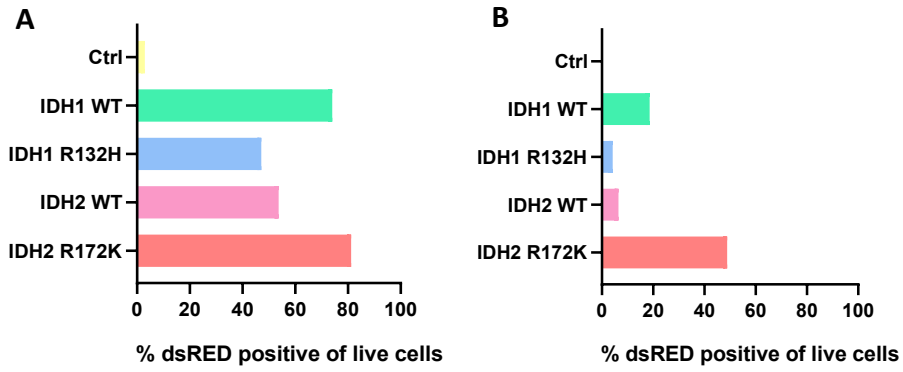

Fig. 42A, B: Intracellular detection of dsRED expression in OCI-M2 cells with inducible overexpression of IDH1 WT, IDH1 R132H, IDH2 WT and IDH2 R172K genes after a 48-hour treatment with 0.6 µg/ml doxycycline shown as the percentage (%) of dsRED positive cells of all live cells 5 days after transfection (A) and 21 days after transfection (B).

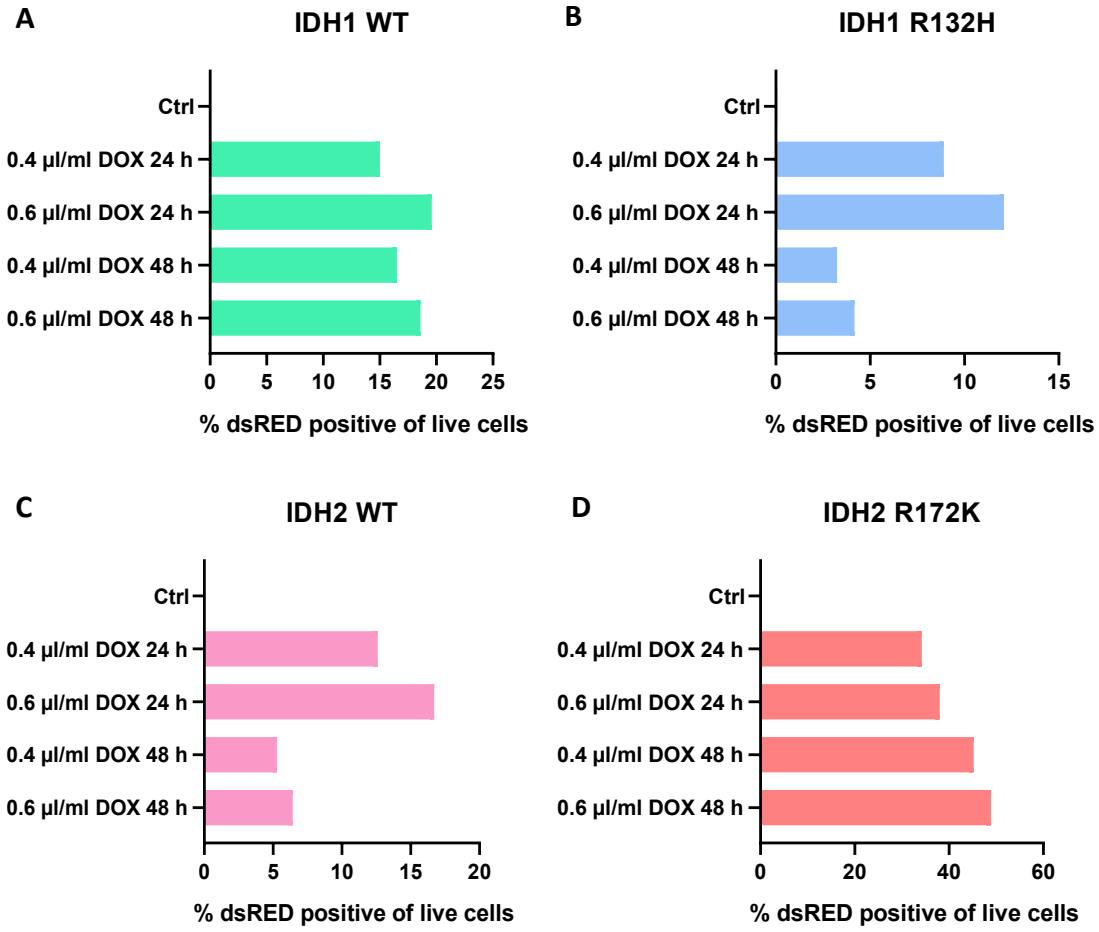

Fig. 43A-D: Intracellular detection of dsRED expression in OCI-M2 cells with inducible overexpression of IDH1 WT, IDH1 R132H, IDH2 WT and IDH2 R172K genes after four treatment conditions: a 24-hour treatment with 0.4 µg/ml doxycycline (0.4 µl/ml DOX 24 h), a 24-hour treatment with 0.6 µg/ml doxycycline (0.6 µl/ml DOX 24 h), a 48-hour treatment with 0.4 µg/ml doxycycline (0.4 µl/ml DOX 48 h) and a 48-hour

treatment with 0.6 µg/ml doxycycline (0.6 µl/ml DOX 48 h), shown as the percentage (%) of dsRED positive cells of all live cells.

Additionally, we isolated the dsRED positive cells through fluorescence-activated cell sorting (FACS) and performed a Western blot analysis to validate the presence of the 3xFLAG-tagged transgenic IDH proteins in the transfected cells following treatment with 0.6 µl/ml Dox for 24 hours. Using a primary antibody specifically binding the Flag peptide, we successfully verified the expression of transgenic IDH proteins in each of the clones (Fig. 44).

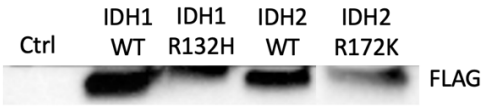

Fig. 44: Immunodetection of FLAG in OCI-M2 cells with inducible overexpression of IDH1 WT, IDH1 R132H, IDH2 WT and IDH2 R172K genes after a 24-hour treatment with 0.6 µg/ml doxycycline.

To measure the oxidative state of the transfected cells, we utilised flow cytometry using the CM-H2DCFDA probe for detecting the oxidative state and ThiolTracker for GSH detection in the samples treated with 0.6 µl/ml Dox for 24 hours. After excluding dead cells using 7-amino actinomycin D (7-AAD), we distinguished populations of dsRED-positive (containing the transfected genes) and dsRED-negative (cells lacking transfected gene expression) based on the PE channel signal. We found a significant decrease in the oxidative state (Fig. 45A) of dsRED-positive cells overexpressing IDH2 WT, accompanied by increased GSH levels (Fig. 45B). Cells overexpressing IDH2 R172K exhibited an even more pronounced decrease in the oxidative state (Fig. 45A) and GSH levels (Fig. 45B). No significant changes were observed in IDH1 overexpressing cells.

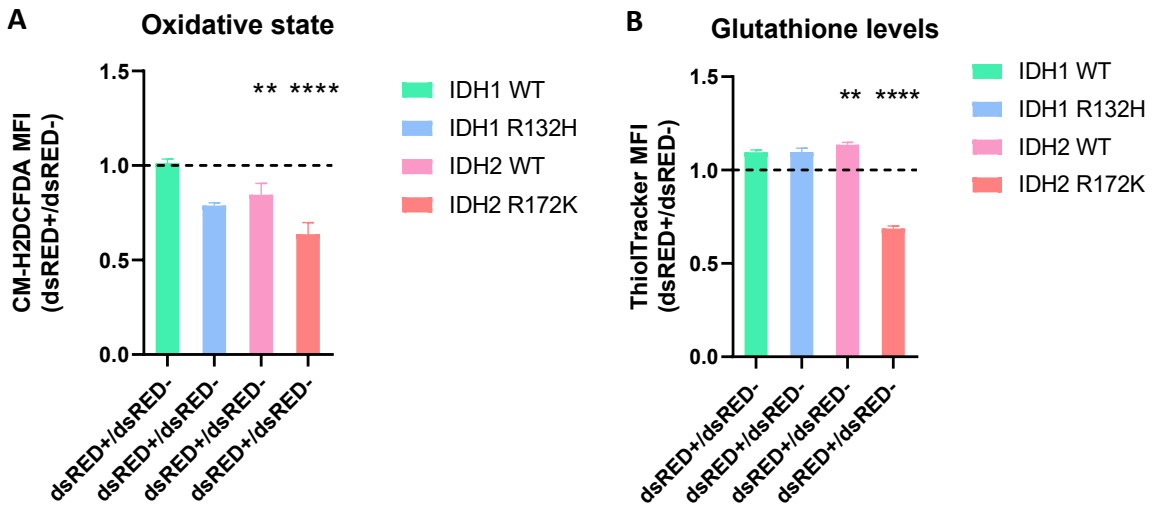

Fig. 45A, B: Intracellular detection of reactive oxidative state (A) and glutathione (B) in OCI-M2 cells with inducible overexpression of IDH1 WT, IDH1 R132H, IDH2 WT and IDH2 R172K, treated with 0.6 µg/ml doxycycline for 24 hours and categorising the events measured based on the presence of dsRED expression (dsRED positive (+) and dsRED negative (-)), displayed as dsRED+/dsRED- ratio of mean fluorescence intensity (MFI).

6 Discussion

Therapy of myelodysplastic syndrome (MDS) and acute myeloid leukaemia (AML) remains challenging, primarily due to the frequent development of drug resistance (Rodriguez-Sevilla, Adema et al. 2023). Enhanced cellular antioxidant system has been shown to drive therapy resistance in AML (Hu, Lu et al. 2010). In this work we studied the redox-related mechanisms underlying resistance to combined 5-azacytidine (AZA)-mediated hypomethylation therapy with Pevonedistat. Our study investigates the impact of NRF2 on redox homeostasis and its role in multi-resistance in MDS upon progression to AML. We found that while NRF2 inhibition impaired the therapeutic effects of AZA and its combination with Pevo, highlighting NRF2's crucial role in therapy efficacy, paradoxically, NRF2 activation was also implicated in resistance to this combined therapy. We observed alterations in the oxidative state during resistance development and potential redox-mediated regulation of autophagy in resistant cells.

AZA is a first-line treatment for MDS and AML and combining it with other agents is a strategy used to increase therapeutic efficacy. One such combination involves AZA with Pevo, which targets the ubiquitin-proteasomal system by inhibiting NEDDylation. We worked with cells resistant to AZA (AZA-R) and cells partially (PEVO-PR) and completely (PEVO-R) resistant to Pevo (Fig. 16). Both PEVO-PR and PEVO-R cells were developed from AZA-R cells and therefore also harbour resistance to AZA. PEVO-PR cells have undergone long-term exposure to Pevo and thus represent an intermediate stage of resistance development, although still exhibiting sensitivity to Pevo.

Our data showed that both AZA and Pevo can alter redox homeostasis in MDS/AML cells. Both drugs increased GSH levels within 24 hours (Fig. 13B, 14B). The impact of nucleoside analogues on redox homeostasis in leukemic cells has been previously described (Fandy, Jiemjit et al. 2014, Montes, Guerra-Librero et al. 2022). One possible explanation for AZA-induced GSH elevation is the activation of defence systems to protect cells against AZA-associated damage (Laranjeira, Hollingshead et al. 2023). Pevo's ability to activate NRF2 and induce the expression of proteins involved in GSH metabolism has been reported

(Andérica-Romero, Hernández-Damián et al. 2016, Jones, Espitia et al. 2023). Therefore, Pevo's effect on GSH levels likely arises from NRF2 activation. Since the studied drugs had a significant impact on redox homeostasis in Pevo-sensitive MDS/AML cells, we investigated whether redox changes play a role in the development of resistance to Pevo. Interestingly, while PEVO-R cells showed no significant alterations in the oxidative state in comparison to AZA-R, cells in the pre-resistant stage (PEVO-PR) exhibited a significant reduction in both ROS and GSH levels compared to PEVO-R and AZA-R cells (Fig. 17A-C). Notably, Pevo treatment induced a distinct oxidative response of AZA-R and PEVO-PR cells (Fig. 21). PEVO-PR cells reacted to Pevo treatment solely by increasing GSH levels (Fig. 21B), consistently with our results from sensitive OCI-M2 cells (Fig. 14B). In contrast, AZA-R cells exhibited decreased ROS levels with no changes in GSH (Fig. 21B, C), suggesting a differential utilisation of newly generated GSH after Pevo treatment. Overall, these findings indicate that at this stage of resistance development, PEVO-PR cells still respond to Pevo with changes in the redox state, unlike the fully resistant PEVO-R cells.

To investigate how Pevo modulates redox homeostasis in Pevo sensitive and resistant MDS/AML cells, we estimated their NRF2 activity. The transcription factor NRF2 is a master regulator of the antioxidant response, controlling expression of genes involved in antioxidant defence (Suzuki, Takahashi et al. 2023). To detect its activity, we measured the nuclear accumulation of NRF2 and the expression of its target protein, NQO1, as described previously (Su, Yang et al. 2021). While our nuclear fraction isolation was successful (showing a minimal presence of the cytosolic protein actin), the cytosolic fraction showed significant levels of the nuclear marker histone H3 (Fig. 18A). Despite this limitation, due to the primary focus on nuclear NRF2 translocation and simultaneous detection of NQO1, we believe that our results reliably reflect the activity of NRF2. In our study, we detected enhanced steady-state activity of NRF2 in PEVO-R cells compared to AZA-R cells sensitive to Pevo (Fig. 18). Interestingly, Pevo treatment induced NRF2 activation in both AZA-R cells and PEVO-PR cells, as evidenced by increased nuclear NRF2 and cytosolic NQO1 levels (Fig. 19, 20). However, PEVO-R cells, which harbour a specific mutation preventing their response to Pevo (as determined by our whole-exome sequencing, data not shown), did not exhibit NRF2 activation in response to Pevo (Fig. 19, 20). Aberrant NRF2 activation has

been shown to promote chemotherapy resistance in various cancers, including AML and MDS (Homma, Ishii et al. 2009, Zheng, Nong et al. 2015, Syu, Chi et al. 2016, Lin, Ren et al. 2019, Mukhopadhyay, Goswami et al. 2020, Hu, Pan et al. 2022). Importantly, we confirmed that Pevo sensitised OCI-M2 cells to AZA through an NRF2-dependent mechanism. Notably, NRF2 inhibition also diminished the response of leukemic cells to AZA alone, highlighting the significance of NRF2 in AZA's mechanism of action (Fig. 15). These findings indicate that the NRF2-mediated antioxidant response is essential for the cytotoxicity of both AZA and Pevo. PEVO-R cells showed a decreased sensitivity to NRF2 inhibition (Fig. 37, 38). These results suggest a dysregulated NRF2 activation in these multi-resistant cells, with the increased levels compensating for NRF2 inhibition. However, the exact mechanism behind the constitutive activation of NRF2 is yet to be determined. Our findings reveal a complex and context-dependent role of NRF2 in AML therapy response. The increased NRF2 activation in PEVO-R cells suggested an important role of NRF2 in resistance to AZA and Pevo, while broad NRF2 inhibition significantly reduced the response of OCI-M2 cells to AZA alone and its combination with Pevo. This underscores the potential harm of non-specific NRF2 targeting and highlights the need for strategies that precisely modulate NRF2 activity for optimal therapy results.

To gain deeper insights into the role of redox homeostasis in Pevo treatment and resistance, we applied a redox proteomics mass spectrometry-based approach (Pan, Chen et al. 2014). We monitored changes in the oxidation rate of specific cysteine residues in AZA-R cells treated with Pevo and in untreated PEVO-R cells, using AZA-R as a common control. We identified 25,309 cysteine-containing peptides and quantified an average of 9,000 cysteine peptides (Fig. 23). Considering cysteine's low abundance in proteins (approximately 2% in humans) (Miseta and Csutora 2000), this represents a high coverage compared to similar studies (Fu, Liu et al. 2017, van der Reest, Lilla et al. 2018, Zamorano Cuervo, Fortin et al. 2021). This comprehensive dataset enabled us to study the influence of Pevo treatment and resistance on protein oxidation within the context of AZA resistance. Our proteomics data showed that Pevo treatment slightly increased the median oxidation of the proteome (Fig. 24), contradicting our flow cytometry findings that showed a decreased oxidative state (Fig. 21A). This highlights that oxidative modifications of protein thiols are tightly controlled and

do not solely reflect the global oxidative state. Redox proteomics allowed us to depict the consequences of subtle redox changes on specific proteins.

Cysteine oxidation is a crucial post-translational modification that influences protein function, stability and interactions, providing detailed insight into the cellular redox state (Sies and Jones 2020). We identified 328 cysteine peptides with significantly altered oxidation after Pevo treatment (Fig. 25) and 241 cysteine peptides with different oxidation state associated with Pevo resistance (Fig. 26). Gene ontology analysis revealed that proteins with increased oxidation following Pevo treatment were involved in regulating protein metabolic processes, cellular response to chemical stimulus, cell cycle, DNA replication or cell migration. Conversely, proteins showing decreased oxidation were found in proteins regulating mitotic spindle organisation, amide biosynthetic process, platelet aggregation or ATP synthesis coupled electron transport (Fig. 30). Pevo resistance showed most significantly increased oxidation in proteins regulating cellular response to chemical stimulus, protein metabolic process, DNA replication, transport, transmembrane receptor protein tyrosine kinase signalling pathway and programmed cell death. Decreased oxidation was seen primarily in proteins involved in nucleobase-containing small molecule metabolic process, chromosome organisation, and nicotinamide nucleotide metabolic process organophosphate metabolic process (Fig. 31)**.** All these biological processes are known to be redox regulated (Tomin, Schittmayer et al. 2021, Pimkova, Jassinskaja et al. 2022, Salovska, Kondelova et al. 2022). The modifications in these processes could potentially play a role in adaptation mechanisms of cells with Pevo resistance and will be the subject of further analysis. In this study, we focused on the findings of oxidative modifications in autophagy, as we found an interesting modification possibly regulating autophagy activity in Pevo resistance.

Our analysis revealed significant changes in cysteine oxidation of proteins involved in autophagy in both Pevo-treated and Pevo-resistant cells. Pevo treatment induced the oxidation of 11 autophagy-related proteins (Fig. 33), while Pevo resistance was associated with increased oxidation of 7 proteins and decreased oxidation of 4 proteins involved in autophagy (Fig. 34). Among the autophagic proteins with significantly oxidised thiols in

AZA-R cells treated with Pevo was KEAP1, a critical regulator of NRF2. Specifically, we found increased oxidation of KEAP1 cysteines 23 and 38. KEAP1 contains seven identified stress-sensing cysteines (151, 226, 273, 288, 613, 622, 624) whose oxidation leads to NRF2 release and subsequent translocation to the nucleus (Suzuki, Takahashi et al. 2023). Here, it activates various genes, including those involved in autophagy activation, such as the autophagy receptor Sequestosome 1 (SQSTM1, also called p62). Although the identified oxidative state of the KEAP1 cysteines was not associated with NRF2 activation, rather than individual cysteines, the overall redox cysteine code of KEAP1 is considered to play a role in redox sensing (Yamamoto, Suzuki et al. 2008).

Our analysis revealed a particularly interesting finding – a significantly increased oxidation of SQSTM1 in PEVO-R cells (Fig. 34). This oxidation occurred at cysteines 26, 27, 44, 289, 290, and 331. SQSTM1, an NRF2 target, is a crucial autophagy receptor that targets ubiquitinated proteins for degradation (Pajares, Jiménez-Moreno et al. 2016). It sequesters these proteins into SQSTM1 droplets, fusing with autophagosomes and ultimately lysosomes, where degradation occurs. Research suggests that cysteine oxidation can regulate SQSTM1's function, potentially influencing autophagy activation (Carroll, Otten et al. 2018). Importantly, recent work by Huang, Yao et al. demonstrated that a specific reversible cysteine modification, S-acylation, at cysteines 289 and 290 is essential for the autophagic degradation of SQSTM1 droplets (Huang, Yao et al. 2023). Huang et al. showed that S-acylation increases the hydrophobicity of SQSTM1, increasing its affinity for microtubule-associated protein 1 light chain 3 (LC3)-positive membranes and promotes the localisation of SQSTM1 to sites of autophagic degradation. Changes in the cysteines' S-acylation and deacylation process serve as a regulatory mechanism for recruiting SQSTM1 droplets to the autophagic membrane, controlling the autophagy of ubiquitinated proteins (Huang, Yao et al. 2023). We detected autophagy using immunodetection and observed that PEVO-R cells exhibited a more active autophagy process compared to AZA-R cells (Fig. 35B). Furthermore, they were more sensitive to autophagy inhibition by chloroquine (Fig. 36). These findings suggest an increased autophagy activity in PEVO-R cells along with an increased dependency on this process. While our redox proteomics method cannot distinguish between specific reversible modifications, the increased oxidation of SQSTM1

cysteines 289 and 290 suggests a potential regulatory role of oxidation in autophagy. Further experiments are needed to distinguish the modification type and its role in autophagy regulation. However, given the increased autophagic activity observed in PEVO-R cells (Fig. 35B), we hypothesise that the modifications we observed on SQSTM1 represent acylation and lead to autophagy activation.

The ubiquitin-proteasome system (UPS) and autophagy are the two major pathways for clearing ubiquitinated proteins in cells. Autophagy can be induced as a compensatory mechanism when the UPS is inhibited, highlighting the complex interplay between these systems (Sun-Wang, Ivanova et al. 2020). The exact mechanism behind this compensation is still under investigation, but the NRF2 accumulation in response to proteasomal inhibition might play an important role as NRF2 activates the expression of autophagy genes (Kageyama, Sou et al. 2014, Pajares, Jiménez-Moreno et al. 2016, Sun-Wang, Ivanova et al. 2020). To investigate the interplay between autophagy and proteasomal degradation in Pevo resistance, we measured the sensitivity of PEVO-R cells to the proteasome inhibitor Bortezomib. Our findings demonstrate that PEVO-R cells are more sensitive to proteasomal inhibition compared to AZA-R cells (Fig. 39, 40). These findings indicate a higher dependency of PEVO-R cells on protein clearance by both autophagy and the UPS.

We aimed to investigate the role of isocitrate dehydrogenase 1 (IDH1) and 2 (IDH2) mutations in AML therapy response. These mutations, found in approximately 20% of AML patients, have been associated with leukemogenesis (Chaturvedi, Araujo Cruz et al. 2013, Medeiros, Fathi et al. 2017). Importantly, IDH mutations directly impair redox homeostasis by depleting NADPH, a crucial cofactor for the regeneration of antioxidants. Studies in gliomas have shown altered ROS and GSH levels, as well as increased NRF2 activation, in IDH1 mutant cells (Shi, Sun et al. 2015, Gelman, Naser et al. 2018, Mugoni, Panella et al. 2019). These findings led us to hypothesise that IDH1/2 mutations can promote therapy resistance in MDS/AML patients through increased NRF2 activity. The observation that patients with these mutations respond better to combined AZA and venetoclax (Ven) supports our hypothesis, as Ven has been shown to inhibit NRF2 (DiNardo, Rausch et al. 2018, Nguyen, Troadec et al. 2019, Lou, Shao et al. 2020).To investigate this further, we

successfully cloned *IDH1 WT*, *IDH R132H*, *IDH2 WT* and *IDH2 R172K* genes into a doxycycline (Dox)-inducible expression system with dsRED and Puromycin selection (Fig. 41). We validated the constructs and generated OCI-M2 leukemic cells with stable Dox-inducible expression of these IDH variants. Even though we validated the presence of IDH-expressing cells via FLAG immunodetection (Fig. 44) and dsRED detection by Flow cytometry, we observed a consistent loss of transfected gene expression over time (Fig. 42A, B). Despite this setback, we obtained interesting preliminary data on the oxidative state of these cells. Overexpression of either IDH2 WT or IDH2 R172K led to a decreased oxidative state compared to wild-type cells (Fig. 45A). Interestingly, IDH2 R172K overexpression was associated with decreased GSH levels (Fig. 45B), potentially reflecting NADPH depletion. These findings align with studies of IDH1-mutant gliomas, further underscoring the impact of IDH mutations on redox balance (Shi, Sun et al. 2015, Tang, Fu et al. 2020). Our results highlight the need for more AML-specific research to fully understand the alterations in the redox state of IDH-mutant cells. We plan to optimise our transfection methods to achieve stable *IDH* gene expression, enabling further investigation of the interplay between IDH mutations, NRF2 activity, and drug resistance.

In this work, we highlighted the complex and context-dependent role of NRF2 in the OCI-M2 cell line's response to combined AZA and Pevo therapy. Our findings demonstrate that while NRF2 inhibition disrupts the therapeutic efficacy of both AZA alone and its combination with Pevo, increased NRF2 activation is associated with resistance to this combined therapy. We further emphasise the importance of protein redox signalling in the adaptive processes occurring in both pre-resistant and fully resistant cells. These findings underscore the need for therapeutic strategies that enable precise and controlled modulation of NRF2 activity and redox homeostasis. Such strategies hold the potential to enhance treatment efficacy while minimising the development of drug resistance.

7 Conclusions

The role of NRF2 in response to anti-leukemic therapy remains complex and not yet fully understood. NRF2 is primarily recognised as a key regulator of antioxidant responses, however, its aberrant activation has also been linked to cancer progression and resistance to chemotherapy. This study investigated the function of NRF2 in sensitivity to combined therapy with 5-azacytidine (AZA) and pevonedistat (Pevo) in MDS/AML cells.

Overview of our most significant results:

1. We have found that Pevo treatment sensitised OCI-M2 cells to AZA through an NRF2-dependent mechanism. NRF2 inhibition impaired the therapeutic efficacy of both AZA and AZA combined with Pevo in OCI-M2 cells.
2. We showed that both AZA and Pevo can alter the redox homeostasis of MDS/AML cells in contrast to resistant cells.
3. We observed that the development of Pevo resistance was associated with the activation of the antioxidant GSH.
4. We observed that Pevo treatment induced NRF2 activation and redox changes in PEVO-PR cells, while PEVO-R cells showed no alterations after the treatment.
5. We found that cells harbouring dual resistance to AZA and Pevo (PEVO-R) showed increased activation of NRF2 and decreased sensitivity to NRF2 inhibition.
6. Applying a redox proteomics approach, we detected increased median protein thiol oxidation in Pevo-sensitive cells after Pevo treatment, one of them being KEAP1, a key regulator of NRF2.
7. We showed that PEVO-R cells displayed an increased dependency on autophagy along with its enhanced activity, possibly regulated by the increased oxidation of Cys289 and Cys290 on Sequestosome 1 (SQSTM1) identified in these cells.
8. We observed an increased dependency of PEVO-R cells on the ubiquitin-proteasome system (UPS), suggesting a dependency of these cells on the turnover of ubiquitylated proteins through both the UPS and autophagy.

9. We successfully cloned *IDH1 WT*, *IDH R132H*, *IDH2 WT* and *IDH2 R172K* genes into a sleeping beauty transposon vector with an inducible expression and transfected OCI-M2 cells with these plasmids.
10. We showed that the IDH2 R172K mutated gene overexpression is associated with significantly decreased GSH levels, implicating the impact of IDH2 mutation on the redox state of AML cells.

8 References

SEER*Explorer: An interactive website for SEER cancer statistics [Internet]. Surveillance Research Program, National Cancer Institute; 2023 Apr 19. [updated: 2023 Nov 16; cited 2023 Nov 22]. Available from: https://seer.cancer.gov/statistics-network/explorer/. Data source(s): SEER Incidence Data, November 2022 Submission (1975-2020), SEER 22 registries.

Adès, L., L. Girshova, V. A. Doronin, M. Díez-Campelo, D. Valcárcel, S. Kambhampati, N. A. Viniou, D. Woszczyk, R. De Paz Arias, A. Symeonidis, A. Anagnostopoulos, E. C. Munhoz, U. Platzbecker, V. Santini, R. J. Fram, Y. Yuan, S. Friedlander, D. V. Faller and M. A. Sekeres (2022). "Pevonedistat plus azacitidine vs azacitidine alone in higher-risk MDS/chronic myelomonocytic leukemia or low-blast-percentage AML." Blood Adv **6**(17): 5132-5145.

Aimiuwu, J., H. Wang, P. Chen, Z. Xie, J. Wang, S. Liu, R. Klisovic, A. Mims, W. Blum, G. Marcucci and K. K. Chan (2012). "RNA-dependent inhibition of ribonucleotide reductase is a major pathway for 5-azacytidine activity in acute myeloid leukemia." Blood **119**(22): 5229-5238.

Al-Gayyar, M. M., L. A. Eissa, A. M. Rabie and A. M. El-Gayar (2007). "Measurements of oxidative stress status and antioxidant activity in chronic leukaemia patients." J Pharm Pharmacol **59**(3): 409-417.

Al-Khallaf, H. (2017). "Isocitrate dehydrogenases in physiology and cancer: biochemical and molecular insight." Cell Biosci **7**: 37.

Andérica-Romero, A. C., J. Hernández-Damián, G. I. Vázquez-Cervantes, I. Torres, I. G. González-Herrera and J. Pedraza-Chaverri (2016). "The MLN4924 inhibitor exerts a neuroprotective effect against oxidative stress injury via Nrf2 protein accumulation." Redox Biol **8**: 341-347.

Asić, K. (2016). "Dominant mechanisms of primary resistance differ from dominant mechanisms of secondary resistance to targeted therapies." Crit Rev Oncol Hematol **97**: 178-196.

Ball, B. J., C. A. Famulare, E. M. Stein, M. S. Tallman, A. Derkach, M. Roshal, S. I. Gill, B. M. Manning, J. Koprivnikar, J. McCloskey, R. Testi, T. Prebet, N. H. Al Ali, E. Padron, D. A. Sallman, R. S. Komrokji and A. D. Goldberg (2020). "Venetoclax and hypomethylating agents (HMAs) induce high response rates in MDS, including patients after HMA therapy failure." Blood Adv **4**(13): 2866-2870.

Barja, G. and A. Herrero (1998). "Localization at complex I and mechanism of the higher free radical production of brain nonsynaptic mitochondria in the short-lived rat than in the longevous pigeon." J Bioenerg Biomembr **30**(3): 235-243.

Battisti, V., L. D. Maders, M. D. Bagatini, K. F. Santos, R. M. Spanevello, P. A. Maldonado, A. O. Brulé, M. o. C. Araújo, M. R. Schetinger and V. M. Morsch (2008). "Measurement of oxidative stress and antioxidant status in acute lymphoblastic leukemia patients." Clin Biochem **41**(7-8): 511-518.

Biteau, B., J. Labarre and M. B. Toledano (2003). "ATP-dependent reduction of cysteine-sulphinic acid by S. cerevisiae sulphiredoxin." Nature **425**(6961): 980-984.

Bleeker, F. E., N. A. Atai, S. Lamba, A. Jonker, D. Rijkeboer, K. S. Bosch, W. Tigchelaar, D. Troost, W. P. Vandertop, A. Bardelli and C. J. Van Noorden (2010). "The prognostic IDH1(R132) mutation is associated with reduced NADP+-dependent IDH activity in glioblastoma." Acta Neuropathol **119**(4): 487-494.

Bordi, M., R. De Cegli, B. Testa, R. A. Nixon, A. Ballabio and F. Cecconi (2021). "A gene toolbox for monitoring autophagy transcription." Cell Death Dis **12**(11): 1044.

Canning, P., F. J. Sorrell and A. N. Bullock (2015). "Structural basis of Keap1 interactions with Nrf2." Free Radic Biol Med **88**(Pt B): 101-107.

Carroll, B., E. G. Otten, D. Manni, R. Stefanatos, F. M. Menzies, G. R. Smith, D. Jurk, N. Kenneth, S. Wilkinson, J. F. Passos, J. Attems, E. A. Veal, E. Teyssou, D. Seilhean, S. Millecamps, E. L. Eskelinen, A. K. Bronowska, D. C. Rubinsztein, A. Sanz and V. I. Korolchuk (2018). "Oxidation of

SQSTM1/p62 mediates the link between redox state and protein homeostasis." Nat Commun **9**(1): 256.
Castro, I., B. Sampaio-Marques and P. Ludovico (2019). "Targeting Metabolic Reprogramming in Acute Myeloid Leukemia." Cells **8**(9).
Challen, G. A. and M. A. Goodell (2020). "Clonal hematopoiesis: mechanisms driving dominance of stem cell clones." Blood **136**(14): 1590-1598.
Chandel, N. S. (2021). "NADPH-The Forgotten Reducing Equivalent." Cold Spring Harb Perspect Biol **13**(6).
Chaturvedi, A., M. M. Araujo Cruz, N. Jyotsana, A. Sharma, H. Yun, K. Görlich, M. Wichmann, A. Schwarzer, M. Preller, F. Thol, J. Meyer, R. Haemmerle, E. A. Struys, E. E. Jansen, U. Modlich, Z. Li, L. M. Sly, R. Geffers, R. Lindner, D. J. Manstein, U. Lehmann, J. Krauter, A. Ganser and M. Heuser (2013). "Mutant IDH1 promotes leukemogenesis in vivo and can be specifically targeted in human AML." Blood **122**(16): 2877-2887.
Chen, C., Y. Liu, C. Lu, J. R. Cross, J. P. Morris, A. S. Shroff, P. S. Ward, J. E. Bradner, C. Thompson and S. W. Lowe (2013). "Cancer-associated IDH2 mutants drive an acute myeloid leukemia that is susceptible to Brd4 inhibition." Genes Dev **27**(18): 1974-1985.
Chiou, J. T., C. C. Hsu, Y. C. Hong, Y. C. Lee and L. S. Chang (2023). "Cytarabine-induced destabilization of MCL1 mRNA and protein triggers apoptosis in leukemia cells." Biochem Pharmacol **211**: 115494.
Creusot, F., G. Acs and J. K. Christman (1982). "Inhibition of DNA methyltransferase and induction of Friend erythroleukemia cell differentiation by 5-azacytidine and 5-aza-2'-deoxycytidine." J Biol Chem **257**(4): 2041-2048.
Dalle-Donne, I., R. Rossi, D. Giustarini, R. Colombo and A. Milzani (2007). "S-glutathionylation in protein redox regulation." Free Radic Biol Med **43**(6): 883-898.
Dang, L., D. W. White, S. Gross, B. D. Bennett, M. A. Bittinger, E. M. Driggers, V. R. Fantin, H. G. Jang, S. Jin, M. C. Keenan, K. M. Marks, R. M. Prins, P. S. Ward, K. E. Yen, L. M. Liau, J. D. Rabinowitz, L. C. Cantley, C. B. Thompson, M. G. Vander Heiden and S. M. Su (2009). "Cancer-associated IDH1 mutations produce 2-hydroxyglutarate." Nature **462**(7274): 739-744.
Day, N. J., M. J. Gaffrey and W. J. Qian (2021). "Stoichiometric Thiol Redox Proteomics for Quantifying Cellular Responses to Perturbations." Antioxidants (Basel) **10**(3).
DiNardo, C. D., B. A. Jonas, V. Pullarkat, M. J. Thirman, J. S. Garcia, A. H. Wei, M. Konopleva, H. Döhner, A. Letai, P. Fenaux, E. Koller, V. Havelange, B. Leber, J. Esteve, J. Wang, V. Pejsa, R. Hájek, K. Porkka, Á. Illés, D. Lavie, R. M. Lemoli, K. Yamamoto, S. S. Yoon, J. H. Jang, S. P. Yeh, M. Turgut, W. J. Hong, Y. Zhou, J. Potluri and K. W. Pratz (2020). "Azacitidine and Venetoclax in Previously Untreated Acute Myeloid Leukemia." N Engl J Med **383**(7): 617-629.
DiNardo, C. D., K. Pratz, V. Pullarkat, B. A. Jonas, M. Arellano, P. S. Becker, O. Frankfurt, M. Konopleva, A. H. Wei, H. M. Kantarjian, T. Xu, W. J. Hong, B. Chyla, J. Potluri, D. A. Pollyea and A. Letai (2019). "Venetoclax combined with decitabine or azacitidine in treatment-naive, elderly patients with acute myeloid leukemia." Blood **133**(1): 7-17.
DiNardo, C. D., C. R. Rausch, C. Benton, T. Kadia, N. Jain, N. Pemmaraju, N. Daver, W. Covert, K. R. Marx, M. Mace, E. Jabbour, J. Cortes, G. Garcia-Manero, F. Ravandi, K. N. Bhalla, H. Kantarjian and M. Konopleva (2018). "Clinical experience with the BCL2-inhibitor venetoclax in combination therapy for relapsed and refractory acute myeloid leukemia and related myeloid malignancies." Am J Hematol **93**(3): 401-407.
DiNardo, C. D., A. C. Schuh, E. M. Stein, P. Montesinos, A. H. Wei, S. de Botton, A. M. Zeidan, A. T. Fathi, H. M. Kantarjian, J. M. Bennett, M. G. Frattini, P. Martin-Regueira, F. Lersch, J. Gong, M. Hasan, P. Vyas and H. Döhner (2021). "Enasidenib plus azacitidine versus azacitidine alone in patients with newly diagnosed, mutant-IDH2 acute myeloid leukaemia (AG221-AML-005): a single-arm, phase 1b and randomised, phase 2 trial." Lancet Oncol **22**(11): 1597-1608.
DiNardo, C. D. and A. H. Wei (2020). "How I treat acute myeloid leukemia in the era of new drugs." Blood **135**(2): 85-96.

Er, T. K., S. M. Tsai, S. H. Wu, W. Chiang, H. C. Lin, S. F. Lin, L. Y. Tsai and T. Z. Liu (2007). "Antioxidant status and superoxide anion radical generation in acute myeloid leukemia." Clin Biochem **40**(13-14): 1015-1019.
Etienne, A., B. Esterni, A. Charbonnier, M. J. Mozziconacci, C. Arnoulet, D. Coso, B. Puig, J. A. Gastaut, D. Maraninchi and N. Vey (2007). "Comorbidity is an independent predictor of complete remission in elderly patients receiving induction chemotherapy for acute myeloid leukemia." Cancer **109**(7): 1376-1383.
Fandy, T. E., A. Jiemjit, M. Thakar, P. Rhoden, L. Suarez and S. D. Gore (2014). "Decitabine induces delayed reactive oxygen species (ROS) accumulation in leukemia cells and induces the expression of ROS generating enzymes." Clin Cancer Res **20**(5): 1249-1258.
Fathi, A. T. (2018). "Pevonedistat, a new partner for 5-azacitidine." Blood **131**(13): 1391-1392.
Forman, H. J., H. Zhang and A. Rinna (2009). "Glutathione: overview of its protective roles, measurement, and biosynthesis." Mol Aspects Med **30**(1-2): 1-12.
Fu, L., K. Liu, M. Sun, C. Tian, R. Sun, C. Morales Betanzos, K. A. Tallman, N. A. Porter, Y. Yang, D. Guo, D. C. Liebler and J. Yang (2017). "Systematic and Quantitative Assessment of Hydrogen Peroxide Reactivity With Cysteines Across Human Proteomes." Mol Cell Proteomics **16**(10): 1815-1828.
Garcia-Manero, G. (2023). "Myelodysplastic syndromes: 2023 update on diagnosis, risk-stratification, and management." Am J Hematol **98**(8): 1307-1325.
Gelman, S. J., F. Naser, N. G. Mahieu, L. D. McKenzie, G. P. Dunn, M. G. Chheda and G. J. Patti (2018). "Consumption of NADPH for 2-HG Synthesis Increases Pentose Phosphate Pathway Flux and Sensitizes Cells to Oxidative Stress." Cell Rep **22**(2): 512-522.
Geurts, A. M., Y. Yang, K. J. Clark, G. Liu, Z. Cui, A. J. Dupuy, J. B. Bell, D. A. Largaespada and P. B. Hackett (2003). "Gene transfer into genomes of human cells by the sleeping beauty transposon system." Mol Ther **8**(1): 108-117.
Ghezzi, P. (2013). "Protein glutathionylation in health and disease." Biochim Biophys Acta **1830**(5): 3165-3172.
Greenberg, P. L., H. Tuechler, J. Schanz, G. Sanz, G. Garcia-Manero, F. Solé, J. M. Bennett, D. Bowen, P. Fenaux, F. Dreyfus, H. Kantarjian, A. Kuendgen, A. Levis, L. Malcovati, M. Cazzola, J. Cermak, C. Fonatsch, M. M. Le Beau, M. L. Slovak, O. Krieger, M. Luebbert, J. Maciejewski, S. M. Magalhaes, Y. Miyazaki, M. Pfeilstöcker, M. Sekeres, W. R. Sperr, R. Stauder, S. Tauro, P. Valent, T. Vallespi, A. A. van de Loosdrecht, U. Germing and D. Haase (2012). "Revised international prognostic scoring system for myelodysplastic syndromes." Blood **120**(12): 2454-2465.
Gu, X., R. Tohme, B. Tomlinson, N. Sakre, M. Hasipek, L. Durkin, C. Schuerger, D. Grabowski, A. M. Zidan, T. Radivoyevitch, C. Hong, H. Carraway, B. Hamilton, R. Sobecks, B. Patel, B. K. Jha, E. D. Hsi, J. Maciejewski and Y. Sauntharajah (2021). "Decitabine- and 5-azacytidine resistance emerges from adaptive responses of the pyrimidine metabolism network." Leukemia **35**(4): 1023-1036.
Haferlach, T., Y. Nagata, V. Grossmann, Y. Okuno, U. Bacher, G. Nagae, S. Schnittger, M. Sanada, A. Kon, T. Alpermann, K. Yoshida, A. Roller, N. Nadarajah, Y. Shiraishi, Y. Shiozawa, K. Chiba, H. Tanaka, H. P. Koeffler, H. U. Klein, M. Dugas, H. Aburatani, A. Kohlmann, S. Miyano, C. Haferlach, W. Kern and S. Ogawa (2014). "Landscape of genetic lesions in 944 patients with myelodysplastic syndromes." Leukemia **28**(2): 241-247.
He, F., X. Ru and T. Wen (2020). "NRF2, a Transcription Factor for Stress Response and Beyond." Int J Mol Sci **21**(13).
Hedley, D. W., E. A. McCulloch, M. D. Minden, S. Chow and J. Curtis (1998). "Antileukemic action of buthionine sulfoximine: evidence for an intrinsic death mechanism based on oxidative stress." Leukemia **12**(10): 1545-1552.
Hole, P. S., J. Zabkiewicz, C. Munje, Z. Newton, L. Pearn, P. White, N. Marquez, R. K. Hills, A. K. Burnett, A. Tonks and R. L. Darley (2013). "Overproduction of NOX-derived ROS in AML promotes proliferation and is associated with defective oxidative stress signaling." Blood **122**(19): 3322-3330.

Homma, S., Y. Ishii, Y. Morishima, T. Yamadori, Y. Matsuno, N. Haraguchi, N. Kikuchi, H. Satoh, T. Sakamoto, N. Hizawa, K. Itoh and M. Yamamoto (2009). "Nrf2 enhances cell proliferation and resistance to anticancer drugs in human lung cancer." Clin Cancer Res **15**(10): 3423-3432.
Hong, F., M. L. Freeman and D. C. Liebler (2005). "Identification of sensor cysteines in human Keap1 modified by the cancer chemopreventive agent sulforaphane." Chem Res Toxicol **18**(12): 1917-1926.
Horie, Y., T. Suzuki, J. Inoue, T. Iso, G. Wells, T. W. Moore, T. Mizushima, A. T. Dinkova-Kostova, T. Kasai, T. Kamei, S. Koshiba and M. Yamamoto (2021). "Molecular basis for the disruption of Keap1-Nrf2 interaction via Hinge & Latch mechanism." Commun Biol **4**(1): 576.
Hu, T., C. Pan, T. Zhang, M. Ni, W. Wang, S. Zhang, Y. Chen, J. Wang and Q. Fang (2022). "Nrf2 overexpression increases the resistance of acute myeloid leukemia to cytarabine by inhibiting replication factor C4." Cancer Gene Ther **29**(11): 1773-1790.
Hu, Y., W. Lu, G. Chen, H. Zhang, Y. Jia, Y. Wei, H. Yang, W. Zhang, W. Fiskus, K. Bhalla, M. Keating, P. Huang and G. Garcia-Manero (2010). "Overcoming resistance to histone deacetylase inhibitors in human leukemia with the redox modulating compound β-phenylethyl isothiocyanate." Blood **116**(15): 2732-2741.
Huang, X., J. Yao, L. Liu, J. Chen, L. Mei, J. Huangfu, D. Luo, X. Wang, C. Lin, X. Chen, Y. Yang, S. Ouyang, F. Wei, Z. Wang, S. Zhang, T. Xiang, D. Neculai, Q. Sun, E. Kong, E. W. Tate and A. Yang (2023). "S-acylation of p62 promotes p62 droplet recruitment into autophagosomes in mammalian autophagy." Mol Cell **83**(19): 3485-3501.e3411.
Iacobini, M., A. Menichelli, G. Palumbo, G. Multari, B. Werner and D. Del Principe (2001). "Involvement of oxygen radicals in cytarabine-induced apoptosis in human polymorphonuclear cells." Biochem Pharmacol **61**(8): 1033-1040.
Itoh, K., T. Chiba, S. Takahashi, T. Ishii, K. Igarashi, Y. Katoh, T. Oyake, N. Hayashi, K. Satoh, I. Hatayama, M. Yamamoto and Y. Nabeshima (1997). "An Nrf2/small Maf heterodimer mediates the induction of phase II detoxifying enzyme genes through antioxidant response elements." Biochem Biophys Res Commun **236**(2): 313-322.
Itoh, K., N. Wakabayashi, Y. Katoh, T. Ishii, K. Igarashi, J. D. Engel and M. Yamamoto (1999). "Keap1 represses nuclear activation of antioxidant responsive elements by Nrf2 through binding to the amino-terminal Neh2 domain." Genes Dev **13**(1): 76-86.
Itoh, K., N. Wakabayashi, Y. Katoh, T. Ishii, T. O'Connor and M. Yamamoto (2003). "Keap1 regulates both cytoplasmic-nuclear shuttling and degradation of Nrf2 in response to electrophiles." Genes Cells **8**(4): 379-391.
Jalali, A., S. Mahmoudi, A. Larki Harchegani, J. Mohammadiasl and A. Ahmadzadeh (2021). "Evaluation of Nrf2, Keap1 and Apoptotic Pathway Genes Expression in Acute Myeloid Leukemia Patients." Iran J Pharm Res **20**(1): 398-407.
Jones, C. L., B. M. Stevens, A. D'Alessandro, R. Culp-Hill, J. A. Reisz, S. Pei, A. Gustafson, N. Khan, J. DeGregori, D. A. Pollyea and C. T. Jordan (2019). "Cysteine depletion targets leukemia stem cells through inhibition of electron transport complex II." Blood **134**(4): 389-394.
Jones, D. P. (2008). "Radical-free biology of oxidative stress." Am J Physiol Cell Physiol **295**(4): C849-868.
Jones, P. A. and S. M. Taylor (1980). "Cellular differentiation, cytidine analogs and DNA methylation." Cell **20**(1): 85-93.
Jones, T. M., C. M. Espitia, J. Chipollini, B. R. Lee, J. A. Wertheim, J. S. Carew and S. T. Nawrocki (2023). "Targeting NEDDylation is a Novel Strategy to Attenuate Cisplatin-induced Nephrotoxicity." Cancer Res Commun **3**(2): 245-257.
Jung, C. H. and J. A. Thomas (1996). "S-glutathiolated hepatocyte proteins and insulin disulfides as substrates for reduction by glutaredoxin, thioredoxin, protein disulfide isomerase, and glutathione." Arch Biochem Biophys **335**(1): 61-72.
Kageyama, S., Y. S. Sou, T. Uemura, S. Kametaka, T. Saito, R. Ishimura, T. Kouno, L. Bedford, R. J. Mayer, M. S. Lee, M. Yamamoto, S. Waguri, K. Tanaka and M. Komatsu (2014). "Proteasome dysfunction activates autophagy and the Keap1-Nrf2 pathway." J Biol Chem **289**(36): 24944-24955.

Kaminskas, E., A. T. Farrell, Y. C. Wang, R. Sridhara and R. Pazdur (2005). "FDA drug approval summary: azacitidine (5-azacytidine, Vidaza) for injectable suspension." Oncologist **10**(3): 176-182.
Kantarjian, H., F. Ravandi, S. O'Brien, J. Cortes, S. Faderl, G. Garcia-Manero, E. Jabbour, W. Wierda, T. Kadia, S. Pierce, J. Shan, M. Keating and E. J. Freireich (2010). "Intensive chemotherapy does not benefit most older patients (age 70 years or older) with acute myeloid leukemia." Blood **116**(22): 4422-4429.
Karathedath, S., B. M. Rajamani, S. M. Musheer Aalam, A. Abraham, S. Varatharajan, P. Krishnamurthy, V. Mathews, S. R. Velayudhan and P. Balasubramanian (2017). "Role of NF-E2 related factor 2 (Nrf2) on chemotherapy resistance in acute myeloid leukemia (AML) and the effect of pharmacological inhibition of Nrf2." PLoS One **12**(5): e0177227.
Karsa, M., A. Kosciolek, A. Bongers, A. Mariana, T. Failes, A. J. Gifford, U. R. Kees, L. C. Cheung, R. S. Kotecha, G. M. Arndt, M. Haber, M. D. Norris, R. Sutton, R. B. Lock, M. J. Henderson and K. Somers (2021). "Exploiting the reactive oxygen species imbalance in high-risk paediatric acute lymphoblastic leukaemia through auranofin." Br J Cancer **125**(1): 55-64.
Kaspar, J. W. and A. K. Jaiswal (2010). "An autoregulatory loop between Nrf2 and Cul3-Rbx1 controls their cellular abundance." J Biol Chem **285**(28): 21349-21358.
Kobayashi, A., M. I. Kang, H. Okawa, M. Ohtsuji, Y. Zenke, T. Chiba, K. Igarashi and M. Yamamoto (2004). "Oxidative stress sensor Keap1 functions as an adaptor for Cul3-based E3 ligase to regulate proteasomal degradation of Nrf2." Mol Cell Biol **24**(16): 7130-7139.
Kobayashi, A., M. I. Kang, Y. Watai, K. I. Tong, T. Shibata, K. Uchida and M. Yamamoto (2006). "Oxidative and electrophilic stresses activate Nrf2 through inhibition of ubiquitination activity of Keap1." Mol Cell Biol **26**(1): 221-229.
Kwak, M. K., K. Itoh, M. Yamamoto and T. W. Kensler (2002). "Enhanced expression of the transcription factor Nrf2 by cancer chemopreventive agents: role of antioxidant response element-like sequences in the nrf2 promoter." Mol Cell Biol **22**(9): 2883-2892.
Laranjeira, A. B. A., M. G. Hollingshead, D. Nguyen, R. J. Kinders, J. H. Doroshow and S. X. Yang (2023). "DNA damage, demethylation and anticancer activity of DNA methyltransferase (DNMT) inhibitors." Sci Rep **13**(1): 5964.
Lee, O. H., A. K. Jain, V. Papusha and A. K. Jaiswal (2007). "An auto-regulatory loop between stress sensors INrf2 and Nrf2 controls their cellular abundance." J Biol Chem **282**(50): 36412-36420.
Li, L. H., E. J. Olin, H. H. Buskirk and L. M. Reineke (1970). "Cytotoxicity and mode of action of 5-azacytidine on L1210 leukemia." Cancer Res **30**(11): 2760-2769.
Lin, P., Y. Ren, X. Yan, Y. Luo, H. Zhang, M. Kesarwani, J. Bu, D. Zhan, Y. Zhou, Y. Tang, S. Zhu, W. Xu, X. Zhou, C. Mei, L. Ma, L. Ye, C. Hu, M. Azam, W. Ding, J. Jin, G. Huang and H. Tong (2019). "The high NRF2 expression confers chemotherapy resistance partly through up-regulated DUSP1 in myelodysplastic syndromes." Haematologica **104**(3): 485-496.
Lindsley, R. C., B. G. Mar, E. Mazzola, P. V. Grauman, S. Shareef, S. L. Allen, A. Pigneux, M. Wetzler, R. K. Stuart, H. P. Erba, L. E. Damon, B. L. Powell, N. Lindeman, D. P. Steensma, M. Wadleigh, D. J. DeAngelo, D. Neuberg, R. M. Stone and B. L. Ebert (2015). "Acute myeloid leukemia ontogeny is defined by distinct somatic mutations." Blood **125**(9): 1367-1376.
Liou, G. Y. and P. Storz (2010). "Reactive oxygen species in cancer." Free Radic Res **44**(5): 479-496.
Lou, Y., L. Shao, L. Mao, Y. Lu, Y. Ma, C. Fan, H. Jiang, J. Li and J. Jin (2020). "Efficacy and predictive factors of venetoclax combined with azacitidine as salvage therapy in advanced acute myeloid leukemia patients: A multicenter retrospective study." Leuk Res **91**: 106317.
Makishima, H., T. Yoshizato, K. Yoshida, M. A. Sekeres, T. Radivoyevitch, H. Suzuki, B. Przychodzen, Y. Nagata, M. Meggendorfer, M. Sanada, Y. Okuno, C. Hirsch, T. Kuzmanovic, Y. Sato, A. Sato-Otsubo, T. LaFramboise, N. Hosono, Y. Shiraishi, K. Chiba, C. Haferlach, W. Kern, H. Tanaka, Y. Shiozawa, I. Gómez-Seguí, H. D. Husseinzadeh, S. Thota, K. M. Guinta, B. Dienes, T. Nakamaki, S. Miyawaki, Y. Sauntharajah, S. Chiba, S. Miyano, L. Y. Shih, T. Haferlach, S.

Ogawa and J. P. Maciejewski (2017). "Dynamics of clonal evolution in myelodysplastic syndromes." Nat Genet **49**(2): 204-212.
Marcucci, G., K. Maharry, Y. Z. Wu, M. D. Radmacher, K. Mrózek, D. Margeson, K. B. Holland, S. P. Whitman, H. Becker, S. Schwind, K. H. Metzeler, B. L. Powell, T. H. Carter, J. E. Kolitz, M. Wetzler, A. J. Carroll, M. R. Baer, M. A. Caligiuri, R. A. Larson and C. D. Bloomfield (2010). "IDH1 and IDH2 gene mutations identify novel molecular subsets within de novo cytogenetically normal acute myeloid leukemia: a Cancer and Leukemia Group B study." J Clin Oncol **28**(14): 2348-2355.
Mardis, E. R., L. Ding, D. J. Dooling, D. E. Larson, M. D. McLellan, K. Chen, D. C. Koboldt, R. S. Fulton, K. D. Delehaunty, S. D. McGrath, L. A. Fulton, D. P. Locke, V. J. Magrini, R. M. Abbott, T. L. Vickery, J. S. Reed, J. S. Robinson, T. Wylie, S. M. Smith, L. Carmichael, J. M. Eldred, C. C. Harris, J. Walker, J. B. Peck, F. Du, A. F. Dukes, G. E. Sanderson, A. M. Brummett, E. Clark, J. F. McMichael, R. J. Meyer, J. K. Schindler, C. S. Pohl, J. W. Wallis, X. Shi, L. Lin, H. Schmidt, Y. Tang, C. Haipek, M. E. Wiechert, J. V. Ivy, J. Kalicki, G. Elliott, R. E. Ries, J. E. Payton, P. Westervelt, M. H. Tomasson, M. A. Watson, J. Baty, S. Heath, W. D. Shannon, R. Nagarajan, D. C. Link, M. J. Walter, T. A. Graubert, J. F. DiPersio, R. K. Wilson and T. J. Ley (2009). "Recurring mutations found by sequencing an acute myeloid leukemia genome." N Engl J Med **361**(11): 1058-1066.
McMahon, M., N. Thomas, K. Itoh, M. Yamamoto and J. D. Hayes (2006). "Dimerization of substrate adaptors can facilitate cullin-mediated ubiquitylation of proteins by a "tethering" mechanism: a two-site interaction model for the Nrf2-Keap1 complex." J Biol Chem **281**(34): 24756-24768.
Medeiros, B. C., A. T. Fathi, C. D. DiNardo, D. A. Pollyea, S. M. Chan and R. Swords (2017). "Isocitrate dehydrogenase mutations in myeloid malignancies." Leukemia **31**(2): 272-281.
Meister, A. (1988). "Glutathione metabolism and its selective modification." J Biol Chem **263**(33): 17205-17208.
Milkovic, L., N. Zarkovic and L. Saso (2017). "Controversy about pharmacological modulation of Nrf2 for cancer therapy." Redox Biol **12**: 727-732.
Minařík, L., K. Pimková, J. Kokavec, A. Schaffartziková, F. Vellieux, V. Kulvait, L. Daumová, N. Dusilková, A. Jonášová, K. S. Vargová, P. Králová Viziová, R. Sedláček, Z. Zemanová and T. Stopka (2022). "Analysis of 5-Azacytidine Resistance Models Reveals a Set of Targetable Pathways." Cells **11**(2).
Miseta, A. and P. Csutora (2000). "Relationship between the occurrence of cysteine in proteins and the complexity of organisms." Mol Biol Evol **17**(8): 1232-1239.
Montes, P., A. Guerra-Librero, P. García, M. E. Cornejo-Calvo, M. D. S. López, T. Haro, L. Martínez-Ruiz, G. Escames and D. Acuña-Castroviejo (2022). "Effect of 5-Azacitidine Treatment on Redox Status and Inflammatory Condition in MDS Patients." Antioxidants (Basel) **11**(1).
Montesinos, P., C. Recher, S. Vives, E. Zarzycka, J. Wang, G. Bertani, M. Heuser, R. T. Calado, A. C. Schuh, S. P. Yeh, S. R. Daigle, J. Hui, S. S. Pandya, D. A. Gianolio, S. de Botton and H. Döhner (2022). "Ivosidenib and Azacitidine in *IDH1*-Mutated Acute Myeloid Leukemia." N Engl J Med **386**(16): 1519-1531.
Mugoni, V., R. Panella, G. Cheloni, M. Chen, O. Pozdnyakova, D. Stroopinsky, J. Guarnerio, E. Monteleone, J. D. Lee, L. Mendez, A. V. Menon, J. C. Aster, A. A. Lane, R. M. Stone, I. Galinsky, J. C. Zamora, F. Lo-Coco, M. K. Bhasin, D. Avigan, L. Longo, J. G. Clohessy and P. P. Pandolfi (2019). "Vulnerabilities in mIDH2 AML confer sensitivity to APL-like targeted combination therapy." Cell Res **29**(6): 446-459.
Mukhopadhyay, S., D. Goswami, P. P. Adiseshaiah, W. Burgan, M. Yi, T. M. Guerin, S. V. Kozlov, D. V. Nissley and F. McCormick (2020). "Undermining Glutaminolysis Bolsters Chemotherapy While NRF2 Promotes Chemoresistance in KRAS-Driven Pancreatic Cancers." Cancer Res **80**(8): 1630-1643.
Nawrocki, S. T., P. Griffin, K. R. Kelly and J. S. Carew (2012). "MLN4924: a novel first-in-class inhibitor of NEDD8-activating enzyme for cancer therapy." Expert Opin Investig Drugs **21**(10): 1563-1573.

Nelson, J. W. and T. E. Creighton (1994). "Reactivity and ionization of the active site cysteine residues of DsbA, a protein required for disulfide bond formation in vivo." Biochemistry **33**(19): 5974-5983.
Nguyen, L. X. T., E. Troadec, A. Kalvala, B. Kumar, D. H. Hoang, D. Viola, B. Zhang, D. Q. Nguyen, I. Aldoss, L. Ghoda, E. Budde, F. Pichiorri, S. Rosen, S. J. Forman, G. Marcucci and V. Pullarkat (2019). "The Bcl-2 inhibitor venetoclax inhibits Nrf2 antioxidant pathway activation induced by hypomethylating agents in AML." J Cell Physiol **234**(8): 14040-14049.
Otsuki, A., M. Suzuki, F. Katsuoka, K. Tsuchida, H. Suda, M. Morita, R. Shimizu and M. Yamamoto (2016). "Unique cistrome defined as CsMBE is strictly required for Nrf2-sMaf heterodimer function in cytoprotection." Free Radic Biol Med **91**: 45-57.
Pajares, M., N. Jiménez-Moreno, Á. García-Yagüe, M. Escoll, M. L. de Ceballos, F. Van Leuven, A. Rábano, M. Yamamoto, A. I. Rojo and A. Cuadrado (2016). "Transcription factor NFE2L2/NRF2 is a regulator of macroautophagy genes." Autophagy **12**(10): 1902-1916.
Palii, S. S., B. O. Van Emburgh, U. T. Sankpal, K. D. Brown and K. D. Robertson (2008). "DNA methylation inhibitor 5-Aza-2'-deoxycytidine induces reversible genome-wide DNA damage that is distinctly influenced by DNA methyltransferases 1 and 3B." Mol Cell Biol **28**(2): 752-771.
Pan, K. T., Y. Y. Chen, T. H. Pu, Y. S. Chao, C. Y. Yang, R. D. Bomgarden, J. C. Rogers, T. C. Meng and K. H. Khoo (2014). "Mass spectrometry-based quantitative proteomics for dissecting multiplexed redox cysteine modifications in nitric oxide-protected cardiomyocyte under hypoxia." Antioxid Redox Signal **20**(9): 1365-1381.
Panieri, E. and M. M. Santoro (2016). "ROS homeostasis and metabolism: a dangerous liason in cancer cells." Cell Death Dis **7**(6): e2253.
Paolillo, R., M. Boulanger, P. Gâtel, L. Gabellier, M. De Toledo, D. Tempé, R. Hallal, D. Akl, J. Moreaux, H. Baik, E. Gueret, C. Recher, J. E. Sarry, G. Cartron, M. Piechaczyk and G. Bossis (2022). "The NADPH oxidase NOX2 is a marker of adverse prognosis involved in chemoresistance of acute myeloid leukemias." Haematologica **107**(11): 2562-2575.
Parsons, D. W., S. Jones, X. Zhang, J. C. Lin, R. J. Leary, P. Angenendt, P. Mankoo, H. Carter, I. M. Siu, G. L. Gallia, A. Olivi, R. McLendon, B. A. Rasheed, S. Keir, T. Nikolskaya, Y. Nikolsky, D. A. Busam, H. Tekleab, L. A. Diaz, J. Hartigan, D. R. Smith, R. L. Strausberg, S. K. Marie, S. M. Shinjo, H. Yan, G. J. Riggins, D. D. Bigner, R. Karchin, N. Papadopoulos, G. Parmigiani, B. Vogelstein, V. E. Velculescu and K. W. Kinzler (2008). "An integrated genomic analysis of human glioblastoma multiforme." Science **321**(5897): 1807-1812.
Pimkova, K., M. Jassinskaja, R. Munita, M. Ciesla, N. Guzzi, P. Cao Thi Ngoc, M. Vajrychova, E. Johansson, C. Bellodi and J. Hansson (2022). "Quantitative analysis of redox proteome reveals oxidation-sensitive protein thiols acting in fundamental processes of developmental hematopoiesis." Redox Biol **53**: 102343.
Prieto-Bermejo, R., M. Romo-González, A. Pérez-Fernández, C. Ijurko and Á. Hernández-Hernández (2018). "Reactive oxygen species in haematopoiesis: leukaemic cells take a walk on the wild side." J Exp Clin Cancer Res **37**(1): 125.
Prébet, T., S. D. Gore, B. Esterni, C. Gardin, R. Itzykson, S. Thepot, F. Dreyfus, O. B. Rauzy, C. Recher, L. Adès, B. Quesnel, C. L. Beach, P. Fenaux and N. Vey (2011). "Outcome of high-risk myelodysplastic syndrome after azacitidine treatment failure." J Clin Oncol **29**(24): 3322-3327.
Rodriguez-Sevilla, J. J., V. Adema, G. Garcia-Manero and S. Colla (2023). "Emerging treatments for myelodysplastic syndromes: Biological rationales and clinical translation." Cell Rep Med **4**(2): 100940.
Rushworth, S. A., K. M. Bowles and D. J. MacEwan (2011). "High basal nuclear levels of Nrf2 in acute myeloid leukemia reduces sensitivity to proteasome inhibitors." Cancer Res **71**(5): 1999-2009.
Salovska, B., A. Kondelova, K. Pimkova, Z. Liblova, M. Pribyl, I. Fabrik, J. Bartek, M. Vajrychova and Z. Hodny (2022). "Peroxiredoxin 6 protects irradiated cells from oxidative stress and shapes their senescence-associated cytokine landscape." Redox Biol **49**: 102212.

Schaefer, M., S. Hagemann, K. Hanna and F. Lyko (2009). "Azacytidine inhibits RNA methylation at DNMT2 target sites in human cancer cell lines." Cancer Res **69**(20): 8127-8132.
Schermelleh, L., F. Spada, H. P. Easwaran, K. Zolghadr, J. B. Margot, M. C. Cardoso and H. Leonhardt (2005). "Trapped in action: direct visualization of DNA methyltransferase activity in living cells." Nat Methods **2**(10): 751-756.
Schreck, R., P. Rieber and P. A. Baeuerle (1991). "Reactive oxygen intermediates as apparently widely used messengers in the activation of the NF-kappa B transcription factor and HIV-1." EMBO J **10**(8): 2247-2258.
Sekeres, M. A. and J. Taylor (2022). "Diagnosis and Treatment of Myelodysplastic Syndromes: A Review." JAMA **328**(9): 872-880.
Sekeres, M. A., J. Watts, A. Radinoff, M. A. Sangerman, M. Cerrano, P. F. Lopez, J. F. Zeidner, M. D. Campelo, C. Graux, J. Liesveld, D. Selleslag, N. Tzvetkov, R. J. Fram, D. Zhao, J. Bell, S. Friedlander, D. V. Faller and L. Adès (2021). "Randomized phase 2 trial of pevonedistat plus azacitidine versus azacitidine for higher-risk MDS/CMML or low-blast AML." Leukemia **35**(7): 2119-2124.
Shi, J., B. Sun, W. Shi, H. Zuo, D. Cui, L. Ni and J. Chen (2015). "Decreasing GSH and increasing ROS in chemosensitivity gliomas with IDH1 mutation." Tumour Biol **36**(2): 655-662.
Shibata, T., A. Kokubu, M. Gotoh, H. Ojima, T. Ohta, M. Yamamoto and S. Hirohashi (2008). "Genetic alteration of Keap1 confers constitutive Nrf2 activation and resistance to chemotherapy in gallbladder cancer." Gastroenterology **135**(4): 1358-1368, 1368.e1351-1354.
Short, N. J., M. Muftuoglu, F. Ong, L. Nasr, W. Macaron, G. Montalban-Bravo, Y. Alvarado, M. Basyal, N. Daver, C. D. Dinardo, G. Borthakur, N. Jain, M. Ohanian, E. Jabbour, G. C. Issa, W. Qiao, X. Huang, R. Kanagal-Shamanna, K. P. Patel, P. Bose, F. Ravandi, R. Delumpa, R. Abramova, G. Garcia-Manero, M. Andreeff, J. Cortes and H. Kantarjian (2023). "A phase 1/2 study of azacitidine, venetoclax and pevonedistat in newly diagnosed secondary AML and in MDS or CMML after failure of hypomethylating agents." J Hematol Oncol **16**(1): 73.
Sies, H. (2017). "Hydrogen peroxide as a central redox signaling molecule in physiological oxidative stress: Oxidative eustress." Redox Biol **11**: 613-619.
Sies, H. and D. P. Jones (2020). "Reactive oxygen species (ROS) as pleiotropic physiological signalling agents." Nat Rev Mol Cell Biol **21**(7): 363-383.
Silkjaer, T., J. M. Nørgaard, A. Aggerholm, L. H. Ebbesen, E. Kjeldsen, P. Hokland and C. G. Nyvold (2013). "Characterization and prognostic significance of mitochondrial DNA variations in acute myeloid leukemia." Eur J Haematol **90**(5): 385-396.
Silverman, L. R., E. P. Demakos, B. L. Peterson, A. B. Kornblith, J. C. Holland, R. Odchimar-Reissig, R. M. Stone, D. Nelson, B. L. Powell, C. M. DeCastro, J. Ellerton, R. A. Larson, C. A. Schiffer and J. F. Holland (2002). "Randomized controlled trial of azacitidine in patients with the myelodysplastic syndrome: a study of the cancer and leukemia group B." J Clin Oncol **20**(10): 2429-2440.
Singh, A., M. Gurav, S. Dhanavade, O. Shetty and S. Epari (2017). "Diffuse glioma - Rare homozygous IDH point mutation, is it an oncogenetic mechanism?" Neuropathology **37**(6): 582-585.
Song, K., M. Li, X. J. Xu, L. Xuan, G. N. Huang, X. L. Song and Q. F. Liu (2014). "HIF-1α and GLUT1 gene expression is associated with chemoresistance of acute myeloid leukemia." Asian Pac J Cancer Prev **15**(4): 1823-1829.
Souers, A. J., J. D. Leverson, E. R. Boghaert, S. L. Ackler, N. D. Catron, J. Chen, B. D. Dayton, H. Ding, S. H. Enschede, W. J. Fairbrother, D. C. Huang, S. G. Hymowitz, S. Jin, S. L. Khaw, P. J. Kovar, L. T. Lam, J. Lee, H. L. Maecker, K. C. Marsh, K. D. Mason, M. J. Mitten, P. M. Nimmer, A. Oleksijew, C. H. Park, C. M. Park, D. C. Phillips, A. W. Roberts, D. Sampath, J. F. Seymour, M. L. Smith, G. M. Sullivan, S. K. Tahir, C. Tse, M. D. Wendt, Y. Xiao, J. C. Xue, H. Zhang, R. A. Humerickhouse, S. H. Rosenberg and S. W. Elmore (2013). "ABT-199, a potent and selective BCL-2 inhibitor, achieves antitumor activity while sparing platelets." Nat Med **19**(2): 202-208.
Sperling, A. S., C. J. Gibson and B. L. Ebert (2017). "The genetics of myelodysplastic syndrome: from clonal haematopoiesis to secondary leukaemia." Nat Rev Cancer **17**(1): 5-19.

Stacy, D. R., K. Ely, P. P. Massion, W. G. Yarbrough, D. E. Hallahan, K. R. Sekhar and M. L. Freeman (2006). "Increased expression of nuclear factor E2 p45-related factor 2 (NRF2) in head and neck squamous cell carcinomas." Head Neck **28**(9): 813-818.
Steensma, D. P., M. R. Baer, J. L. Slack, R. Buckstein, L. A. Godley, G. Garcia-Manero, M. Albitar, J. S. Larsen, S. Arora, M. T. Cullen and H. Kantarjian (2009). "Multicenter study of decitabine administered daily for 5 days every 4 weeks to adults with myelodysplastic syndromes: the alternative dosing for outpatient treatment (ADOPT) trial." J Clin Oncol **27**(23): 3842-3848.
Steensma, D. P., K. V. Heptinstall, V. M. Johnson, P. J. Novotny, J. A. Sloan, J. K. Camoriano, J. Niblack, J. M. Bennett and R. A. Mesa (2008). "Common troublesome symptoms and their impact on quality of life in patients with myelodysplastic syndromes (MDS): results of a large internet-based survey." Leuk Res **32**(5): 691-698.
Strati, P., H. Kantarjian, F. Ravandi, A. Nazha, G. Borthakur, N. Daver, T. Kadia, Z. Estrov, G. Garcia-Manero, M. Konopleva, T. Rajkhowa, M. Durand, M. Andreeff, M. Levis and J. Cortes (2015). "Phase I/II trial of the combination of midostaurin (PKC412) and 5-azacytidine for patients with acute myeloid leukemia and myelodysplastic syndrome." Am J Hematol **90**(4): 276-281.
Su, H., F. Yang, R. Fu, X. Li, R. French, E. Mose, X. Pu, B. Trinh, A. Kumar, J. Liu, L. Antonucci, J. Todoric, Y. Liu, Y. Hu, M. T. Diaz-Meco, J. Moscat, C. M. Metallo, A. M. Lowy, B. Sun and M. Karin (2021). "Cancer cells escape autophagy inhibition via NRF2-induced macropinocytosis." Cancer Cell **39**(5): 678-693.e611.
Sun-Wang, J. L., S. Ivanova and A. Zorzano (2020). "The dialogue between the ubiquitin-proteasome system and autophagy: Implications in ageing." Ageing Res Rev **64**: 101203.
Suzuki, T., J. Takahashi and M. Yamamoto (2023). "Molecular Basis of the KEAP1-NRF2 Signaling Pathway." Mol Cells **46**(3): 133-141.
Swords, R. T., H. P. Erba, D. J. DeAngelo, D. L. Bixby, J. K. Altman, M. Maris, Z. Hua, S. J. Blakemore, H. Faessel, F. Sedarati, B. J. Dezube, F. J. Giles and B. C. Medeiros (2015). "Pevonedistat (MLN4924), a First-in-Class NEDD8-activating enzyme inhibitor, in patients with acute myeloid leukaemia and myelodysplastic syndromes: a phase 1 study." Br J Haematol **169**(4): 534-543.
Swords, R. T., K. R. Kelly, P. G. Smith, J. J. Garnsey, D. Mahalingam, E. Medina, K. Oberheu, S. Padmanabhan, M. O'Dwyer, S. T. Nawrocki, F. J. Giles and J. S. Carew (2010). "Inhibition of NEDD8-activating enzyme: a novel approach for the treatment of acute myeloid leukemia." Blood **115**(18): 3796-3800.
Syu, J. P., J. T. Chi and H. N. Kung (2016). "Nrf2 is the key to chemotherapy resistance in MCF7 breast cancer cells under hypoxia." Oncotarget **7**(12): 14659-14672.
Tang, X., X. Fu, Y. Liu, D. Yu, S. J. Cai and C. Yang (2020). "Blockade of Glutathione Metabolism in." Mol Cancer Ther **19**(1): 221-230.
Testa, U., G. Castelli and E. Pelosi (2020). "Isocitrate Dehydrogenase Mutations in Myelodysplastic Syndromes and in Acute Myeloid Leukemias." Cancers (Basel) **12**(9).
Theodore, M., Y. Kawai, J. Yang, Y. Kleshchenko, S. P. Reddy, F. Villalta and I. J. Arinze (2008). "Multiple nuclear localization signals function in the nuclear import of the transcription factor Nrf2." J Biol Chem **283**(14): 8984-8994.
Tomin, T., M. Schittmayer, S. Sedej, H. Bugger, J. Gollmer, S. Honeder, B. Darnhofer, L. Liesinger, A. Zuckermann, P. P. Rainer and R. Birner-Gruenberger (2021). "Mass Spectrometry-Based Redox and Protein Profiling of Failing Human Hearts." Int J Mol Sci **22**(4).
Tonelli, C., I. I. C. Chio and D. A. Tuveson (2018). "Transcriptional Regulation by Nrf2." Antioxid Redox Signal **29**(17): 1727-1745.
Tong, K. I., Y. Katoh, H. Kusunoki, K. Itoh, T. Tanaka and M. Yamamoto (2006). "Keap1 recruits Neh2 through binding to ETGE and DLG motifs: characterization of the two-site molecular recognition model." Mol Cell Biol **26**(8): 2887-2900.
Tong, K. I., A. Kobayashi, F. Katsuoka and M. Yamamoto (2006). "Two-site substrate recognition model for the Keap1-Nrf2 system: a hinge and latch mechanism." Biol Chem **387**(10-11): 1311-1320.

Trombetti, S., E. Cesaro, R. Catapano, R. Sessa, A. Lo Bianco, P. Izzo and M. Grosso (2021). "Oxidative Stress and ROS-Mediated Signaling in Leukemia: Novel Promising Perspectives to Eradicate Chemoresistant Cells in Myeloid Leukemia." Int J Mol Sci **22**(5).
Tsuji-Takayama, K., T. Inoue, Y. Ijiri, T. Otani, R. Motoda, S. Nakamura and K. Orita (2004). "Demethylating agent, 5-azacytidine, reverses differentiation of embryonic stem cells." Biochem Biophys Res Commun **323**(1): 86-90.
Turrens, J. F. (2003). "Mitochondrial formation of reactive oxygen species." J Physiol **552**(Pt 2): 335-344.
Turrens, J. F. and A. Boveris (1980). "Generation of superoxide anion by the NADH dehydrogenase of bovine heart mitochondria." Biochem J **191**(2): 421-427.
van der Reest, J., S. Lilla, L. Zheng, S. Zanivan and E. Gottlieb (2018). "Proteome-wide analysis of cysteine oxidation reveals metabolic sensitivity to redox stress." Nat Commun **9**(1): 1581.
Vardiman, J. W., N. L. Harris and R. D. Brunning (2002). "The World Health Organization (WHO) classification of the myeloid neoplasms." Blood **100**(7): 2292-2302.
Wang, E. S., P. Montesinos, M. D. Minden, J. H. Lee, M. Heuser, T. Naoe, W. C. Chou, K. Laribi, J. Esteve, J. K. Altman, V. Havelange, A. M. Watson, C. Gambacorti-Passerini, E. Patkowska, S. Liu, R. Wu, N. Philipose, J. E. Hill, S. C. Gill, E. S. Rich and R. V. Tiu (2022). "Phase 3 trial of gilteritinib plus azacitidine vs azacitidine for newly diagnosed FLT3mut+ AML ineligible for intensive chemotherapy." Blood **140**(17): 1845-1857.
Wang, X. J., Z. Sun, N. F. Villeneuve, S. Zhang, F. Zhao, Y. Li, W. Chen, X. Yi, W. Zheng, G. T. Wondrak, P. K. Wong and D. D. Zhang (2008). "Nrf2 enhances resistance of cancer cells to chemotherapeutic drugs, the dark side of Nrf2." Carcinogenesis **29**(6): 1235-1243.
Ward, P. S., C. Lu, J. R. Cross, O. Abdel-Wahab, R. L. Levine, G. K. Schwartz and C. B. Thompson (2013). "The potential for isocitrate dehydrogenase mutations to produce 2-hydroxyglutarate depends on allele specificity and subcellular compartmentalization." J Biol Chem **288**(6): 3804-3815.
Ward, P. S., J. Patel, D. R. Wise, O. Abdel-Wahab, B. D. Bennett, H. A. Coller, J. R. Cross, V. R. Fantin, C. V. Hedvat, A. E. Perl, J. D. Rabinowitz, M. Carroll, S. M. Su, K. A. Sharp, R. L. Levine and C. B. Thompson (2010). "The common feature of leukemia-associated IDH1 and IDH2 mutations is a neomorphic enzyme activity converting alpha-ketoglutarate to 2-hydroxyglutarate." Cancer Cell **17**(3): 225-234.
Welch, J. S., T. J. Ley, D. C. Link, C. A. Miller, D. E. Larson, D. C. Koboldt, L. D. Wartman, T. L. Lamprecht, F. Liu, J. Xia, C. Kandoth, R. S. Fulton, M. D. McLellan, D. J. Dooling, J. W. Wallis, K. Chen, C. C. Harris, H. K. Schmidt, J. M. Kalicki-Veizer, C. Lu, Q. Zhang, L. Lin, M. D. O'Laughlin, J. F. McMichael, K. D. Delehaunty, L. A. Fulton, V. J. Magrini, S. D. McGrath, R. T. Demeter, T. L. Vickery, J. Hundal, L. L. Cook, G. W. Swift, J. P. Reed, P. A. Alldredge, T. N. Wylie, J. R. Walker, M. A. Watson, S. E. Heath, W. D. Shannon, N. Varghese, R. Nagarajan, J. E. Payton, J. D. Baty, S. Kulkarni, J. M. Klco, M. H. Tomasson, P. Westervelt, M. J. Walter, T. A. Graubert, J. F. DiPersio, L. Ding, E. R. Mardis and R. K. Wilson (2012). "The origin and evolution of mutations in acute myeloid leukemia." Cell **150**(2): 264-278.
Winer, E. S. and R. M. Stone (2019). "Novel therapy in Acute myeloid leukemia (AML): moving toward targeted approaches." Ther Adv Hematol **10**: 2040620719860645.
Winterbourn, C. C. and D. Metodiewa (1999). "Reactivity of biologically important thiol compounds with superoxide and hydrogen peroxide." Free Radic Biol Med **27**(3-4): 322-328.
Xu, W., H. Yang, Y. Liu, Y. Yang, P. Wang, S. H. Kim, S. Ito, C. Yang, M. T. Xiao, L. X. Liu, W. Q. Jiang, J. Liu, J. Y. Zhang, B. Wang, S. Frye, Y. Zhang, Y. H. Xu, Q. Y. Lei, K. L. Guan, S. M. Zhao and Y. Xiong (2011). "Oncometabolite 2-hydroxyglutarate is a competitive inhibitor of α-ketoglutarate-dependent dioxygenases." Cancer Cell **19**(1): 17-30.
Yamamoto, T., T. Suzuki, A. Kobayashi, J. Wakabayashi, J. Maher, H. Motohashi and M. Yamamoto (2008). "Physiological significance of reactive cysteine residues of Keap1 in determining Nrf2 activity." Mol Cell Biol **28**(8): 2758-2770.

Yan, H., D. W. Parsons, G. Jin, R. McLendon, B. A. Rasheed, W. Yuan, I. Kos, I. Batinic-Haberle, S. Jones, G. J. Riggins, H. Friedman, A. Friedman, D. Reardon, J. Herndon, K. W. Kinzler, V. E. Velculescu, B. Vogelstein and D. D. Bigner (2009). "IDH1 and IDH2 mutations in gliomas." N Engl J Med **360**(8): 765-773.
Yu, X., Y. Wang, J. Tan, Y. Li, P. Yang, X. Liu, J. Lai, Y. Zhang, L. Cai, Y. Gu and L. Xu (2024). "Inhibition of NRF2 enhances the acute myeloid leukemia cell death induced by venetoclax via the ferroptosis pathway." Cell Death Discov **10**(1): 35.
Yu, Y., Di Trapani, G., Tonissen, K.F. (2022). Thioredoxin and Glutathione Systems. In: Chakraborti, S., Ray, B.K., Roychoudhury, S. (eds) Handbook of Oxidative Stress in Cancer: Mechanistic Aspects. Springer, Singapore. https://doi.org/10.1007/978-981-15-9411-3_143
Zamorano Cuervo, N., A. Fortin, E. Caron, S. Chartier and N. Grandvaux (2021). "Pinpointing cysteine oxidation sites by high-resolution proteomics reveals a mechanism of redox-dependent inhibition of human STING." Sci Signal **14**(680).
Zeidan, A. M., U. Borate, D. A. Pollyea, A. M. Brunner, F. Roncolato, J. S. Garcia, R. Filshie, O. Odenike, A. M. Watson, R. Krishnadasan, A. Bajel, K. Naqvi, J. Zha, W. H. Cheng, Y. Zhou, D. Hoffman, J. G. Harb, J. Potluri and G. Garcia-Manero (2023). "A phase 1b study of venetoclax and azacitidine combination in patients with relapsed or refractory myelodysplastic syndromes." Am J Hematol **98**(2): 272-281.
Zhang, D. D., S. C. Lo, J. V. Cross, D. J. Templeton and M. Hannink (2004). "Keap1 is a redox-regulated substrate adaptor protein for a Cul3-dependent ubiquitin ligase complex." Mol Cell Biol **24**(24): 10941-10953.
Zhang, P., A. Singh, S. Yegnasubramanian, D. Esopi, P. Kombairaju, M. Bodas, H. Wu, S. G. Bova and S. Biswal (2010). "Loss of Kelch-like ECH-associated protein 1 function in prostate cancer cells causes chemoresistance and radioresistance and promotes tumor growth." Mol Cancer Ther **9**(2): 336-346.
Zhao, S., Y. Lin, W. Xu, W. Jiang, Z. Zha, P. Wang, W. Yu, Z. Li, L. Gong, Y. Peng, J. Ding, Q. Lei, K. L. Guan and Y. Xiong (2009). "Glioma-derived mutations in IDH1 dominantly inhibit IDH1 catalytic activity and induce HIF-1alpha." Science **324**(5924): 261-265.
Zheng, H., Z. Nong and G. Lu (2015). "Correlation Between Nuclear Factor E2-Related Factor 2 Expression and Gastric Cancer Progression." Med Sci Monit **21**: 2893-2899.
Zipper, L. M. and R. T. Mulcahy (2002). "The Keap1 BTB/POZ dimerization function is required to sequester Nrf2 in cytoplasm." J Biol Chem **277**(39): 36544-36552.

9 Attachment

9.1 Table of peptides with significant changes in cysteine oxidation in Pevo-treated or Pevo-resistant cells compared to Pevo-sensitive cells

Uniprot ID	Cys positions	mean % OX AR	mean % OX PR	mean % OX AR+P	-Log Student's T-test p-value PR_AR	-Log Student's T-test p-value AR+P_AR
Q13085	407	4.07	1.71	6.22	1.6773	NaN
O95831	441	2.30	1.76	1.57	1.6254	0.8181
Q8NI99	410	50.25	67.21	52.68	1.6032	0.3272
P20073	298	2.60	4.83	3.51	1.6278	0.8082
P61966	47	2.99	2.51	3.09	1.6450	NaN
Q96CW1	212	2.27	4.10	4.18	1.3243	0.4560
P15514	172	47.67	58.04	46.72	1.7739	0.4204
O14497	1827	6.21	10.04	5.72	2.1332	0.2033
O95671	333	1.85	0.95	2.68	1.4251	0.8386
Q5T9A4	515	3.67	2.20	3.49	1.8916	0.1593
Q6DD88	371	1.49	0.81	2.84	1.5070	NaN
P98194	409;411	3.42	6.48	4.88	1.6665	0.6952
P38606	138	3.23	2.06	NaN	1.4246	NaN
Q14CW9	209	8.66	23.78	23.90	1.9365	0.5826
O14965	49	6.38	3.60	6.68	1.3544	0.4068
Q8NFC6	1742	3.64	6.07	4.49	2.3514	0.5966
Q15059	387	8.18	5.77	NaN	1.4414	NaN
Q8IYL3	92;124	4.63	3.53	NaN	1.7600	NaN
P17655	405	1.24	2.70	2.13	1.4525	NaN
P42575	436;440	4.79	5.78	9.56	1.4593	0.6615
O95319	161	3.77	2.85	3.85	1.3672	0.0258
P23528	39	3.19	5.49	6.38	1.3105	1.0694
O14967	185	48.12	32.15	51.63	1.8401	0.3972
Q9HAW4	915	3.93	4.74	4.90	1.9799	0.3254
O75153	184	3.92	5.50	NaN	1.4055	NaN
O75153	588	1.29	3.04	1.82	2.2098	NaN
P09543	158	8.62	3.81	11.13	1.4563	0.1466
Q9UKF6	655	1.65	2.40	2.87	1.8754	0.9289
P32929	109	3.87	5.78	3.63	1.6625	0.1156
Q9UER7	720	6.73	8.53	13.69	1.5286	0.6723
Q9UJW0	344	3.62	5.17	4.20	1.3672	0.2321
P09622	69	29.72	22.08	29.91	1.9644	0.0491
P31689	149;150;153	8.91	12.38	9.21	1.5243	0.0694

O60884	280	8.70	5.79	5.78	2.2520	0.8482
Q96EY1	236	9.73	13.50	8.37	1.5910	0.3046
P26358	1221;1226	3.54	2.90	4.34	1.3147	NaN
P29692	247	7.13	9.38	9.02	1.3594	NaN
P13639	369	7.80	4.14	NaN	2.2086	NaN
Q8N9N8	89	5.40	3.24	4.77	1.4061	0.9489
P41091	96;101	3.39	5.48	3.23	1.6819	0.1357
Q09472	1753;1758	3.58	2.41	3.42	2.4772	0.0952
P11171	224	2.29	4.88	NaN	1.7408	NaN
Q2NKX8	825	4.74	2.80	6.21	1.5715	NaN
Q9BS26	301	77.13	68.42	72.21	1.5209	0.2632
P49327	634;642	2.26	4.98	3.50	1.3608	NaN
Q14315	1469	1.42	4.29	1.08	1.7491	0.3613
Q14315	198;203	1.42	4.75	1.05	1.5730	0.3808
Q14315	1348	0.84	5.95	1.37	3.8083	NaN
Q9BTY2	277	44.07	34.81	46.54	1.5864	0.2817
Q92538	1707	2.84	2.01	2.19	1.3285	NaN
Q92896	444	88.64	92.29	87.76	1.5743	0.1838
Q92896	1071	74.54	78.21	79.27	1.4655	1.1367
Q92896	480	83.46	88.69	81.05	1.6991	0.2338
Q9HC38	197	4.88	7.27	5.17	1.5294	0.0653
P04899	326	1.79	3.18	2.75	1.3363	0.3482
P08754	66	1.97	4.53	5.12	1.9887	0.6722
P36915	410;412	6.75	4.22	4.70	3.0580	0.3491
Q14789	395	35.94	41.93	33.55	1.4824	0.1760
Q9NPB8	584	4.30	2.05	3.52	1.7457	0.8916
P43304	385	4.45	2.70	6.31	1.3014	1.0212
Q9UHW5	281	2.10	3.89	2.64	1.4546	0.3194
O14964	212;215	4.20	5.01	5.02	1.4624	0.2723
P01893	283	29.15	39.67	32.90	1.4486	0.1164
P52272	676	6.74	2.61	6.36	1.7280	0.2425
Q1KMD3	308	3.45	1.76	2.79	1.7546	1.0124
Q5SSJ5	359	6.11	4.25	6.45	1.7863	0.0748
P34932	167	1.90	2.53	2.28	1.3720	0.2393
Q92598	167	1.71	3.01	3.53	1.6179	NaN
O14879	73	4.40	5.35	5.42	1.4782	NaN
P08069	1367	5.04	10.07	9.08	1.3720	NaN
Q08334	188	68.01	75.47	58.21	1.9931	1.1015
Q7Z5L9	37	4.77	7.73	7.34	1.3090	0.7910
P08514	96	56.11	63.46	62.07	2.4450	1.0413
P05106	299	49.43	36.06	56.12	1.7049	0.3626
P05106	75	55.58	69.78	47.12	1.4678	0.4648
Q9Y287	89	17.04	29.24	14.65	1.8299	0.5501

Q9Y287	38	9.58	15.41	14.58	1.4671	1.2119
P28290	673	8.48	4.58	NaN	1.5755	NaN
Q8NHM5	770	5.90	4.30	7.40	1.5618	0.1823
P41229	327	6.69	4.22	4.21	1.7885	NaN
Q02241	483	3.61	2.47	4.77	1.8557	0.9302
O95239	977	8.67	6.29	8.88	1.8493	0.6066
Q1ED39	172	6.78	4.68	6.57	1.3613	0.0820
Q9Y4W2	316	3.02	2.49	3.74	2.0793	0.3374
Q8N3X6	75	7.48	4.97	8.76	1.3113	0.2579
O15243	66	5.79	8.42	6.35	1.6842	0.1862
Q5TKA1	435	6.07	3.60	6.96	1.6419	0.9002
Q7Z4F1	381;387	53.41	70.26	48.27	1.4138	0.2561
Q9Y561	166;168	61.15	65.71	68.60	1.7612	0.9520
Q5SQ64	184	67.06	77.27	64.76	1.7846	0.2183
Q5SQ64	141;146	59.74	66.96	57.37	1.9876	0.2090
P49137	224	7.95	4.23	8.47	1.5819	NaN
Q7KZI7	210	9.14	3.55	8.83	1.7288	NaN
Q7Z434	20;33	8.06	6.83	6.17	2.1215	NaN
P33992	221	3.16	4.61	4.77	1.4266	0.9662
Q9NVC6	15	5.30	2.43	4.69	1.8405	NaN
P46013	958	4.63	2.67	6.97	1.5444	NaN
O95297	203	6.90	11.63	9.26	1.4555	0.6329
Q9UBG0	942;950	77.05	52.59	81.72	1.8045	0.2655
Q96H55	227	9.72	5.87	12.95	1.7435	0.3820
P51970	110	93.83	94.46	94.81	2.9869	0.3319
Q9H3P2	471	4.36	3.54	2.56	1.3051	NaN
Q99519	265	52.18	34.67	42.26	2.2957	0.3765
Q9BYG3	237	6.26	3.65	5.46	1.3451	0.2350
Q9UKK9	91	6.41	10.02	NaN	1.3549	NaN
Q14980	299	11.61	6.39	8.77	1.4208	0.5872
Q96E22	77	5.64	6.73	8.99	1.7074	0.7983
Q9UBU9	588	12.05	5.67	1.55	1.5949	NaN
Q8N543	143	9.87	5.98	NaN	1.5430	NaN
Q9NTK5	55	4.32	7.26	6.21	1.8472	0.5964
Q9UNF0	233	4.85	2.78	3.45	1.3245	0.7293
Q9UKS6	421	2.43	4.27	3.47	2.9380	0.6611
P09874	429	8.84	3.95	8.83	1.3226	0.0018
Q96KB5	70	5.69	3.52	9.99	1.8952	0.2294
O95613	2446	3.83	2.23	6.16	1.7818	0.5357
P11177	263	2.91	2.45	3.81	1.5664	0.7561
O00541	272	3.31	1.61	2.93	1.3372	NaN
O60825	158	4.79	2.02	NaN	2.0354	NaN
P17858	708	2.16	3.18	2.82	1.4085	0.2851

A6NDG6	217	3.77	4.88	3.38	2.8682	0.1455
Q92643	280	37.98	24.70	39.92	1.3185	0.1761
P14618	358	5.32	3.50	NaN	2.9339	NaN
Q15149	4454	5.16	2.64	6.26	1.3299	NaN
Q9BX97	389	64.47	74.62	67.04	3.0535	0.1737
Q9BX97	272	45.42	65.43	54.16	1.7740	0.5081
Q13794	25	7.72	12.84	11.14	1.3920	0.8758
P49005	447	4.16	6.13	5.24	1.3909	NaN
P62875	7;10	25.77	19.37	21.12	2.3532	0.9450
Q969H6	146	3.92	1.73	4.47	2.1731	0.1006
Q9H2U2	161;171	7.72	4.49	8.76	1.3215	0.2425
P49643	384	27.78	22.67	28.17	1.4892	0.2736
O43395	630	4.96	3.50	8.35	1.3071	0.2060
Q13523	962	5.02	2.63	NaN	1.5394	NaN
P07602	482	83.05	94.50	88.65	3.4582	0.7906
P35998	377	2.07	3.55	4.41	1.7094	1.1808
P49023	358;361	3.01	5.52	6.05	2.0720	0.7279
Q9H0R6	88	5.02	2.59	4.05	2.9049	NaN
Q6IQ22	68;71	5.85	7.82	8.24	1.9048	0.5244
P62834	48;51	5.56	8.32	9.01	1.3599	0.8840
P61224	51	3.89	8.47	7.04	1.8380	0.5598
Q9P2N5	49	5.96	2.11	4.44	1.7431	NaN
P46063	493	3.72	2.57	6.05	1.8136	0.8961
Q96TC7	288	3.57	4.46	2.71	1.3121	0.4037
O75792	181	4.66	9.51	9.32	1.7456	0.8130
P10155	305	2.30	3.83	3.95	1.8776	0.9673
O75116	330	3.35	1.62	3.26	1.5286	0.0476
Q9Y3U8	48	4.46	7.84	4.01	1.6049	0.2921
Q96P16	100	6.41	2.88	7.00	2.7808	NaN
O76021	96	4.09	2.80	5.49	1.5286	0.6398
Q96T51	351	8.12	4.58	NaN	1.5802	NaN
Q9UBE0	146	3.14	4.19	3.27	1.5053	0.0351
Q99590	346	5.67	3.03	4.44	1.5815	NaN
Q96EE3	30	13.86	7.24	21.64	1.3452	0.9960
Q9C0C4	99	49.89	41.05	52.42	1.5269	0.1595
O75533	1035	2.66	1.67	2.48	2.4344	0.0984
Q8N8R3	181	2.74	1.95	4.65	3.0269	1.1527
A6NHR9	505	3.55	2.24	3.09	1.3673	0.1006
Q5T280	151	5.11	3.30	5.11	1.3459	0.0004
Q13501	26;27;44	11.03	21.72	9.41	1.5777	0.3327
Q13501	331	4.34	6.34	3.15	1.9756	0.8806
Q13501	289;290	5.41	12.84	4.75	1.5747	0.1630
P78362	223	2.87	4.30	4.13	1.6510	0.6952

Q9UQ35	1480	35.85	18.61	28.01	1.4772	0.9638
Q96SI9	40	3.90	2.59	NaN	1.7140	NaN
P49848	130	4.25	3.46	4.45	1.4709	0.0662
Q9Y2W6	419	7.02	4.54	6.30	1.5855	0.3205
Q02763	877	10.27	6.22	10.48	1.6318	NaN
P10646	250	62.93	74.28	75.64	1.5799	1.0437
P48307	122	62.32	75.24	70.95	2.4271	0.9019
P52888	682;689	1.20	2.05	2.52	1.3275	0.7708
Q9UDY2	601	3.98	4.52	5.82	1.4443	0.4609
P04183	79	4.47	2.53	3.96	1.3436	0.1780
P29401	206;225	41.87	29.55	42.00	1.7985	0.0400
Q9Y490	1045	2.34	1.53	NaN	1.3430	NaN
Q92973	164	2.13	3.87	3.30	1.6646	0.3435
Q9UPQ9	202	6.04	4.18	NaN	2.3009	NaN
P11388	1145	2.76	1.41	5.05	1.5414	1.1546
Q9Y3C4	13	6.05	3.67	5.19	1.6844	NaN
P48553	1126	5.40	2.96	NaN	2.2252	NaN
Q9BQ61	165	6.07	3.41	5.78	2.2044	0.0257
Q9NXH9	150	2.33	1.37	3.00	1.7310	0.3658
Q9NXH9	287	3.66	1.90	4.02	1.9429	0.2915
Q8IZ69	463	3.94	2.58	4.46	1.8995	NaN
Q5TAX3	302	4.87	4.56	5.69	2.4021	0.2165
P10599	73	5.33	7.64	5.12	2.3201	NaN
Q9NZ09	81	4.33	2.13	6.14	1.4306	NaN
P61081	65	3.83	5.90	5.36	1.3414	0.7555
Q9H832	243	2.97	3.77	3.58	1.5201	0.3724
P17480	328	7.47	5.99	6.57	1.3474	0.2179
O94763	420	7.90	4.81	10.79	1.3716	NaN
Q9Y4E8	791	1.40	2.68	3.38	1.4743	0.4234
Q9UPU5	172	4.23	2.36	3.73	2.1016	0.7588
O95292	121	3.29	5.31	3.14	1.5359	NaN
O95292	173	8.43	4.35	NaN	1.4318	NaN
P18206	85	11.62	23.88	14.69	1.6740	NaN
Q9UK41	60;70	4.65	5.86	3.80	1.9384	0.3986
Q9NP79	155	3.02	4.42	4.54	1.6513	1.2578
Q9H7D7	656	2.11	1.11	2.39	1.3517	0.0722
Q6RFH5	277;287	4.32	1.79	2.62	1.8157	NaN
Q9BRX9	205	3.08	8.16	6.07	2.1770	0.8688
Q9BYP7	927	3.58	4.78	6.14	1.8304	0.3498
Q9Y5A9	433	4.17	2.00	2.11	1.3391	NaN
Q9NUD5	170;178	2.68	3.63	5.20	1.3590	0.5887
Q8IUH4	10	6.98	10.44	8.62	1.5951	0.5509
P37275	962	7.83	5.34	7.90	2.5303	0.0192

Q9Y4E5	150	3.92	2.44	9.77	1.9517	0.6306
Q9ULM2	377	22.77	4.17	20.03	1.3715	0.0581
Q8TF50	334;337	13.07	6.67	16.15	2.4747	0.3654
Q5MCW4	300;303	7.34	4.46	7.19	1.3719	0.0270
Q3KQV3	212	4.71	3.06	5.48	1.5192	0.1781
Q8NHG8	225	6.97	11.51	16.50	2.4661	NaN
Q96B67	368	11.37	14.30	13.96	1.6621	2.3056
Q6PL18	1388	3.15	2.36	5.66	1.5427	1.4064
P31939	325	9.24	6.31	4.41	1.8229	2.0568
P30530	588	5.84	11.75	9.04	2.6408	1.4013
P20810	381	2.08	4.31	5.09	1.9575	1.7920
Q8TBM8	11	6.75	4.56	5.98	1.4484	2.9325
Q5T3I0	333	4.99	3.64	5.48	2.9014	1.7211
Q9Y5Q8	242	3.77	2.07	4.96	3.1503	1.3431
Q13111	7	1.93	3.76	6.53	1.5626	2.3091
Q9Y6K9	396;397	3.84	4.88	5.01	2.2150	3.4746
P01130	452	26.13	39.73	33.45	3.0177	2.1002
Q9BQ69	246	7.98	2.78	4.29	2.4044	1.9610
P53582	22;25	3.19	4.35	4.68	1.7042	2.0483
Q9Y3A3	119	2.55	3.35	3.93	1.3014	2.1714
P27815	218	10.50	6.10	13.95	3.1874	2.0601
Q9BZM1	67	70.76	76.80	83.77	1.7404	2.0759
P60510	52	3.43	5.57	6.52	1.5873	2.3801
P60900	115	59.78	63.26	56.18	2.1867	1.9122
P62191	399	2.41	3.45	4.15	1.4906	1.3231
Q9NW13	392	2.91	5.70	2.26	2.0098	1.9387
O76038	193	10.22	5.04	21.08	1.4940	1.8044
O75410	482	4.27	6.40	7.81	1.7323	1.7742
Q96J01	134	2.83	5.32	6.10	1.6924	1.6998
P29401	133	78.08	58.54	83.26	4.2307	1.8290
Q9Y490	1045	2.60	1.34	1.39	1.6590	1.4502
O43715	37	86.57	80.40	75.65	1.5541	2.7461
Q8TBZ6	37	12.62	7.08	7.56	2.3856	1.4169
Q6IPR3	49	2.36	3.79	4.66	1.6446	2.5810
Q70CQ2	741	3.08	5.68	6.03	2.3320	1.3986
Q7Z5K2	293	5.88	3.67	3.86	1.3938	1.3292
P61221	65	37.36	33.36	28.43	0.8269	1.5028
Q99798	385	7.02	6.08	7.49	1.1089	2.2856
Q15067	449	2.91	2.46	4.10	0.2863	1.3024
P12814	154	3.98	4.28	2.42	0.1052	1.7771
O14672	173	30.37	29.19	36.43	0.1288	1.5911
O14672	524;530	83.11	89.93	90.64	1.2404	1.3046
Q96A54	54	7.76	6.94	9.90	0.4674	1.3591

Q96SZ5	239	3.10	5.23	7.32	0.8328	1.6844
Q99943	229	2.78	3.45	4.89	0.6900	1.9404
O43572	110	3.26	4.83	5.13	0.6923	1.3925
Q9H1A4	1074	1.16	1.56	2.70	0.1925	1.4601
Q92625	849;866	2.49	2.56	5.85	0.0417	3.0409
Q06481	116	87.25	87.76	84.01	0.3936	1.6118
Q9UH17	247	1.97	2.04	3.84	0.0463	1.5443
P02649	130	10.39	10.82	14.61	0.1302	1.5477
Q92974	306	2.44	3.04	5.86	0.1634	1.6087
Q8NCT1	72	11.98	15.41	16.39	0.9784	1.3628
Q8N3C0	131	2.57	3.75	4.94	0.3154	1.7589
Q9BZE9	224;225	2.94	3.53	7.70	0.2512	1.3090
P16615	635	4.90	5.19	8.40	0.0653	1.8092
O43505	182	55.87	59.97	73.79	0.3179	2.2178
Q9UL15	360	9.95	13.96	15.01	0.2544	2.0268
Q14692	101	1.33	1.62	2.51	0.1358	1.4537
Q6PH81	16;19;27	2.51	2.81	7.36	0.5839	1.4964
Q8IYL3	61	5.04	6.17	8.72	1.0169	1.6759
Q9BRJ6	107	3.02	3.16	6.59	0.0613	1.4192
Q9H7E9	42;44;50	7.75	8.29	12.95	0.1023	1.9627
P27708	986	2.06	2.50	4.09	0.1359	1.3978
P27797	105	30.08	29.81	32.46	0.0911	2.4459
P27797	137	52.98	51.57	58.34	0.2085	2.0026
P52907	124	3.28	6.71	6.53	0.6415	1.9570
O75081	556;559	9.04	8.91	14.89	0.0263	1.5153
P29279	103	39.68	47.22	84.34	0.3362	2.5735
P29279	148	19.69	27.19	72.26	0.6879	1.9018
P40227	406	2.49	3.60	1.28	0.5464	1.8640
P16070	53	94.18	94.42	95.72	0.1125	1.7193
P13987	88;89	70.47	75.16	80.79	0.2032	1.7083
Q14008	1317	2.66	3.13	4.07	0.1777	1.9175
O00299	178	4.85	3.69	1.22	0.4293	1.5272
Q9NYJ1	54;64	64.16	65.37	42.60	0.1378	2.0985
Q9NYJ1	34;44	73.47	76.83	49.62	0.3037	1.6428
Q9NYJ1	64	76.19	76.58	46.63	0.0560	3.6378
P31146	24	4.70	3.84	7.95	0.4289	1.6456
P14854	65	81.78	77.45	70.84	0.6900	2.3406
P14854	65	88.50	85.33	83.71	0.5423	1.6644
Q96SW2	441	2.29	3.00	3.63	0.4574	1.7599
P41240	119;122	3.87	5.82	5.88	0.5250	1.5905
P07858	211	59.39	47.03	71.20	0.6523	1.5638
Q5TAQ9	272;273	3.25	4.15	4.29	0.4856	1.6196
O00148	164	1.82	1.95	2.81	0.1057	1.6712

P26196	102	3.18	2.69	2.45	0.8422	2.2892
Q9H2U1	261	2.03	2.73	2.81	0.9528	1.4032
P09622	484	14.71	12.24	12.75	0.7150	1.3375
P09622	477	16.87	14.60	12.31	0.7921	1.3417
Q9UKB3	41	5.80	6.50	9.27	NaN	1.4245
Q96G46	171;177	3.82	5.04	7.37	1.2119	1.6178
P26641	266	2.22	1.36	0.90	1.1218	1.7370
Q8N3D4	346	2.91	2.17	5.30	0.3242	1.4995
O75821	139	4.27	4.56	1.79	0.0785	1.5162
Q13347	160	7.28	4.32	2.53	0.9623	1.3600
P11308	85	6.53	5.71	10.27	0.4486	1.8190
Q15910	523	3.41	2.58	5.90	1.1028	2.0928
Q9Y5Q0	24	2.99	2.25	4.40	0.7746	1.7721
Q9UNN5	120	2.69	2.42	3.38	0.2818	1.3735
Q96EK7	392	2.80	2.91	4.62	0.1470	1.9535
Q52LJ0	63	3.91	5.50	9.75	0.4398	1.5973
Q96ME1	423	3.17	5.44	4.92	0.4674	1.4945
Q8TB52	723;725	3.06	1.93	1.77	1.0365	2.5128
P39748	182	2.97	2.31	5.17	0.4537	1.6652
Q13451	339;340	3.18	2.77	4.72	0.3527	1.5878
Q9BQS8	719	9.61	10.87	17.47	0.5280	1.8883
Q10472	442	72.27	62.94	77.52	0.6951	4.5084
Q7Z7M9	873	69.21	65.58	67.92	1.0233	1.5315
P22102	200;202	1.99	3.40	4.06	1.1371	1.3916
P50440	64	3.32	2.82	6.44	0.2408	1.4587
Q92538	1110	2.16	2.87	3.73	0.6290	1.5111
Q5VTD9	165	6.93	8.10	10.07	0.2206	1.6519
Q5VTD9	194;197	4.08	5.11	11.09	0.1859	1.3588
Q86VQ1	297	8.32	10.92	15.87	0.3187	1.7373
P00367	172	3.94	2.45	1.01	0.5168	1.6573
P04899	352	2.55	4.05	5.49	0.5930	1.3745
P36915	294	3.68	4.39	6.13	0.5383	1.3248
Q9NVN8	490	3.02	3.00	4.12	0.0170	1.6420
Q9NVN8	89	2.66	2.79	4.18	0.0598	1.5634
Q9Y4H4	160	3.78	5.21	7.54	0.6642	1.4953
P25098	340	2.85	2.85	4.58	0.0001	1.8926
P00390	102;107	14.09	20.44	26.94	0.5145	1.6088
P00390	467	15.43	16.67	31.30	0.0940	1.4214
P00390	278	23.57	26.29	47.42	0.3603	2.6375
P00390	484	15.01	23.89	42.57	1.0584	2.0337
P00390	467	19.76	25.40	50.39	0.5149	3.3301
P00390	278	24.05	29.99	54.69	0.5173	2.4594
P00390	377	20.52	33.06	53.21	0.9803	1.5210

P21266	91	3.32	3.17	6.47	0.0927	1.9587
P32780	246	2.42	2.70	3.39	0.3323	1.5905
P12081	174;191	2.87	5.80	6.08	0.8965	1.3051
Q8TF76	219	3.85	3.37	7.75	0.5418	2.6986
P53701	35;46	8.05	7.86	12.93	0.0417	2.6683
P07686	551	75.44	73.95	82.82	0.1591	1.4525
Q8NCD3	663	5.74	7.22	13.20	0.1656	1.5065
Q00839	289;295	10.56	6.16	15.78	0.6617	1.4858
Q8IWL3	79	4.16	5.87	8.75	1.0729	1.8230
P38646	366	7.91	8.34	5.07	0.1015	1.7201
Q7Z6Z7	1832	1.86	2.65	3.74	0.8415	1.5845
Q13111	761	4.59	3.88	7.55	0.5743	2.5251
Q9Y6H1	134	68.89	71.82	53.12	0.2262	2.3547
Q9NX63	112	8.55	7.31	12.15	0.4936	1.3912
O15111	658	1.06	1.58	2.35	0.2837	1.4734
P48551	93	67.72	72.02	61.05	0.9937	1.8320
P18065	98	85.26	85.20	89.97	0.0143	1.3573
Q12906	116	3.92	3.09	2.03	0.7140	1.5475
Q13418	239	2.05	1.78	4.41	0.2233	1.5416
Q8IU81	207	3.24	6.23	8.48	0.6632	1.5382
Q14653	222	2.50	3.12	5.55	0.3865	1.6697
O14896	249	6.28	5.90	4.32	0.1129	1.3148
Q8WZA9	152;158	10.46	10.76	15.04	0.0254	2.5197
P26006	904	60.62	66.19	72.68	0.2829	1.8083
P05556	64	86.67	85.64	89.54	0.5327	1.3988
P05556	553;555;560	81.22	85.41	89.87	0.3224	1.4309
P05106	258	32.20	32.52	48.76	0.0182	1.5634
Q9H9L4	311	14.85	17.19	23.33	0.4983	1.3266
Q7L273	353;358	4.07	4.20	3.07	0.1662	1.8747
Q14145	23;38	2.73	3.50	4.14	0.6331	1.4990
O95235	860;866	2.41	2.81	4.75	0.1263	2.4644
O95235	87	3.26	3.00	6.87	0.0585	1.3054
Q99661	40	2.16	2.44	3.98	0.1662	1.8173
O95239	965	3.81	2.70	6.72	1.2179	2.2452
Q9BXK1	189;192	4.42	7.52	9.76	1.2157	1.5352
P24043	1557;1560	3.31	3.47	8.02	0.1105	2.1025
P07942	170	63.18	63.88	74.63	0.0617	1.8022
Q9NS86	169;174	6.55	5.66	5.25	0.9125	1.4995
Q9Y4W2	504	2.02	3.28	3.90	0.5325	1.4766
Q8NC56	355	68.41	65.80	72.93	0.4404	1.4712
P48357	604	46.64	49.65	65.20	0.5087	2.2589
P25791	94;97	4.91	5.30	7.71	0.2232	1.7440
P25791	94;97	6.21	5.19	10.74	0.4092	1.4374

O94898	902;905	11.98	21.85	28.80	0.4157	2.1967
Q9H9A6	54	2.74	2.63	4.47	0.0631	1.4368
Q9BXY0	44	24.93	24.42	35.73	0.0409	1.3954
P25205	263	1.32	2.19	4.24	0.5323	1.4351
Q14566	91	2.53	2.81	5.36	0.1266	1.7722
Q14566	180	3.23	3.02	6.26	0.2237	3.4515
Q14676	2042;2049	9.76	7.60	16.73	0.4835	1.5572
Q09328	649	50.73	55.28	78.13	0.4157	1.7271
Q5TGZ0	13	43.20	41.42	62.81	0.1249	1.3127
P46013	643	2.99	1.94	6.89	1.1899	2.5163
P82663	139;141;149	9.86	8.29	14.02	0.4726	2.5039
P43246	404	2.48	2.92	3.65	0.1984	1.4378
Q13126	136;145	5.18	6.17	7.28	0.4071	1.4362
Q6UB35	778;779	1.40	2.42	2.40	0.8658	2.9470
Q2M296	113	3.76	4.33	5.52	0.4225	1.4863
P46199	711	4.19	7.80	7.23	0.8555	1.5346
Q99707	120	2.28	2.59	4.07	0.1383	1.3093
Q9BQG0	614;623	3.74	3.31	4.80	0.1980	1.3784
Q9BQG0	890	3.89	3.23	5.20	0.2332	1.5832
P35579	896	2.69	3.20	1.25	0.4051	1.4311
Q99733	247;250	5.86	4.78	3.21	0.8742	1.3997
Q9BPX3	509	1.02	1.03	2.19	0.0246	1.4469
Q9NZQ3	700	2.31	2.04	6.09	0.1076	1.5778
Q9BTX1	468	2.83	3.34	6.14	0.3479	1.6845
O14777	342	5.09	5.84	10.57	0.2846	2.0306
P49821	142	19.02	18.10	25.81	0.2683	1.9404
P49821	206	18.49	20.65	27.27	0.3314	2.1694
Q12986	92	4.69	4.05	9.30	0.2908	1.8971
Q6KC79	52;56	4.03	3.16	5.82	0.5123	2.1824
O15226	453	1.33	1.92	3.25	0.6430	1.7446
P51843	38;41;43	3.50	7.25	8.37	0.9490	1.4786
P49116	134;137	3.50	4.96	7.00	0.5998	1.5168
P53384	22;25	5.51	6.29	9.88	0.3754	1.5029
Q9Y5Y2	54	3.72	3.74	6.89	0.0059	1.5654
Q96RS6	111	2.49	3.71	4.35	0.5875	1.4702
Q14980	375	1.99	2.69	4.16	0.5910	2.3054
Q12769	65	1.27	3.38	3.46	0.3676	2.2300
Q9Y530	33;38	4.82	5.19	7.95	0.0873	1.3257
P11926	11	1.43	1.81	2.79	0.9972	1.9718
P11926	89	3.85	3.23	5.92	0.5419	2.0527
O60313	786	8.84	11.16	12.79	0.9111	1.8305
P22059	609	4.63	3.98	2.27	0.3819	1.5362
Q96FW1	23	1.46	2.03	2.86	0.6584	2.1623

O15460	529	21.21	16.92	28.99	1.2065	2.1022
Q13177	352	3.20	4.61	5.60	0.3393	1.3416
P49585	139	16.51	16.54	13.47	0.0075	2.1252
Q8N8D1	281	6.40	7.26	11.80	1.2205	1.4994
O00541	391	3.40	5.23	4.68	0.9162	1.4902
Q92576	402	2.05	2.98	4.05	0.3480	1.3321
Q9NRX4	69;71;73	4.90	9.62	12.09	0.5952	2.5898
Q16512	942	1.45	1.78	3.74	0.2108	1.5315
Q6IQ23	310;313	5.29	4.99	9.22	0.0620	2.0733
Q96S99	21	2.27	3.16	3.52	0.9422	1.4627
O75439	62	1.91	1.95	3.14	0.0924	2.2118
P09884	1180	1.95	2.88	5.08	0.3960	1.4646
Q9NVU0	103	3.46	3.03	2.54	1.0024	1.7643
Q9H2U2	161;171	4.78	5.29	7.30	0.2310	1.9013
Q06203	503;506	23.37	30.35	31.57	0.5836	1.3688
P30153	310;317	3.20	4.20	7.48	0.2077	2.7448
P50897	152;160	83.23	77.19	89.77	0.9884	1.4832
Q96BP3	287	5.65	4.60	4.24	0.3541	2.7272
P42785	233	58.74	57.63	69.04	0.0737	1.4108
P31323	149	3.08	3.28	5.81	0.1278	1.4586
P05771	572	2.49	2.95	5.91	0.6454	1.6308
O94906	513	2.00	1.81	3.84	0.2396	2.2065
Q86TP1	8	2.26	2.42	3.46	0.2088	1.7760
P20618	82;89	67.42	69.36	75.29	0.3946	2.0203
Q15397	185	1.83	1.73	3.28	0.1381	1.6150
Q9Y606	260	4.26	3.63	6.10	0.2121	2.1391
Q15276	533;536	4.77	5.20	7.36	0.5925	1.8116
O60216	585	4.10	3.81	2.72	0.2759	1.3671
P49792	2982	3.97	4.64	6.53	0.1358	1.4534
O94762	977;987	4.99	6.60	9.03	0.5579	1.4030
P52758	71	20.36	13.84	28.57	0.9318	1.5493
Q9Y508	173;176	6.42	6.36	4.95	0.0232	1.5139
Q969K3	325	5.49	7.05	7.96	0.8900	1.6098
O60942	419	1.97	2.14	4.65	0.0734	1.4475
P13489	199;209;216	2.57	3.66	5.12	0.4218	1.5096
O75116	804	4.87	6.59	9.66	0.2862	1.3068
P40429	38	1.63	1.78	2.27	0.3682	1.9715
Q02543	16	3.84	3.36	2.79	0.1559	2.2756
P04843	545	1.89	1.88	3.06	0.0139	1.5923
P62249	25	1.47	1.78	2.33	0.3930	1.4726
Q15418	552	2.21	2.47	4.72	0.1211	2.1982
O76021	96	3.47	3.60	5.09	0.1037	1.3218
Q9Y3I0	19	11.04	9.48	8.38	0.1674	1.7571

Q16799	104;113	5.69	5.75	3.13	0.0225	3.1104
O95197	390	5.84	6.96	8.31	0.3881	1.3799
Q9UQR0	350	3.11	3.60	6.61	0.3732	1.3674
Q99470	80	81.65	76.73	86.03	0.6920	1.8293
Q15437	434	8.43	9.77	22.86	0.1004	1.4593
Q9UBV2	168	49.72	50.39	56.23	0.0280	1.3613
P41440	220	5.43	5.81	9.61	0.3207	1.5919
P30825	628	3.06	6.74	7.21	0.7558	1.8807
Q9H4L7	575	1.78	1.82	4.09	0.0225	1.6098
Q8TAD8	299	4.26	4.31	7.87	0.0227	1.5120
Q9UNH7	347;348	2.47	2.85	4.79	0.1455	1.3452
Q9HB58	468	4.43	4.86	7.60	0.6892	1.5233
Q8N0X7	562	4.35	3.36	3.83	0.5696	2.2252
Q8NBT2	155	2.97	4.59	8.35	0.6020	1.4959
Q15005	17;26	4.55	4.21	6.86	0.2983	2.8073
O43291	38	83.87	85.97	79.32	0.2740	1.6162
O15269	438	5.16	6.81	9.42	0.5418	1.4333
Q9Y5M8	100	3.79	4.01	5.59	0.1361	1.3327
Q9UQ35	872	6.57	6.26	9.18	0.1799	1.6994
P27105	87	36.06	37.44	44.48	0.1561	1.3558
P53597	172;181	5.39	4.35	2.05	0.2978	1.5559
A2RTX5	43;49	6.01	4.05	7.69	0.9610	1.3451
P17987	147	1.66	1.61	2.57	0.0299	1.5548
Q9UBB9	391;400	2.27	1.70	3.11	0.5261	1.4436
Q6YHU6	588	2.57	2.73	5.12	0.1465	1.3344
Q5T1C6	68	3.84	4.55	7.46	0.7197	2.1019
Q6I9Y2	38	2.01	2.77	4.51	0.6520	1.6205
P62072	50	88.80	86.39	87.52	0.5145	1.3170
O60830	17	31.83	29.71	48.09	0.2299	1.3377
Q9Y5J9	55;59	84.53	82.49	76.65	0.2621	1.4768
O15321	445	4.94	7.30	8.54	0.8250	2.4182
Q6NUQ4	392	2.87	3.77	4.92	0.2011	1.3517
Q96K49	139	66.34	61.56	80.40	1.0316	2.6189
P42166	330	4.22	3.88	7.57	0.2650	3.3844
O00220	204	85.55	87.01	90.71	0.4345	1.3404
O96008	74;76;86	5.63	6.36	8.40	0.1689	1.4261
P11388	455	2.33	2.51	6.11	0.1150	1.5706
Q02880	271	1.41	1.20	3.05	0.3068	1.6607
P67936	247	6.95	5.31	4.50	0.9097	2.0376
P51580	132;133	1.59	2.09	4.80	0.9873	2.2767
Q96Q05	141	3.50	4.07	6.56	0.1510	1.5576
P14373	43;53;56	2.52	2.98	3.33	0.2265	2.0468
Q13263	65;68	3.05	5.01	6.22	0.7936	1.4069

Q13263	232	9.12	10.45	14.51	0.7409	1.5629
O95857	140;144	49.51	53.47	61.18	0.2532	1.3483
P68366	347	1.70	1.59	2.95	0.0751	1.5225
P23258	201	4.04	4.15	3.39	0.0778	1.7313
Q5TAX3	852	5.77	6.66	11.03	0.4686	1.8707
Q16881	515;533	6.66	9.61	45.54	0.7605	1.6190
Q16881	209;214	15.98	20.06	55.84	1.0329	1.4694
Q16881	577	10.17	12.38	50.76	0.1502	4.4193
Q16881	577	8.93	9.54	55.74	0.0849	1.6529
Q9BZF9	598	8.43	8.14	16.69	0.0331	1.3814
Q05086	108	4.83	3.23	7.44	0.8936	1.3492
Q6ZU65	562	4.48	3.78	6.28	0.7854	1.6329
O94874	641;649	2.50	2.41	3.97	0.0429	2.0351
P07919	67	71.91	73.12	79.98	0.5547	1.7138
Q9Y5T5	77;82	3.32	3.68	5.66	0.2882	1.7653
P45974	219	6.06	5.63	3.50	0.1556	1.9646
Q9NYH9	524	2.73	3.09	7.26	NaN	2.1018
Q9Y277	65	2.41	3.74	6.88	0.6500	1.7001
Q14119	327	3.31	4.57	5.03	0.7030	1.4968
Q4G0F5	334	1.96	2.65	3.06	0.5904	1.6585
Q7Z3J2	315	1.78	2.67	3.32	0.5859	1.5402
Q99986	205	5.05	3.14	8.16	1.0114	1.4611
P23381	305;309	2.84	2.86	1.49	0.0094	1.4229
O00401	431	2.69	4.04	7.03	1.1505	1.3309
Q8WV99	57;60	8.49	8.32	6.30	0.0366	1.6748
Q9HBF4	623;628;631	4.66	8.03	9.45	0.6129	2.3595
Q5VZL5	341;344	1.95	1.98	3.73	0.0288	2.0870
Q8ND82	734	1.86	2.26	2.71	0.8596	1.9676
Q9ULM2	224	3.45	5.46	10.20	0.8242	1.4368
Q96KM6	512;515	4.46	5.48	9.98	0.1564	1.9719
Q9BS34	325	2.77	5.91	7.10	1.0947	1.5971
Q8NDX6	159	5.56	4.02	11.77	0.6752	1.7590
Q15696	214	5.26	3.90	8.88	0.6077	1.3233